

STATIC STRUCTURAL STUDIES ON REINFORCED TUBULAR T-JOINTS OF OFFSHORE JACKET STRUCTURES

Thesis

submitted in partial fulfillment of the requirements for the degree of

DOCTOR OF PHILOSOPHY

by

N. MURUGAN
(165102AM16F04)



**DEPARTMENT OF WATER RESOURCES AND OCEAN ENGINEERING
NATIONAL INSTITUTE OF TECHNOLOGY KARNATAKA
SURATHKAL, MANGALORE - 575 025, INDIA**

JUNE, 2023

STATIC STRUCTURAL STUDIES ON REINFORCED TUBULAR T-JOINTS OF OFFSHORE JACKET STRUCTURES

Thesis
submitted in partial fulfillment of the requirements for the degree of
DOCTOR OF PHILOSOPHY

by

N. MURUGAN
(165102AM16F04)

Under the guidance of

Dr. VADIVUCHEZHIAN KALIVEERAN
Assistant Professor
and
Dr. SUBRAHMANYA KUNDAPURA
Assistant Professor

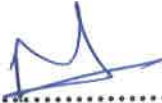


**DEPARTMENT OF WATER RESOURCES AND OCEAN ENGINEERING
NATIONAL INSTITUTE OF TECHNOLOGY KARNATAKA
SURATHKAL, MANGALORE - 575 025, INDIA**

JUNE, 2023

DECLARATION

I hereby declare that the Ph.D. Thesis entitled “**STATIC STRUCTURAL STUDIES ON REINFORCED TUBULAR T-JOINTS OF OFFSHORE JACKET STRUCTURES**” which is being submitted to **National Institute of Technology Karnataka, Surathkal**, for the partial fulfillment of the requirement for the award of degree of **Doctor of Philosophy** in the **Department of Water Resources and Ocean Engineering** is a bonafide report of the work carried out by me. The material contained in this Ph.D. Thesis has not been submitted to any university or Institution for the award of any degree.



.....
N.MURUGAN (165102AM16F04)

Department of Water Resources and Ocean Engineering
National Institute of Technology Karnataka, Surathkal

Place: NITK, SURATHKAL.

Date: 12/06/2023

CERTIFICATE

This is to certify that the Ph.D. Thesis entitled “**STATIC STRUCTURAL STUDIES ON REINFORCED TUBULAR T-JOINTS OF OFFSHORE JACKET STRUCTURES**” submitted by **N. MURUGAN (165102AM16F04)**, as the record of the work carried out by him, is accepted as the Ph.D. Thesis submission in partial fulfillment of the requirements for the award of the degree of **Doctor of Philosophy** in the **Department of Water Resources and Ocean Engineering, National Institute of Technology Karnataka, Surathkal**, is a bonafide work carried out by him under our supervision and guidance.


.....
Dr. VADIVUCHEZHIAN KALIVEERAN

Assistant Professor

Department of Water Resources and Ocean Engineering
National Institute of Technology Karnataka, Surathkal


.....
Dr. SUBRAHMANYA KUNDAPURA

Assistant Professor

Department of Water Resources and Ocean Engineering
National Institute of Technology Karnataka, Surathkal


.....
Chairman - DRPC

Department of Water Resources and Ocean Engineering
National Institute of Technology Karnataka, Surathkal
Dept. of Water Resources & Ocean Engineering



ACKNOWLEDGEMENT

First and foremost, I would like to thank my supervisor, **Dr. Vadivuchezhian K.**, for providing me with the opportunity to conduct this Ph.D. research, as well as for his constant enthusiasm and helpful guidance over the years. I would like to thank him for sharing his extensive knowledge with me as well as many other technical aspects of my work. These years would have been far more difficult without his invaluable assistance. Thank you for your assistance, support, and love

I am also grateful to **VDK sir's family members** for their love and support throughout this research process. Thank you very much!

I would also like to thank my co-supervisors, **Dr. Subrahmanya K.** and **Prof. M. K. Nagaraj**, for providing me with the opportunity to conduct this Ph.D. research, as well as for their constant support and useful guidance over the years. Thank you for your assistance, support, and love

I am also thankful to **Prof. G. S. Dwarakish**, **Prof. Amai Mahesha**, **Prof. Amba Shetty** and **Prof. B.M. Dodamani** former Heads of the Department and **Prof. K. Varija**, present Head of the Department of Water Resources and Ocean Engineering, NITK, Surathkal for permitting me to carry out my research work and to make use of institutional infrastructure facilities.

I am grateful to Research Progress Appraisal Committee members, **Prof. Subba Rao**, **Prof. Katta Venkataramana** for their thoughtful comments on my work and the stimulating discussions we had during my research seminars.

At work, I met many people who inspired, supported, and guided me not only in my research but also in my personal challenges. I am grateful to my friend **Dr. Muralidhar**, who assisted and supported me a lot during my research phase and continues to do so. Thank you for your assistance, support, and love

I would like to thank my friend **Dr. Kumaran V**, who helped me in any way he could during difficult times in my life and was always there for me when I needed him. Thank you for your assistance, support, and love.

I am deeply grateful to my friend **Raveesh R M**, who supported me a lot in learning and doing numerical modelling and to carry out the experiments. Thanks for your valuable time. Thank you for your assistance, support, and love

I sincerely thank **Dr. Ramachandra rao, Dr. Srinivasala reddy, Dr. Palani Kumar Dr. Rajapandi, Mrs. T S Sahana, Mrs. Vijayalakshmi, Mr. Pugalvendhan, Mr. Balan, Mr. Venkatesh** and others for their support to conduct experiments. I sincerely acknowledge and express my heartfelt gratitude to all of the above research scholars for their unfailing assistance.

I want to thank my friend **Dr. Vijay**, an assistant professor in the department of ocean engineering at IIT Madras, for his advice and candid conversations. I appreciate your help, love, and support.

I would also like to thank the research scholars for their time and support (**Dr. Sahaj K V, Salma, Abdul Sharif, Ayilobeni, Vasala SaiCharan, Sonia Xavier, Dr. Rajesh Kumar, Dr. Vivek, Dr. Ajuy, and Dr. Nidhul**) of our own department and other departments.

I sincerely acknowledge the help and support of **Balu Anna, Prathima Mam, Seetharam sir, Jagadish Sir, Anil Anna, Anand Anna, Padmanaban Anna, Gopal Anna** and **all other non-teaching staff** of Department of Water Resources and Ocean Engineering, NITK, Surathkal, in completing the work. A very special gratitude to everyone in the Administrative block and Accounts section for their cooperation. I am also grateful to the operators, fabrication specialists and machine suppliers from Chennai who gave me a support to conduct my experiments.

I would like to thank my friend **C. Mariappan and his family** for their support throughout my life.

I would like to thank my sisters and their family, **N. Ponselvi, N. Paneerselvi, N. Kanaku, N. Latha, C. Dhanalakshmi** and **C.Triveni** for their unending support and encouragement throughout my life. Thank you very much.

I would like to express my heartfelt gratitude to my elder sister (and family) **S. Suganthi, & Dr. S. R. S. Selvakuthalingam, S.Rispremika**, well-wishers who prayed for me, supported me during my difficult times, and encouraged me greatly.

I would like to thank my wife **S. Saranya** for her patience, love and the support.

Finally, I would like to express my gratitude to my parents, **C. Natarajan** and **N. Ezhilarasi**, for their unwavering support and encouragement in my studies. Without them, I would never have travelled such a long distance. I love you both and am grateful for everything you have done for me. I dedicate this thesis for my beloved family

I dedicate all of my studies to my **Amma N. Ezhilarasi & Appa Natarajan** for their unconditional love, support, and liberty.

N. MURUGAN

ABSTRACT

The oil discovery was one of the most important discoveries in the twentieth century. At the turn of the twentieth century, exploration started based on land-based resources and as the demands increased, the exploration was into sea-based resources. It started in shallow water and later in deep water regions. The jacket platform is the most commonly employed one in the shallow water depths.

Stiffening is a reinforcing mechanism that essentially improves the strength as well as enhances the lifetime of the structures. Owing to greater mechanical properties and economic advantages, tubular structures are preferably used in offshore jacket structures. The present study investigates the stiffening effect on the behavior of static strength and stiffness of the tubular T joint of an offshore jacket platform structure subjected to axial compressive load. The tubular T model selected for this study, as per the API (American Petroleum Institute) standard, has the following dimensions: Chord length is 400 mm, diameter is 100 mm, thickness is 4 mm, and brace length is 200 mm, diameter is 50 mm, and thickness is 3 mm. The structural steel material with a Young's modulus of 205 GPa and a Poisson ratio of 0.3 was considered for the analysis. The axial compressive load of 20 kN to 300 kN with an interval of 20 kN is applied on top of the brace section and the support conditions at the chord end are simply supported. Three-dimensional static structural analysis using the ANSYS software package was carried out to evaluate the effect of stiffeners placed over the chord section of the tubular T joint. An experimental program has been carried out in the laboratory, and the results are presented. A comparative study is conducted between the experimental and numerical for the validation of results. The stiffened configurations considered are: Can around the joint with 6 rings and 4 strips, Can around the joint with 6 rings and 6 strips, Can around the joint with 6 rings and 8 strips. For the given axial compressive load of 20kN, the joint stiffness of the unstiffened tubular T joint is 67.929N/mm. The stiffened configuration increases the joint's local stiffness by more than 100 percent, and a maximum of 140 percent is observed.

Keywords: Tubular T joint, Compressive load, Static Strength, Stiffness, Finite element analysis, Offshore jacket structures

TABLE OF CONTENTS

ABSTRACT	i
TABLE OF CONTENTS	ii
LIST OF FIGURES	v
LIST OF TABLES	ix
NOMENCLATURE	x
CHAPTER 1	
INTRODUCTION	1
1.1 INTRODUCTION	1
1.1.1 Tubular joints	1
1.1.2 Failure modes of tubular connections	4
1.1.3 Types of Stiffening Mechanisms	6
1.1.4 Material used for present work	10
1.2 MOTIVATION	11
1.3 STRUCTURE OF THE THESIS	12
CHAPTER 2	
LITERATURE REVIEW	13
2.1 INTRODUCTION	13
2.2 REVIEWS ON RING STIFFENERS	13
2.3 REVIEWS ON DOUBLER/COLLAR PLATES	18
2.4 REVIEWS ON FIBER REINFORCED POLYMERS (FRP)	22
2.5 RESEARCH GAPS	23
2.6 OBJECTIVES OF RESEARCH WORK	24
CHAPTER 3	
EXPERIMENTAL STUDY	25
3.1 INTRODUCTION	25
3.2 MATERIAL COMPOSITION	25
3.3 MODEL PREPARATION	27

3.4	EXPERIMENTAL DETAILS	30
3.5	MAJOR STUDY: T-JOINT MODEL DETAILS	31
3.6	INSTRUMENTATION	36
CHAPTER 4		
COMPUTATIONAL STUDY		41
4.1	INTRODUCTION	41
4.2	LINEAR STATIC ANALYSIS	41
4.3	GEOMETRIC MODELLING	41
4.4	MESHING AND ELEMENT DETAILS	42
4.5	LOADING AND BOUNDARY CONDITIONS	42
4.6	NON-LINEAR ANALYSIS	43
4.7	GEOMETRIC MODEL	44
4.8	MESHING AND ELEMENT DETAILS	49
4.9	MESH CONVERGENCE STUDY	54
4.10	LOADING AND BOUNDARY CONDITIONS	55
CHAPTER 5		
RESULTS AND DISCUSSIONS		59
5.1	INTRODUCTION	59
5.2	FAILURE MECHANISM	59
5.3	VON-MISES STRESS VARIATION	59
5.4	LOAD-OVALIZATION RELATIONSHIP	60
5.5	LOAD-OVALIZATION DEFINITION	61
5.6	UNSTIFFENED T-JOINT	68
5.7	BEHAVIOUR OF STIFFENED TUBULAR T-JOINT	71
5.8	ULTIMATE CAPACITY OF THE CHORD	72
5.9	VERIFICATION OF NUMERICAL RESULTS WITH EXPERIMENTAL DATA	73
CHAPTER 6		
CONCLUSIONS		77

6.1	CONCLUSIONS FROM EXPERIMENTAL STUDY	77
6.2	CONCLUSIONS FROM NUMMERICAL STUDY	77
6.3	LIMITATIONS OF THE STUDY	78
6.4	SCOPE FOR FURTHER STUDY	78
	REFERENCES	79
	PUBLICATIONS BASED ON PRESENT RESEARCH WORK	84
	CURRICULUM VITAE	85

LIST OF FIGURES

Figure 1.1	Tubular KT-joint	2
Figure 1.2a	Types of uniplanar tubular joints	2
Figure 1.2b	Example of multi-planar joints (a) Multi-planar XT joint and (b) Multi-planar XX joint.	3
Figure 1.3	Simple tubular joint	3
Figure 1.4	Ring stiffened joint	4
Figure 1.5	Failure at branch adjacent to weld toe	4
Figure 1.6	Failure in the weld	5
Figure 1.7	Ductile failure of chord wall	5
Figure 1.8	Buckling of chord wall	6
Figure 1.9	Lamellar tearing of chord wall	6
Figure 1.10	Local collapse of chord wall	6
Figure 1.11	Pass- through Gusset Plate	7
Figure 1.12	External ring stiffeners	8
Figure 1.13	Overlap K-joint geometry	8
Figure 1.14	Internal ring stiffeners for large diameter chords	9
Figure 1.15	Thickening of chord wall near the connection	9
Figure 1.16	Doubler plate reinforced T-joint	9
Figure 1.17	Collar plate reinforced T-joint	10
Figure 1.18	FRP stiffened T-Joint	10
Figure 2.1	Configuration of the stiffened specimen used in static tests	14
Figure 2.2	Load-Deformation curves of the stiffened and unstiffened T-joint	14
Figure 2.3	Ring stiffened T-joint	16
Figure 2.4	Typical undamaged stiffened T-joint	17
Figure 2.5	Typical undamaged stiffened Y-joint	17
Figure 2.6	Load-deformation curves for T-joints with external stiffeners	18
Figure 3.1	Specimen for Spectrometric analysis of material	26
Figure 3.2	Tested specimen for Spectrometric analysis of material	26
Figure 3.3	Pipe cutting using grinder cutting machine	27
Figure 3.4	Chord and brace members	27

Figure 3.5	Edge preparation	28
Figure 3.6	Hole preparation for joining brace member	28
Figure 3.7	Welding of chord and brace member	29
Figure 3.8	Tubular T-joint model	29
Figure 3.9	Experimental setup	30
Figure 3.10	Experimental setup with dial gauges	30
Figure 3.11	Schematic arrangement of T joint specimen	31
Figure 3.12	Tubular T-joint Specifications	32
Figure 3.13	Unreinforced tubular T-joint	33
Figure 3.14	Reinforced tubular T-joint Can -Ring- 6 strips	33
Figure 3.15	Reinforced tubular T-joint Can -Ring- 8 strips	34
Figure 3.16a	Schematic diagram of specimen on saddle support	35
Figure 3.16b	Saddle Support 150 mm x 300 mm x12 mm	35
Figure 3.16c	Fabricated saddle support	36
Figure 3.17	Strain Gauge pasted over specimen	37
Figure 3.18	Experimental setup with specimen (Unreinforced)	38
Figure 3.19	Experimental setup with specimen (Reinforced)	39
Figure 4.1	The geometry of Tubular T joint model with 5 grooves	42
Figure 4.2	Meshed model 5 grooves 2mm model	42
Figure 4.3	Boundary conditions for tubular T joint with 5 grooves	43
Figure 4.4	Material model for finite element input	43
Figure 4.5	Tubular T-joint Specifications	44
Figure 4.6	Unreinforced tubular T-joint model	45
Figure 4.7	Reinforced tubular T-joint model (4 strips)	46
Figure 4.8	Reinforced tubular T-joint model (6 strips)	47
Figure 4.9	Reinforced tubular T-joint model (8 strips)	48
Figure 4.10	Finite element mesh	49
Figure 4.11	The geometry of SOLID186 element	50
Figure 4.12	The geometry of SOLID187 element	50
Figure 4.13	Finite element mesh unreinforced model	51
Figure 4.14	Finite element mesh 4 strips model	52

Figure 4.15	Finite element mesh 6 strips model	53
Figure 4.16	Finite element mesh 8 strips model	54
Figure 4.17	Convergence study	55
Figure 4.18	Boundary conditions for tubular T joint	56
Figure 4.19	Boundary conditions for tubular T joint (4 strips)	56
Figure 4.20	Boundary conditions for tubular T joint (6 strips)	57
Figure 4.21	Boundary conditions for tubular T joint (8 strips)	57
Figure 5.1	Shape of the cross-section of a chord member before (a) and after (b) applying a load	59
Figure 5.2	Load vs chord ovalization	60
Figure 5.3	Definition of Ovalization	62
Figure 5.4	(a) Failure at support and (b) Ovalization Curve (case 1)	63
Figure 5.5	a) Ovalized specimen	64
Figure 5.5	(b) Ovalization Curve (case 2)	65
Figure 5.6	Unstiffened T- joint (a) Local collapse of chord wall	65
Figure 5.6	(b) Load ovalization curve	66
Figure 5.7	4 strips (a) Local collapse of chord wall	66
Figure 5.7	(b) Load ovalization curve	67
Figure 5.8	8 strips (a) Local collapse of chord wall	68
Figure 5.8	(b) Load ovalization curve	68
Figure 5.9	Load-deformation curve for unstiffened joint	69
Figure 5.10	Unstiffened T joint (a) After-testing image of the specimen (experiment) (b) The von Mises stress distribution (Numerical simulation) (c) Variation of Equivalent plastic strain (Numerical simulation)	70
Figure 5.11	Figure 5.11: 4 strips stiffened T joint (a) After-testing image of the specimen (experiment) (b) The von Mises stress distribution (Numerical simulation)	71
Figure 5.11	(c) Variation of Equivalent plastic strain (Numerical simulation)	72
Figure 5.12	Comparison of Load v/s Vertical deflection between experimental and FE-simulated data for Unstiffened T-Joint	74

Figure 5.13	Comparison of Load v/s Vertical deflection between experimental and FE-simulated data for 4 strip stiffened T-Joint	74
Figure 5.14	Comparison of Load v/s Vertical deflection between experimental and FE-simulated data for 6 strip stiffened T-Joint	75
Figure 5.15	Comparison of Load v/s Vertical deflection between experimental and FE-simulated data for 8 strip stiffened T-Joint Pipeline.	75

LIST OF TABLES

Table 1.1	Chemical composition of SS304 alloy	11
Table 3.1	Spectrometric analysis of material	26
Table 3.2	Specimen Details (Measured Dimensions)	32
Table 5.1	Joint local stiffness for T joint model	61
Table 5.2	Ultimate capacity variation (kN)	72
Table 5.3	Joint Local Stiffness variation (N/mm)	73
Table 5.4	Variation of load	76

NOMENCLATURE

L	Chord member Length, mm
D	Chord member Diameter, mm
T	Chord member Thickness, mm
l	Brace member Length, mm
d	Brace member Diameter, mm
t	Brace member Thickness, mm
a	Length of edge strip, mm
b	Length of the strip, mm
c	Ring length, mm
e	Distance between two rings, mm
f	Distance between Can and first ring, mm
g	Can length, mm
h	Brace member diameter, mm
Δ_t	top displacement of the chord member, mm
Δ_b	Bottom displacement of the chord member, mm

CHAPTER 1

INTRODUCTION

1.1 Introduction

Drilling, production, storage, and distribution facilities in the ocean are supported by offshore platforms. The jacket platform is the most popular offshore platform used at shallow water depths (up to 200 m) (T. S. Thandavamoorthy., 2000). Offshore installations frequently use steel tubular sections. When compared to standard steel sections, the tubular sections have a greater strength-to-weight ratio and can withstand hydrodynamic forces (Saini et al., 2016). Because they are more advantageous in the construction of offshore constructions, cylindrical steel tube sections are more frequently used (Chen et al., 1985). For offshore oil drilling and production platforms, tens of thousands of massive tubular constructions have been built over the last 60 years. Over 7000 offshore platforms have been installed globally (Digre et al., 1994).

1.1.1. Tubular joints:

A connection between two or more tubular sections, between vertical member, i.e., chord and horizontal/inclined members, i.e., brace is referred as tubular joint (Figure 1.1). The larger diameter pipe in a tubular joint made of two pipes of differing diameters is known as the chord, while the smaller pipe is known as the brace (Hamid Ahmadi et al., 2013).

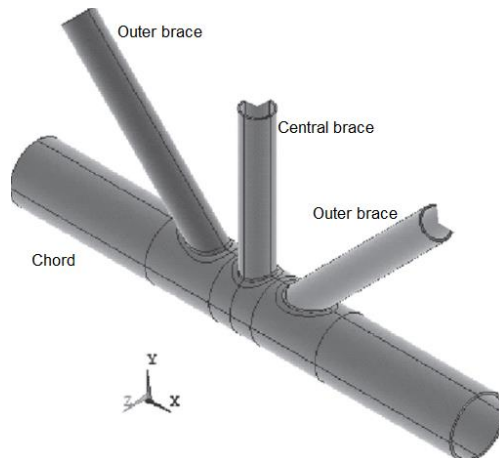


Figure 1.1: Tubular KT-joint (Hamid Ahmadi *et al.*, 2013)

Few uni-planar (Figure 1.2a) and multi-planar (Figure 1.2b) joints utilized in offshore structures were presented by Saini *et al.* (2016). H. Qu *et al.*, (2014) reported that the tubular joints are critical structural members playing an important role in transferring the loads in an offshore platform structure. Due of their geometric discontinuity, joints are a significant component of offshore structures, according to research by T. C. Fung *et al.* (2015).

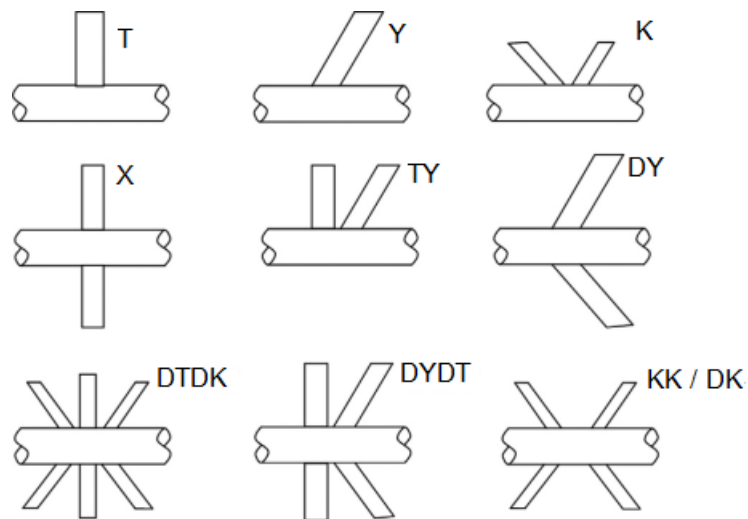


Figure 1.2a: Types of uniplanar tubular joints (Saini *et al.*, 2016)

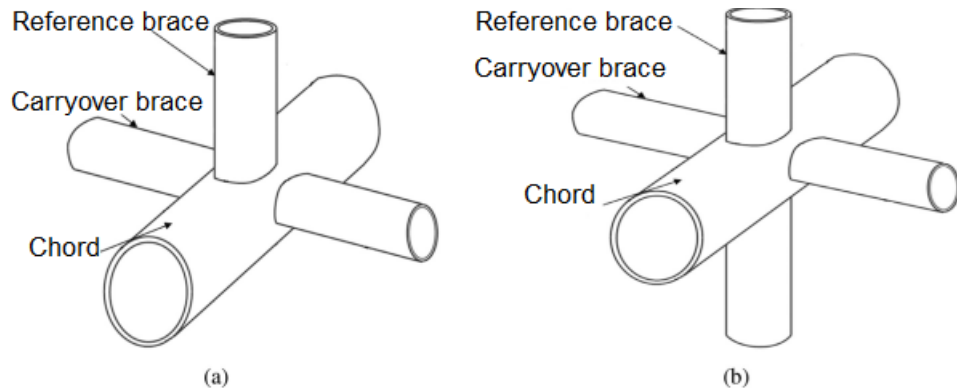


Figure 1.2b: Example of multi-planar joints

(a) Multi-planar XT joint and (b) Multi-planar XX joint. (*Saini et al.*, 2016)

W. Visser (1975) classified tubular joints based on reinforcement. The simple unstiffened joint shown in Figure 1.3 is a joint without any reinforcement. The bending effect plays an essential role in the stress transmission through the joint.

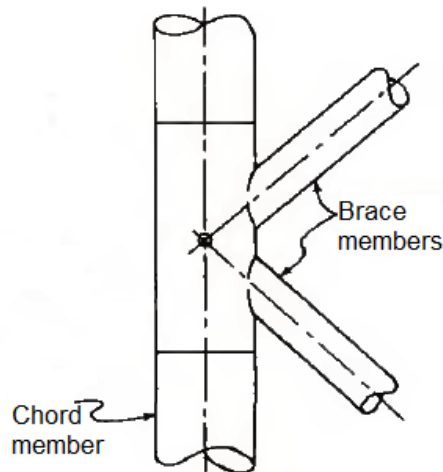


Figure 1.3: Simple tubular joint (*Marshall, P.W. & Toprac, A. A. 1974*)

The term "stiffened joint" refers to the joint that has reinforcement (Figure 1.4). The stiffening or reinforcement techniques used for structures are:

- (i) Techniques implemented during design (e.g., joint can, ring, rack/rib, and doubler plate)
- (ii) Techniques implemented during service and/or design (e.g., Collar plates, FRP, and external rings) (*Hossein Nassiraei et al.*, 2016)

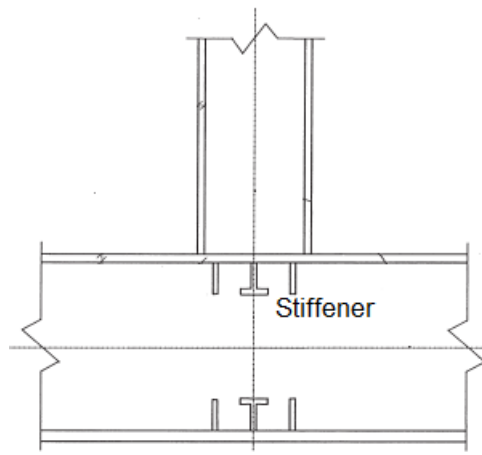


Figure 1.4: Ring stiffened joint (M. M. K. Lee. and A. Llewelyn-Parry, 1999)

1.1.2. Failure modes of tubular connections:

A list of unreinforced tubular T and X joint failure types was compiled by R. P. Pan et al. in 1977. Both compressive and tensile forces may have contributed to the breakdown. Tensile failures can either be ductile or brittle and are characterized by a material fracture or parting. The branch member's elongation is depicted in Figure 1.5. This model develops a branch's maximum strength and is a very ductile failure. The failure scenario when the weld metal fractures is depicted in Figure 1.6. The complete design load of the member should be developed through the weld in order to prevent this kind of failure.

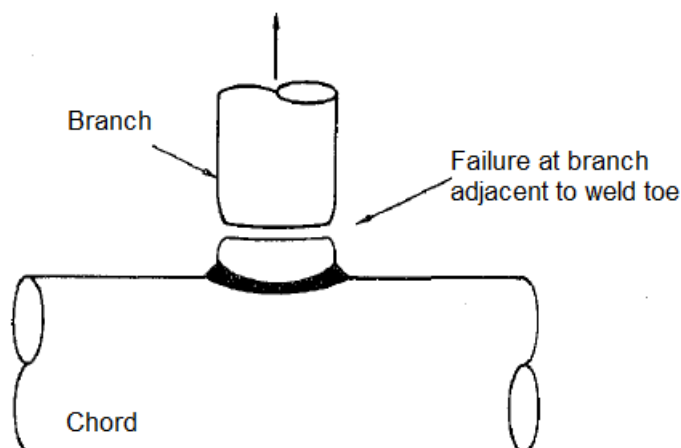


Figure 1.5: Failure at branch adjacent to weld toe (R. P. Pan *et al.*, 1977)

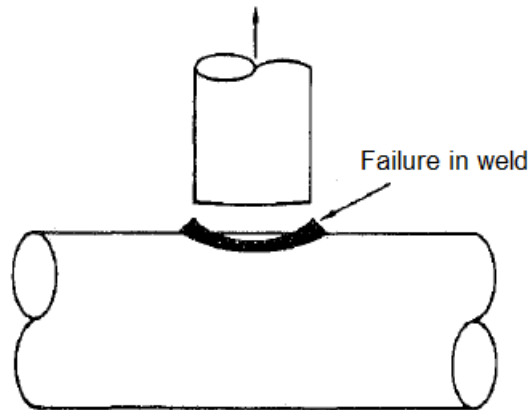


Figure 1.6: Failure in the weld (R. P. Pan *et al.*, 1977)

In the failure mechanism depicted in Figure 1.7, the chord wall experiences significant plastic deformation that is later followed by fracture at the weld toe. Another potential T-joint failure mode is depicted in Figure 1.8, especially when the chord component has a long, unsupported length. It is not a true joint failure and is brought on by bending compressive forces in the chord wall. When the wall thickness exceeds 1 in. to 2 in., lamellar ripping becomes primarily a metallurgical issue. As seen in Figure 1.9, it typically happens close to the welds due to significant local temperature strains and potential weak points in the chord wall (produced by impurities that are stretched during the plane-rolling process).

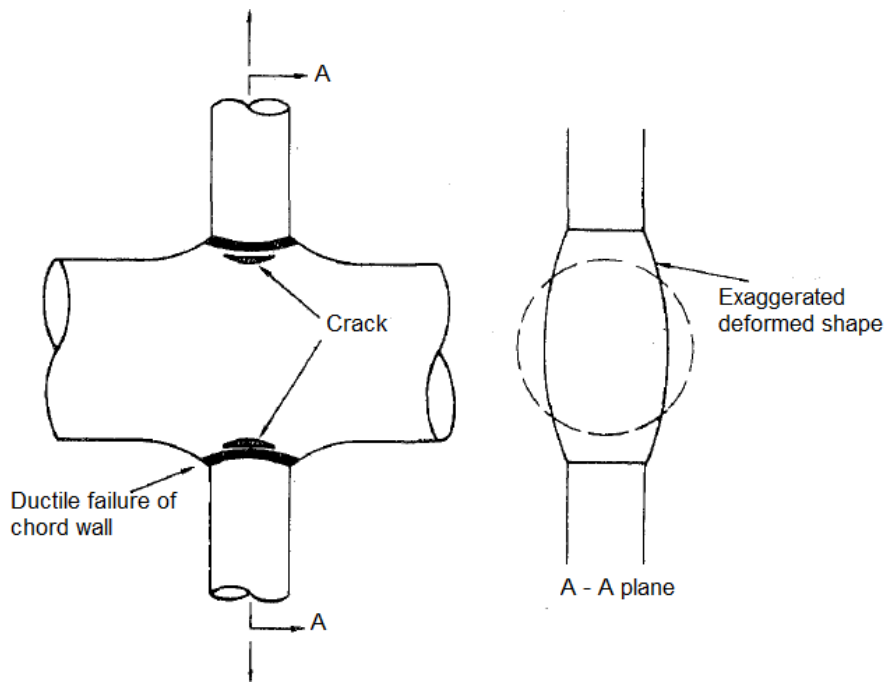


Figure 1.7: Ductile failure of chord wall (R. P. Pan *et al.*, 1977)

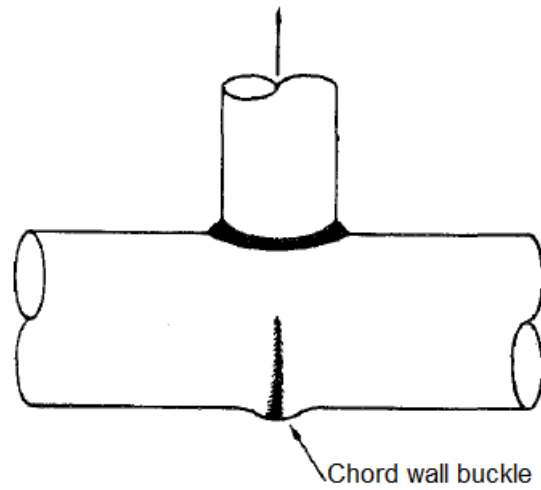


Figure 1.8: Buckling of chord wall (R. P. Pan *et al.*, 1977)

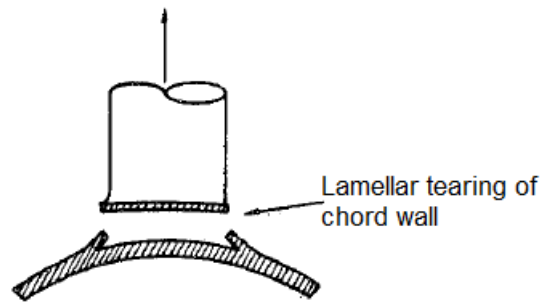


Figure 1.9: Lamellar tearing of chord wall (R. P. Pan *et al.*, 1977)

As demonstrated in Figure 1.10, a local buckling or collapse of the chord wall close to the branch intersection characterizes the compressive failure of a T-joint. The compressive loading generally governs the design as the value of compressive load is less than that of the tensile load.

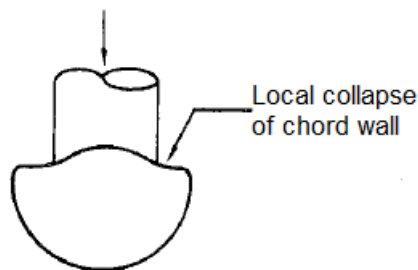


Figure 1.10: Local collapse of chord wall (R. P. Pan *et al.*, 1977)

1.1.3.Types of Stiffening Mechanisms:

Various stiffening mechanisms were used to strengthen the brace chord tubular

connections in offshore structures. The stiffening mechanisms are as follows:

- Gusset plates
- External ring stiffeners
- Overlap braces
- Internal ring stiffeners
- Joint can
- Doubler / collar plates
- Fiber Reinforced polymer

1. **Gusset plates:** Gusset plates (Figure 1.11) were first tried as a stiffening mechanism in offshore structures. These were welded in between the brace ends and the chords during late 1950s and early 1960s (W.J. Craff, 1981). Sometimes pass-through gusset plates were used (G. Raghava *et al.*, 1989). In or around 1965, it was discovered that gusset plates created unfavourable stress concentrations that reduced the joint's ability to withstand fatigue.

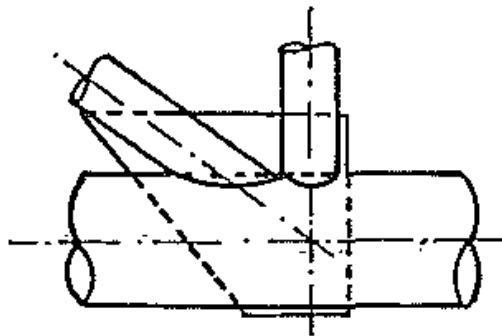


Figure 1.11: Pass- through Gusset Plate (G. Raghava *et al.*, 1989)

2. **External ring stiffeners:** Owing to the disadvantages of gusset plates, the industry trend was toward reinforcing joints with external ring stiffeners (Figure 1.12). Although this is the simplest method of local stiffening, it encourages additional wave forces (Shiyerkar *et al.*, 1983).

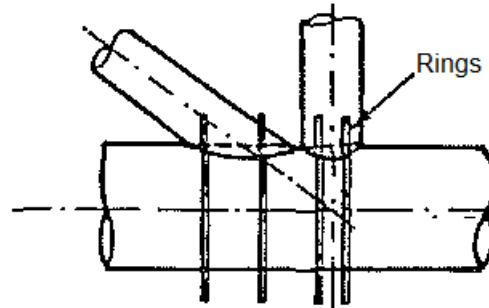


Figure 1.12. External ring stiffeners (G. Raghava *et al.*, 1989)

3. **Overlap braces:** During the early 1960s it became common practice to use overlap braces (Figure 1.13) in order to transmit part of the load directly from one brace to another.

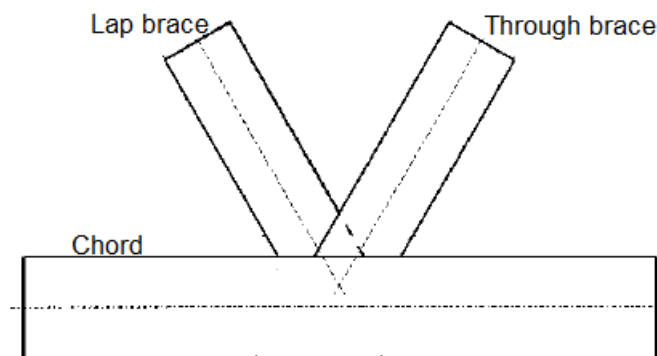


Figure 1.13: Overlap K-joint geometry (E. M. Dexter and M. M. K. Lee, 1999)

4. **Internal ring stiffeners:** Early in the 1970s, platforms in the North Sea were constructed with substantially larger jacket legs, leading to the employment of internal ring stiffeners (Figure 1.14) (Craff, 1981). The benefits of internal ring stiffeners include a longer fatigue life and a decreased susceptibility to corrosive attack (G.Raghava *et al.*, 1989). This has the drawback of lowering the chord's interior clear diameter (Shiyerkar *et al.*, 1983). The chord should be stiffened with three internal rings (ideally), one in the centre and the other two at the branch faces. This is the most efficient approach to strengthen a tubular joint. Compared to an equal joint Can, a ring-stiffened joint more effectively minimizes the stress concentration.

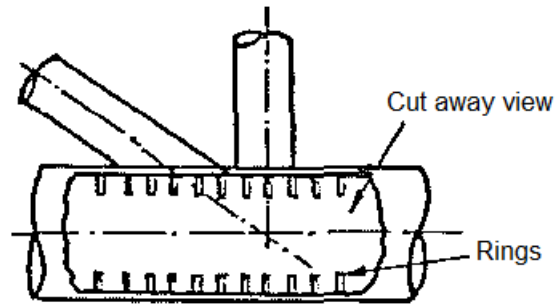


Figure 1.14: Internal ring stiffeners for large diameter chords (G. Raghava *et al.*, 1989)

5. **Joint can:** API suggested making the chord sections around the intersection of the tubular joints thicker in order to strengthen them. The term "joint can" (Figure 1.15) refers to this short chord (API, 2014).

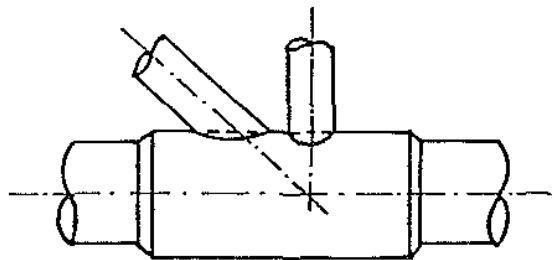


Figure 1.15: Thickening of chord wall near the connection (G. Raghava *et al.*, 1989)

6. **Doubler/ Collar plates**

Y. S. Choo *et al.* (2005) discovered that the doubler plate (Figure 1.16) and collar forms (Figure 1.17) of reinforcement are both effective at distributing the axial stress of the brace across a greater area of the chord, resulting in a strengthening effect.

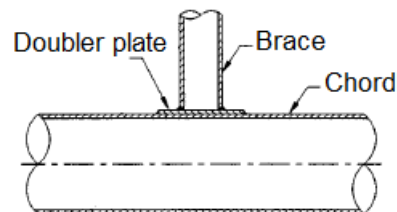


Figure 1.16: T-joints with reinforced doubler plates (Y. S. Choo *et al.*, 2005)

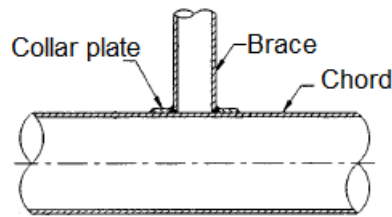


Figure 1.17: T-joints with reinforced Collar plates (Y. S. Choo *et al.*, 2005)

7. Fiber Reinforced Polymer (FRP)

Lesani et al. (2014) looked at how stiffeners made of fibre-reinforced polymer affected the ultimate capacity of tubular joints that were subjected to axial loading. When compared to an unstiffened joint, it was shown that fibre reinforced polymer joints (Figure 1.18) significantly increased ultimate strength.

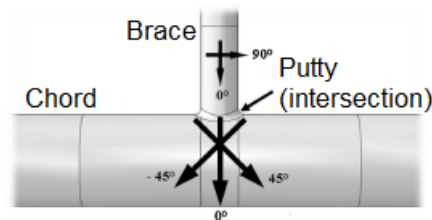


Figure 1.18: FRP stiffened T-Joint (M. Lesani *et al.*, 2014)

1.1.4. Material used for present work:

SS 304 is chosen for their wide spread applications in offshore industry and ease of procurement. Stainless steel alloys are grouped according to the structure of their crystals. Adding nickel creates the structure used in marine applications, called austenitic. Austenitic stainless steels are identified by their 300-series designation. Most of the stainless produced today is type 304, a low-carbon variation which is also called 18-8, because it's made of 18% chromium and 8% nickel. Type 304 has good resistance to corrosion by a great number of chemicals. Consequently, it satisfies a broad demand for adequate performance at an affordable price. Table 1.1 lists the elements, composition and mechanical properties of SS304 alloy.

Table 1.1. Chemical composition of SS304 alloy

Element	% Composition
Carbon	0.08 max
Manganese	2 max
Phosphorus	0.045 max
Sulphur	0.03 max
Silicon	1 max
Nickel	08-11
Chromium	18-20
Molybdenum	0
Tensile Strength (Mpa)	505
Yield Strength (Mpa)	205
Poisson ratio	0.296
Density (kg/m ³)	7800
Hardness (Rockwell)	70

This chapter gives the motivation behind the chosen work, a detailed literature review and a review of different stiffener configurations. Finally, it provides the objectives of work and an overview of the consecutive research chapters.

1.2 MOTIVATION

Oil and Natural Gas Corporation (ONGC) has planned to requalify the fixed, jacket type-platforms installed during 1970s to avoid decommissioning and to extend the use of these structures. More than 265 platforms were subject to structural testing as part of the project, the majority of which had reached the end of their 25-year design life. The primary focus of the project involves the identification of platforms functioning beyond their service life, providing stiffening measures and strengthening measures to 90% of the platforms and recertification of platforms to ensure implementation of industrial safety requirements. Offshore Structural Analysis and Computer System (SACS) was used for structural analysis of platform life extension/requalification. Studies conducted during the analysis include dent modeling, member strengthening, joint component strengthening and additional pile modeling. (Offshore Oil and Gas magazine, Volume 77, Issue 4, 2017).

1.3 STRUCTURE OF THE THESIS

In **Chapter 1**, an introduction to the tubular T joint is discussed. This chapter explains the different configurations of tubular joints, failure modes of T joints under axial load, various types of stiffening mechanisms, and the motivation for the present study.

In **Chapter 2**, a review on literature is made of available stiffening mechanisms focusing on its experimental and numerical study. The ring stiffeners, Doubler/Collar plates and Fiber reinforced polymers are discussed in detail. Finally, it provides the research gap and objectives for this study.

In **Chapter 3**, discussion on a preliminary experimental study to understand the behavior of T joint at the outset is done. For major experimental study, it discusses the details about experimental setup, support facilities, and instrumentation.

Chapter 4 describes the finite element analysis of unstiffened and stiffened tubular T-joints under axial compressive force. It covers boundary conditions, meshing, and geometric modelling.

Chapter 5 describes the results of experimental and numerical studies of the reinforced and unreinforced tubular T-joints in tubing that are compressed axially. The deformation and ovalization, failure patterns, the effect of stiffening mechanisms on the static strength and stiffness of the joint are discussed.

In **Chapter 6**, the conclusions are drawn from this study; limitations of the present study and scope for future work are presented followed by references and publications.

CHAPTER 2

LITERATURE REVIEW

2.1 Introduction

Existing literature on various joint configurations used in the design of offshore jacket structures was studied with a specific focus on ultimate capacity of the joint, joint behaviour and failure mechanisms of unreinforced and reinforced joint configurations. The reinforcement methods improve the ultimate strength and thereby, enhance the load bearing capacity of the joint.

2.2 Reviews on Ring stiffeners

Older platforms had a typical practice of providing reinforcement in the form of rings welded to the can region of the joint for large diameter chord members in offshore jacket structures. Worldwide, many joints with internal ring stiffeners are still in use (Wimpey offshore, 1991). On T-joints stiffened with an internal ring stiffener, static tests and fatigue testing were carried out by Y. Sawada et al. in 1979. For the experimental study, a total of nine specimens (two unstiffened joints and seven stiffened joints) with rings stiffeners of various widths, wall thicknesses, and materials were utilized. A single internal ring was included to strengthen the junction (Figure 2.1). They observed that the deformation at low load levels indicate the joint deformation can be significantly reduced by stiffening. The estimated value of ultimate static strength of unstiffened and stiffened T-joints have good agreement with the equation (1) given by API. The load deformation curve for stiffened and unstiffened joints is shown in Figure 2.2. The ultimate strength of the joint increased by 50 % - 150 % due to the stiffening.

$$p_u = \pi dT \frac{\sigma_y}{0.5\gamma^{0.7}}; \quad \text{where } \gamma = D/2T \dots\dots (1)$$

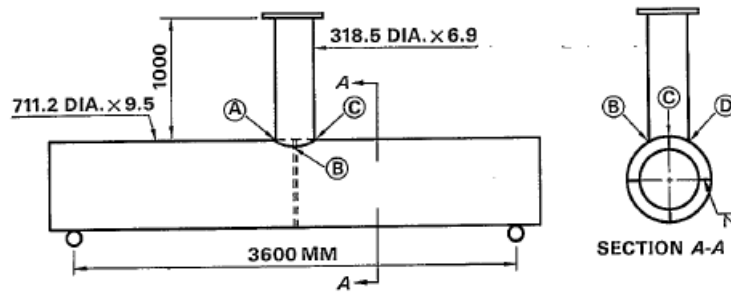


Figure 2.1: Configuration of the stiffened specimen used in static tests
(Y. Sawada *et al.*, 1979)

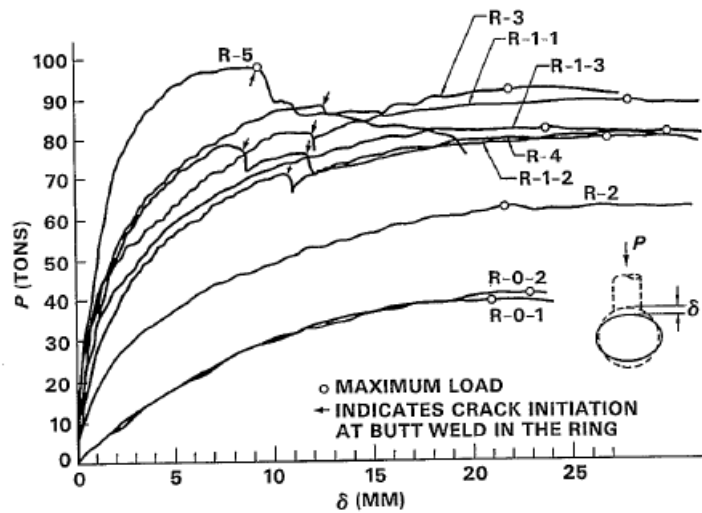


Figure 2.2: Load-Deformation curves of the stiffened and unstiffened T-joint
(Y. Sawada *et al.*, 1979)

An experimental and computational investigation on the impact of internal ring stiffeners for welded tubular T-joints in traditional jacket type offshore constructions was undertaken by M. R. Shiyekar *et al.* in 1983. For the purpose of an experimental study, four tubular joint models were created. They noticed that the three-ring configuration strengthened the joint in a practical sense. When there are three rings, the axial load transfer from the branch to the chord becomes more uniform, and adding more rings has not boosted the joint's strength.

An analytical and experimental investigation on the behaviour of an unstiffened and a stiffened steel tube welded T-joint under axial brace loading was undertaken by G. Raghava et al. in 1989 (Figure 2.3). The internal chord perimeter of the chord had three rectangular-shaped ring stiffeners that stiffened the joint. Failure occurs as a result of the plug being punched into or pulled out from the side of the chord in the case of unstiffened joints with d/D less than 0.3. The chord collapses when the d/D number is greater than 0.8. The chord tube flattened out at the intersection during failure in the case of the intermediate value of $d/D=0.67$. Failure was sudden and mostly caused by the tubular structure collapsing. Failure of stiffened joint was gradual due to simultaneous local buckling of the chord and the brace adjacent to the intersection. The equation (2) given by Y. Sawada *et al.* (1979) was used to calculate ultimate strength of the joint. They observed that the ultimate load increased from 53.75 t for the unstiffened joint to 89.50 t for the stiffened joint (67 % increase in ultimate strength).

$$P_u = \frac{7.3F_y T^2}{(1-0.833\beta)} + \frac{2hT_s F_y'}{\sqrt{3}} \quad \text{for } 15 \leq D/T \leq 100 \text{ and } 0.2 \leq \beta \leq 1.0 \dots\dots\dots (2)$$

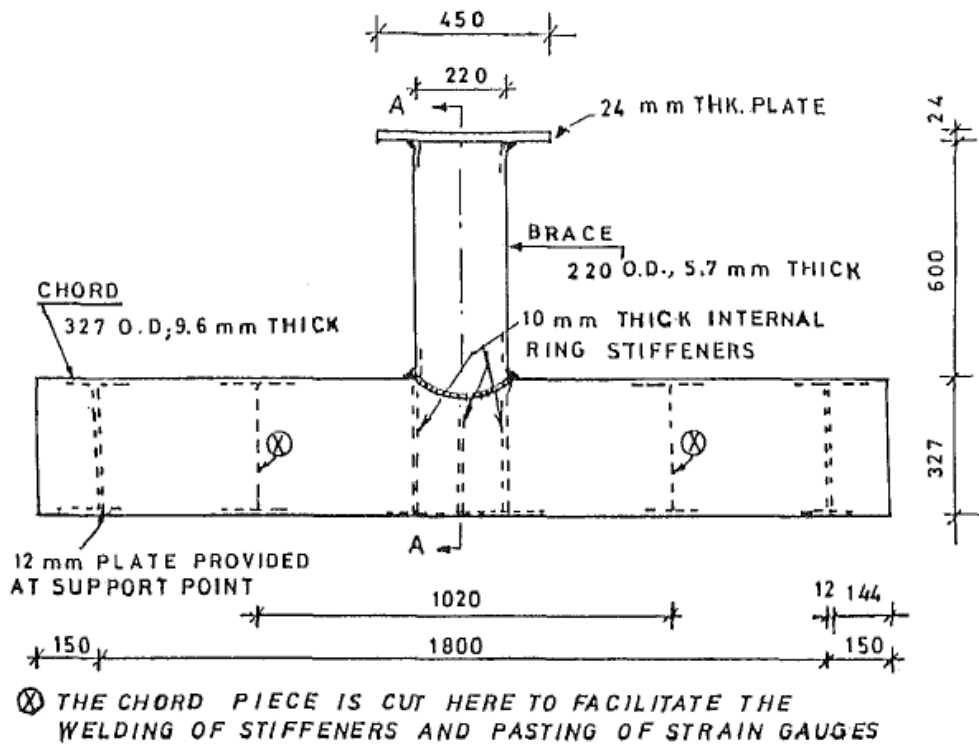


Figure 2.3: Ring stiffened T-joint (G.Raghava *et al.*, 1989)

Static tests were carried out by D. S. Ramachandra Murthy et al. (1992) to examine the impact of stiffening tubular T and Y joints that were exposed to compressive loading, in-plane moment, and out-of-plane moment. The preparation of eleven specimens for experimental investigation. All of the specimens had a chord that was 324 mm in diameter and 12 mm thick. All of the specimens' braces were 219 mm in diameter and 8.18 mm thick, with the exception of one, whose brace was 324 mm in diameter and 10.31 mm thick. The chord and bracing for the Y joint formed a 60° angle. They noticed that an unstiffened joint lost rigidity at failure stress, whereas a stiffened joint remained intact and may retain some strength. The ultimate strength of stiffened T and Y-joints are increased by 66.6 % and 73 % respectively.

Using internal ring-stiffeners to stiffen tubular T and Y joints (Figures 2.4 and 2.5) that were being compressed by an axial brace, T. S. Thandavamoorthy (2000) conducted experimental and numerical studies on the issue. There was an experimental investigation done with four samples. The most common cause of failure of an internally ring strengthened joint was chord bending. The local bending and ovalization of the chord wall near the welded intersection were removed by three annular ring stiffeners that were welded inside the chord. The joint's behaviour changed from punching shear to bending deflection as a result of the stiffener arrangement. To evaluate the strength of T and Y-joints strengthened with internal rings, they created a linear analytical model. The ultimate strength of unstiffened joint was calculated based on equation (3) suggested by Yamasaki *et al.* (1979). The strength of internal ring stiffened joints were found to be almost twice that of similar unstiffened joints. The values are $T_{\text{stiffened}} = 1887.60 \text{ kN}$, $T_{\text{unstiffened}} = 985.60 \text{ kN}$, $Y_{\text{stiffened}} = 1834.00 \text{ kN}$, $Y_{\text{unstiffened}} = 996.20 \text{ kN}$.

$$P_u = \frac{4.5}{K \sin^{1.5} \theta} \sigma_y \quad \text{where } K = 0.62 D_0^{0.70} t^{-1.6} .d^{-1.1} \dots\dots\dots (3)$$

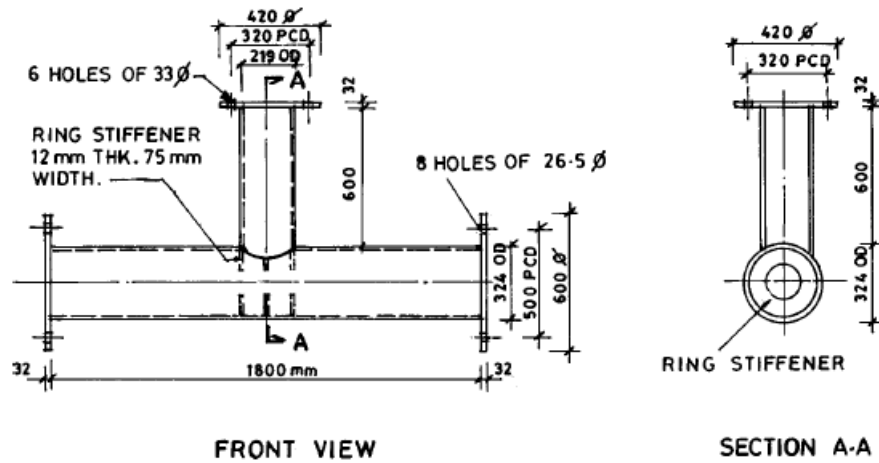


Figure 2.4: Typical undamaged stiffened T-joint (T. S. Thandavamoorthy, 2000)

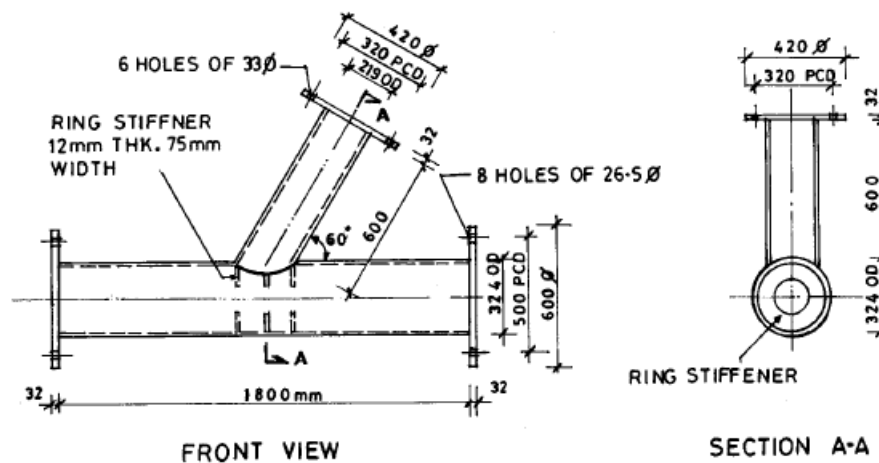


Figure 2.5: Typical undamaged stiffened Y-joint (T. S. Thandavamoorthy, 2000)

Numerous numerical tests on tube joints strengthened with internal ring stiffeners were conducted by Lee et al. (1999 and 2005). The numerical analysis has examined a database of 40 stiffened joints. Since stiffened joints attain their maximal strengths at roughly the same deformation level as their unstiffened counterparts, they found that internal ring stiffeners have no effect on the ductility of tube joints. Instead of failing by shear yielding, stiffeners failed via the creation of plastic hinges from bending. The strength improvement that is produced by the stiffeners is significantly influenced by the joint parameters chord to brace diameter ratio and chord radius to thickness ratio. Stiffeners can boost joint strength by at least 50% and as much as 140% when $d/D=0.33$. They discovered that the T-shape stiffener's flange contributes to the stiffener's

strength, but that the influence of the thickness is more than that of the breadth. Positioned stiffeners at the saddle position increase strength more effectively than those at the crown positions.

Experimental research on the static strength of tubular T-joints strengthened with external stiffening rings was conducted by Zhu et al. in 2016. Six specimens were evaluated to ascertain their compressive load capacity: three unreinforced and three reinforced joints with ratios of brace to chord diameter of 0.26, 0.51, and 0.74, respectively. They discovered that the external stiffening ring significantly improved the compressive strength of the joint (Figure 2.6), and that the ultimate load capacity could be determined using the plastic bending moment at the crown point. When the chords were subjected to the compressive loading of the brace, the reinforced joints demonstrated almost little ovalization and behaved like a beam.

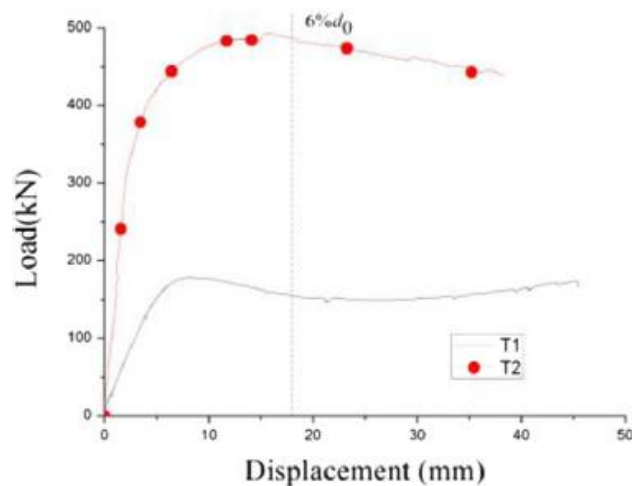


Figure 2.6: Load-deformation curves for T-joints with external stiffeners
(Zhu *et al.*, 2016)

2.3 Reviews on Doubler/Collar Plates

The codes ISO (1999), API (2000), DNV (2000) suggested that strengthening a circular hollow section (CHS) joint by using a joint can in offshore industry is a usual practice, in which a thicker chord wall is provided near the brace-chord intersection. This is an effective method to improve the structural strength of the joint. However, there are occasions where joint reinforcement is required subsequent to fabrication, whereby the joint is found to be lacking in strength. For these cases, a possible solution is suggested

by Y. S. Choo et al. (2004) wherein the profiled parts of steel plates termed collar plates are attached externally to the joint. The collar plate reinforcement scheme may be adopted for repairing joints in old platform structures.

A computational analysis and an experimental test were both carried out on T-joints reinforced with doubler plate by Fung et al. (1999). Axial compression, axial tension, in-plane bending, and out-of-plane bending were all successfully resisted by the doubler plate, the researchers discovered. They noticed that the usage of the doubler plate had greatly raised the maximum capacities for axial compression, axial tension, in-plane bending, and out-of-plane bending by 65%, 35%, 55%, and 66%, respectively.

Y. S. Choo et al. (2005) and van der vegte et al. (2005) conducted four experimental and numerical studies on T-joints strengthened with collar plates under brace compression and tension. They stated that collar plate reinforcing can result in a significant increase in strength. T-joints strengthened with doubler plates and subjected to brace compression and tension stresses were the topic of various experimental and numerical tests by Y. S. Choo et al. (2005) and van der vegte et al. (2005). They showed that the ultimate strength of a doubler plate reinforced T-joint can be up to 220% higher than that of an unreinforced joint when subjected to brace compression.

Fenq Qi and tan Jia-hua (2005) studied the static strength of doubler plate reinforced Y-joints subjected to compression loading using finite element analysis. They observed that doubler plate had significantly increased the ultimate capacity more than 200% for axial compression. The geometric parameters, brace to chord diameter ratio and doubler plate to chord wall thickness ratio have great influence on the ultimate strength of reinforced joints with doubler plate. The combination of higher plate length and thickness greatly enhanced the ultimate strength of joints.

According to J. X. Liang et al. (2003), the penetration weld between the brace and chord allows both the compressive and tensile brace loads to be transferred to the chord for an unreinforced X-joint during out-of-plane bending. A significant amount of the compressive load is conveyed for joints reinforced with doubler plates through contact interaction between the doubler plate and the chord outer surface. On the tensile side, contact interaction has little effect, and brace load is transferred through the penetration weld between the brace and the plate, and the fillet welds between the plate and the chord. The increment in plate thickness is effective to obtain more strength

enhancement for joints reinforced with longer doubler plates, whereas the effect of plate thickness is less important for joints reinforced with shorter doubler plates.

J. X. Liang et al. (2003) reported the results for doubler plate reinforced X-joints under out-of-plane bending. They observed that the ultimate strength of a CHS X-joint reinforced with appropriately proportioned doubler plates can be up to 290% to its unreinforced counterpart. The geometric parameters chord diameter-to-thickness ratio, brace-to-chord diameter ratio did not show any significant effects on strength ratio. The plate thickness plays an important role in the joints reinforced with longer doubler plate.

The findings of an experimental investigation to examine the static strength of T-joints in circular hollow sections (CHS), reinforced with a doubler plate or collar plate, and subjected to brace axial compression or tension were presented by Y.S. Choo et al. in 2004. Twelve specimens, made up of four joints in each configuration—unreinforced, doubler, and collar plate reinforced joints—and each with a different geometric ratio—were tested until failure. It was noticed that the chord around the reinforcement's perimeter plastified when a brace under compression failed. The chord cross section buckles in an inelastic manner in the case of joints under tension with $d/D=0.54$ and considerable plastification around the chord-brace junction area. Chord plastification developed throughout the loading period for the joint under tension with $d/D=0.28$ whereas brittle fracture around the brace diameter indicated the completion of the tests. Strength increase was up to 39% for brace compression and 16% for brace tension for specimens with diameter ratio $d/D=0.54$, while it was 53% for brace compression and 28% for brace tension for specimens with $d/D=0.28$. The results of the experiment were utilized to confirm those of the finite element analysis, and after that, a comprehensive numerical parametric study was carried out to look at how plate sizes and thicknesses affected the ultimate strength of reinforced joints.

The findings of a comprehensive parametric study to examine the static strength of doubler plate reinforced X-joints in circular hollow sections that were reinforced with a doubler plate or collar plate and subjected to an in-plane bending (IPB) moment were published by Y. S. Choo et al. (2004). 120 doubler plate joints and 8 unreinforced joints altogether were examined. Investigations on the load-transfer mechanisms and failure modes of doubler plate reinforced joints as well as assessments of the effects of key geometrical parameters on the joints' ultimate strength were conducted.

Establishing and evaluating empirical relations for the ultimate strength of doubler plate reinforced X-joints subjected to in-plane bending

The doubler/collar plate reinforced CHS X-joints subjected to in-plane bending pressure were studied by Y. S. Choo et al. in 2004. It was observed that the strength of a collar plate reinforced joint can be up to 280% stronger than an unreinforced joint, and that the strength of doubler plate reinforced joints can be up to 240% stronger. Collar plate reinforcement was shown to be more effective than doubler plate reinforcement in increasing the strength of CHS X-joints exposed to in-plane bending when these two plate reinforcements were compared. The strength of reinforced joints is significantly influenced by the ratios of doubler and collar plates' plate-to-chord thickness and plate-length-to-chord diameter. While the collar plate reinforced junction failed with a rather wide plastic zone close to the intersection of the brace chords, the doubler plate reinforced joint failed with plastic hinges in the chord wall or in the doubler plate. The collar plate thickness parameter has a greater impact than the doubler plate thickness parameter, according to the strength ratio function (ratio between ultimate moment of collar plate reinforced joint under in-plane bending and ultimate moment of unreinforced joint under in-plane bending). This is because the collar plate is more integrated to the chord wall through the additional welds.

Results of doubler plate reinforced tubular T-joints and Y-joints subjected to brace compression, tension, and in-plane bending were presented by Hossein Nassiraei et al. in 2016 and 2017. To investigate the impact of joint geometry and doubler plate size on the ultimate strength, initial stiffness, strength ratios, and failure mechanisms of doubler plate reinforced T-joints and Y-joints, 210 finite element models, verified against the data available from eight experimental specimens, were generated. Under brace compression and in-plane load, the ultimate strength of doubler plate reinforced T-joints and Y-joints can reach 295% to 330% of the capacity of the corresponding un-strengthened joint. The maximum strength of the joints was also increased by 168% when a doubler plate was put under tension.

According to Hossein Nassiraei et al. (2017), the collar plate increases the chord thickness, brace thickness, and brace diameter at the junction of the chord and brace, hence strengthening the joint by increasing the thickness of the joint in the critical

location. One of the best ways to raise the static capacity of tubular connections is collar plate reinforcement.

The findings of an experimental and computational research of the static capacity in collar plate strengthened X-joints under axially compressive pressures were presented in Hossein Nassiraei et al. (2017). Three joints without reinforcement and three joints with collar plate reinforcement underwent analysis. In comparison to the comparable deformation of unreinforced joints, the deformation of reinforced joints in the vicinity of joint intersection is more uniform. The tubular X-joints' axial compressive load strength can be increased by the collar plate by 55%, 57%, and 66%, respectively, for small, middle, and large values of d/D . For all types of joints, the brace chord interaction is where the maximum displacement position is found.

2. 4 Reviews on Fiber Reinforced Polymers (FRP)

In recent years, researchers have begun to comprehend how fibre reinforced polymers (FRP) affect the behaviour of tubular joints and their ultimate carrying capacity. The experimental and numerical examination of FRP-strengthened tubular T-joints subjected to axial compressive loads was done by M.Lesani et al. in 2013 and 2014. Due to the combined action of steel and composite against the compressive stress, the numerical modelling results showed that the influence of FRP wrap in joint resulted in an increase of ultimate strength capacity from 22% to 68%. Additionally, the state of stresses, deformations, and ovalization all improved, indicating an improvement in joint behaviour as a whole. Local bending of the chord member, punched shear from ovalization, and plastic failure of the chord were all prevented by the FRP-strengthened joints. FRP reinforcement in the critical locations of the tubular joint in the crown line direction reduces the stresses and deflections and also beneficial in hoop line direction. FRP plies could bear at least 50% of the joint's maximum load without showing any signs of failure. The saddle point and the nearby-ovalized section of the chord shell were the crucial areas of the plies. It was found that the composite plays a significant role in supporting the steel during the loading regime based on the failure modes of composite plies. Before the maximum load level, no evident failure or delamination was noticed. In addition, increasing the number of layers would increase the potential of ply failure in low loads. The numerical model assuming a perfect binding condition

between the FRP and steel was validated up to the ultimate load threshold due to the good agreement between experimental and computational data.

Y. Fu *et al.* (2016) examined the static performance of carbon fibre reinforced polymer (CFRP) composite-reinforced CHS gap K-joints experimentally and numerically and provided an equation for evaluating the impact of factors on the static capacity.

Alireza Sadat Hosseini *et al.* (2017) performed the finite element analysis using ABAQUS software package to study stress concentration factors of FRP reinforced tubular T-joint subjected to in-plane bending and out of-plane bending moments. The strengthening was done on chord, brace, and combined chord & brace to study the strengthening effects.

Z. Li, X. Jiang & G. Lodewijks (2017) reviewed the latest reinforcement techniques used in tubular joints to enhance the load bearing capacity and ultimate strength of the joints. The latest FRP reinforcement technique showed advantages due to its excellent mechanical and physical characteristics when compared with traditional reinforcement methods. Further investigations need to be carried out to clearly understand the FRP- reinforcement mechanism, in order to improve the understanding of Carbon Fiber reinforced Polymer (CFRP) reinforcement method and increase its applications in the real scenario.

2.5 RESEARCH GAPS

- From the literature review, it can be seen that researchers have done extensive experimental and numerical study to understand the structural behaviour of joints of various configurations under different loading schemes applied to stiffened and unstiffened joints.
- The research work on the stiffening with various configurations is limited. It can be further extended considering various configurations of joints under different loading schemes.

2.6 OBJECTIVES OF RESEARCH WORK

The objectives of the study are as follows:

- To carry out Finite element analysis of joint configurations with proposed stiffeners subjected to axial compressive load.
- To conduct experiments using the experimental rig and fixtures for the *SS304* stiffened joint configurations subjected to various loading conditions to investigate the ultimate strength of the joint configurations and failure mechanisms.

CHAPTER 3

EXPERIMENTAL STUDY

3.1. Introduction

This chapter deals with material details, specimen preparation, instrumentation, fixture set up preparation, and testing of the tubular T joint specimens. Here a preliminary experimental study is carried out to understand the behaviour of unstiffened T-joints initially. Then major experimental study is done to study the effect of reinforcements on the strength and failure mechanism of the joint.

3.2. Material Composition

The behaviour of tubular T-joint under axial compressive load is studied by using an experimental setup. The tubular T joint model is having dimensions (based on API RP 2A) of chord length = 494 mm, chord diameter = 141 mm, chord thickness = 5 mm, and brace length = 237 mm, brace diameter = 90 mm, brace thickness = 4.5 mm and the corresponding dimensionless parameters are Brace to chord diameter ratio ($\text{Beta} = d/D$) = 0.64, Chord wall slenderness ratio ($\text{gamma} = D/2T$) = 14.1, and Brace to Chord wall thickness ratio ($\text{tau} = t/T$) = 0.9. In total, three specimens are prepared for the experimental study to understand the behaviour of tubular T-joints and their failure mechanisms.

To know the composition of the material used for T-joint specimen, a small piece of specimen is taken from the tubular pipes and cleaned to identify the location to carry out the spectrometric analysis. The figures 3.1 and 3.2 show the specimens before and after the spectrometric analysis.



Figure 3.1: Specimen for Spectrometric analysis of material



Figure 3.2: Tested specimen for Spectrometric analysis of material

From the spectrometric analysis, the composition of the material is identified. The various elements compose the material is given in the table 3.1. The standard followed for spectrometric analysis is ASTM E-415 and the material is mild steel. The chemical analysis by using spectrometric analysis test method is done at GWASF Quality Castings (P) Ltd.

Table 3.1. Spectrometric analysis of material

Element %	C	Mn	Si	S	P	Cr	Ni	Mo	Cu	V	W	Nb	Co	Fe
1	0.18	0.99	0.052	0.013	0.017	0.010	0.005	0.001	0.009	0.002	0.003	0.002	0.003	98.71
2	0.078	0.47	0.15	0.017	0.024	0.006	0.004	0.001	0.008	0.001	0.002	0.001	0.002	99.23

3.3. Model Preparation:

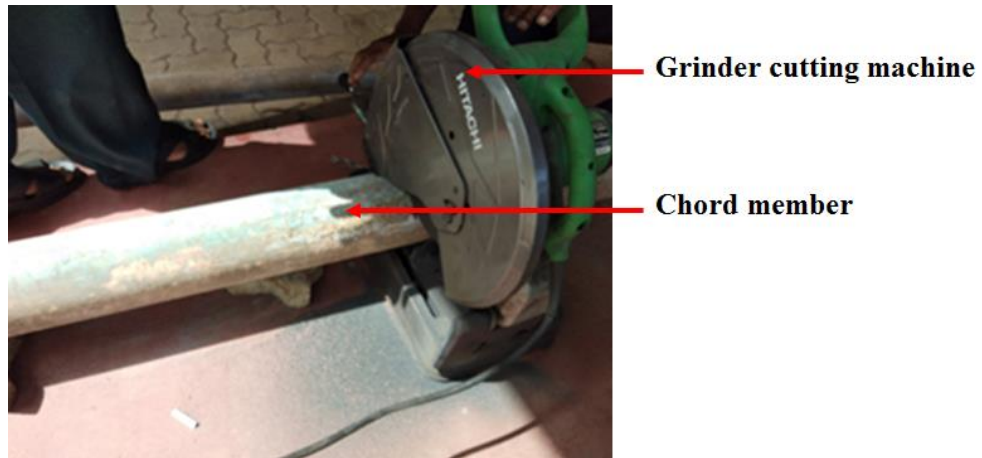


Figure 3.3: Pipe cutting using grinder cutting machine

The specimens as per the dimensions are prepared for the present study. Initially, the raw long pipe was cut into the specimens by using a grinder-cutting machine as shown in Figure 3.3.



Figure 3.4: Chord and brace members

The cutting machine is an industrial power tool that uses an abrasive wheel for cutting the material. The pipes are held tightly by using a clamp mechanism at the grinding machine, and then the cutting process is done. The chord and brace members prepared after the cutting process are displayed in Figure 3.4.

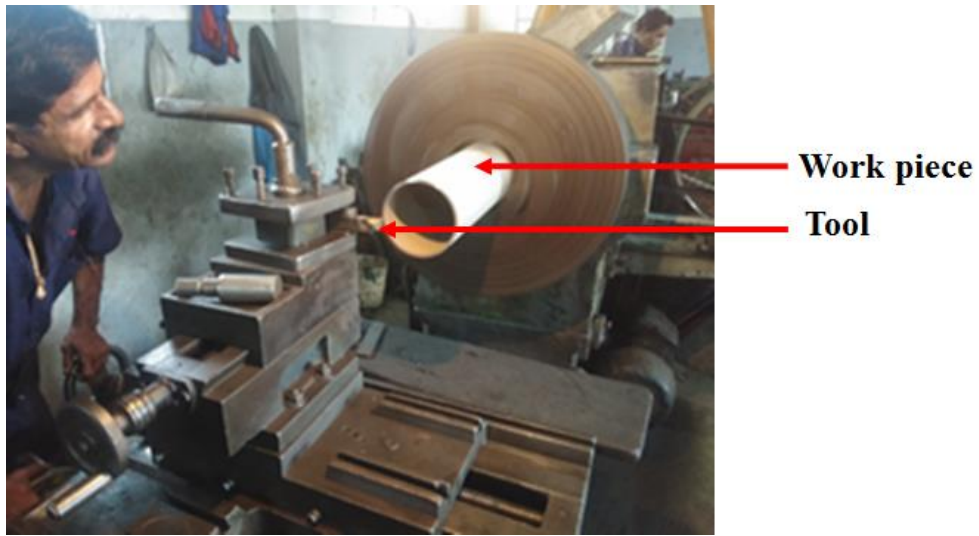


Figure 3.5: Edge preparation

The edge of these members is non-uniform. The non-uniformity of members' edges is made uniform by means of facing operation in the lathe. In this process, work piece (specimen) is placed on the machine; a cutting tool is pressed against it at the end (Figure 3.5).

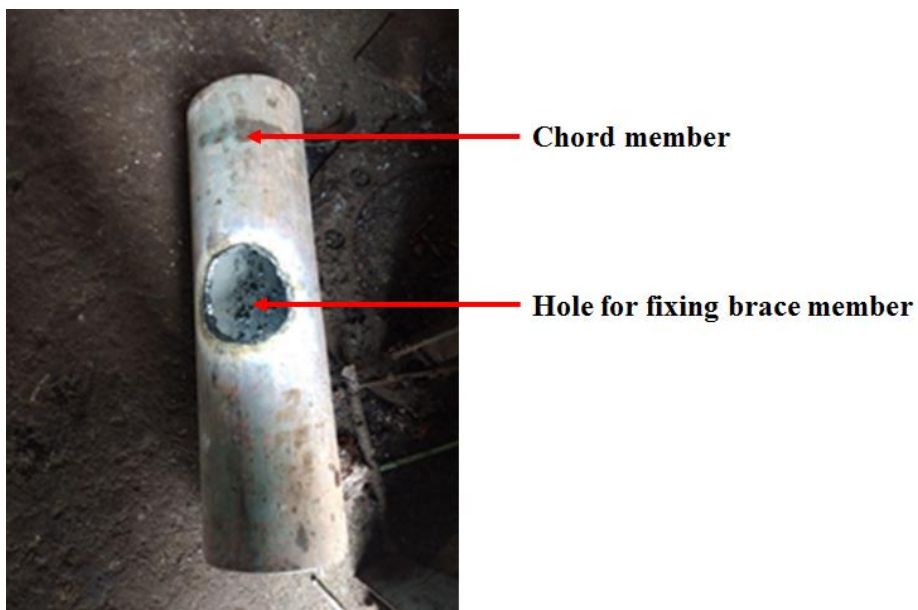


Figure 3.6: Hole preparation for joining brace member

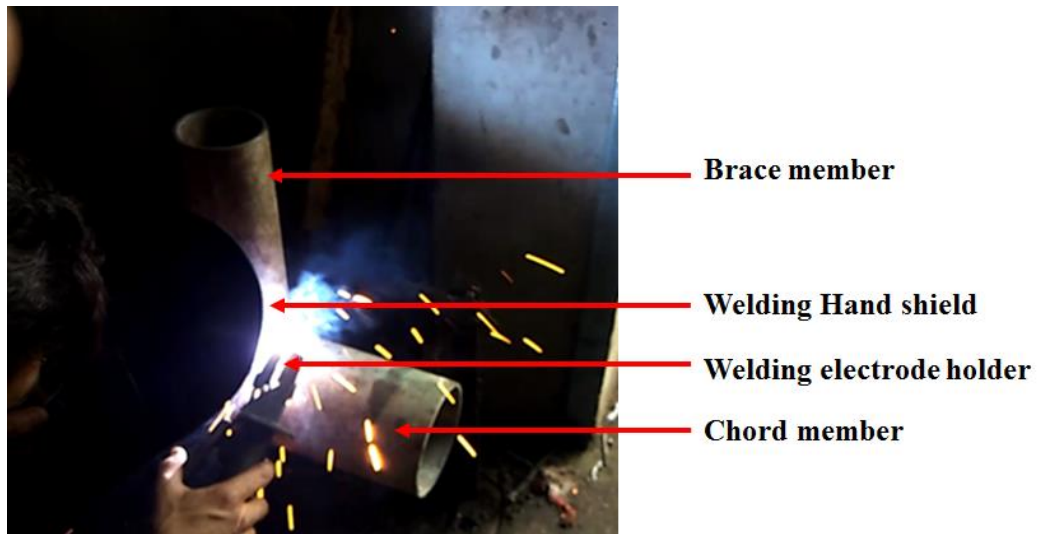


Figure 3.7: Welding of chord and brace member

The material removal is done by the rotation of cutting tool over the work piece. To join the brace member with the chord member a circular hole with a diameter of 9 cm is made on the chord member by gas cutting process depicted in Figure 3.6. Then the members are connected through the welding process (Figure 3.7) and yield in the final tubular T-joint specimen Figure 3.8.



Figure 3.8: Tubular T-joint model

3.4. Experimental details:

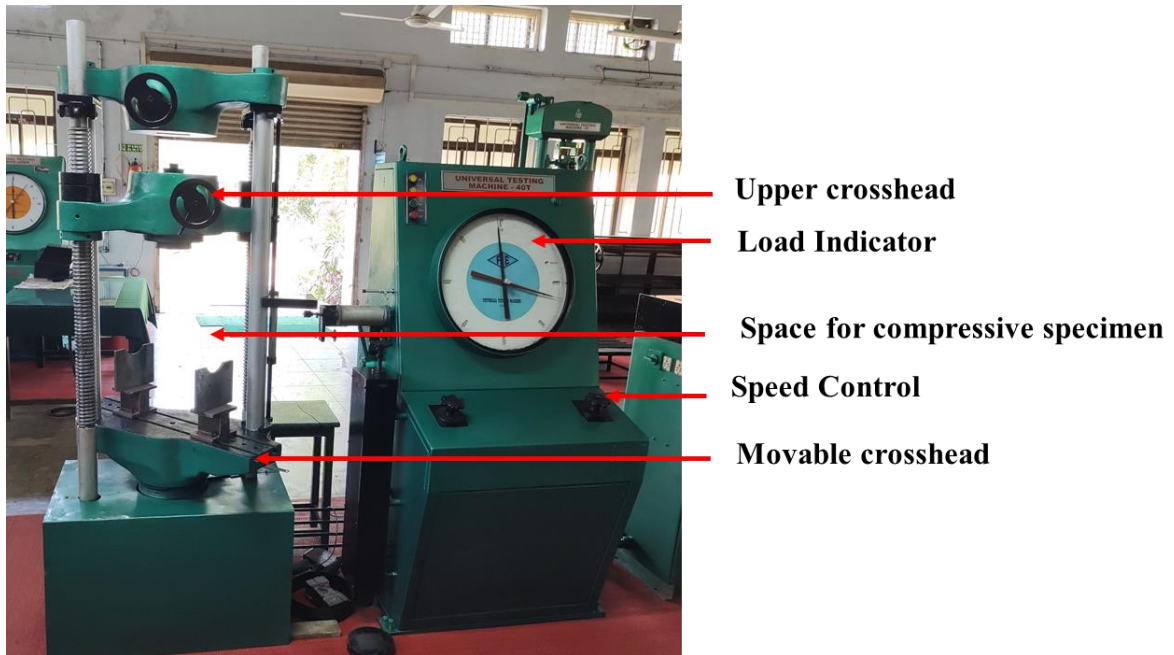


Figure 3.9: Experimental setup

The experimental setup used for the present study is shown in Figure 3.9. The dial gauges are placed to measure the chord ovalization of the tubular joint. The specimen is simply supported at the chord ends by means of saddle supports.

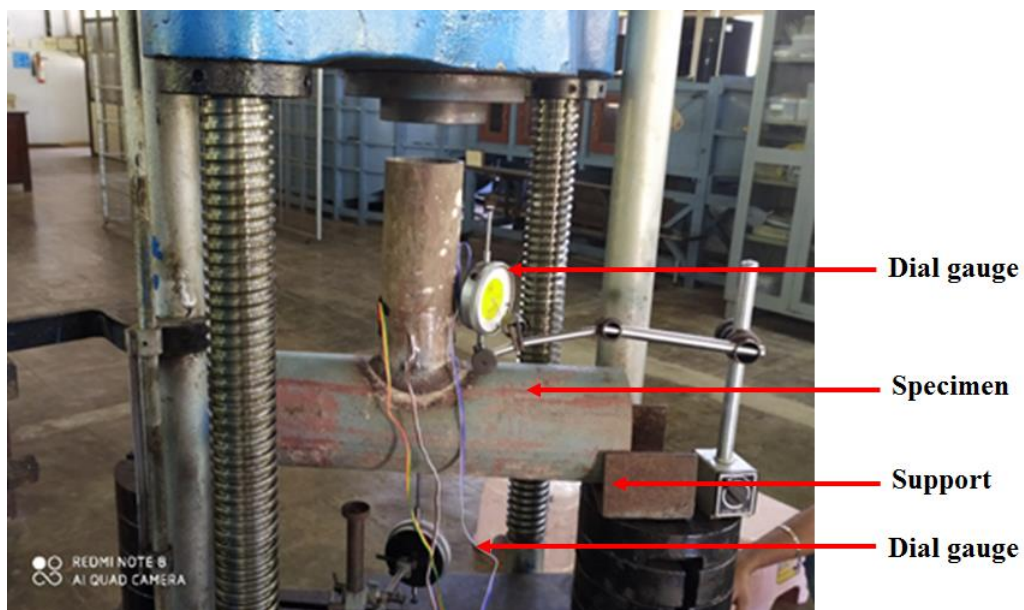


Figure 3.10: Experimental setup with dial gauges

For each specimen, the instrumentation consists of dial gauges to measure displacements at the chosen locations and strain gauges wrapped around the brace member to measure the strain distributions at the hot spots (Figure 3.10). The 40T load-controlled actuator is used. Each test involves applying a starting brace load of 0 kg (0 N) and gradually increasing it by 50 kg (490 N) increments until the specimen fails.

3.5. Major Study: T-joint model Details

The schematic arrangement of the T-joint specimen and the corresponding variables are shown in Figure 3.11.

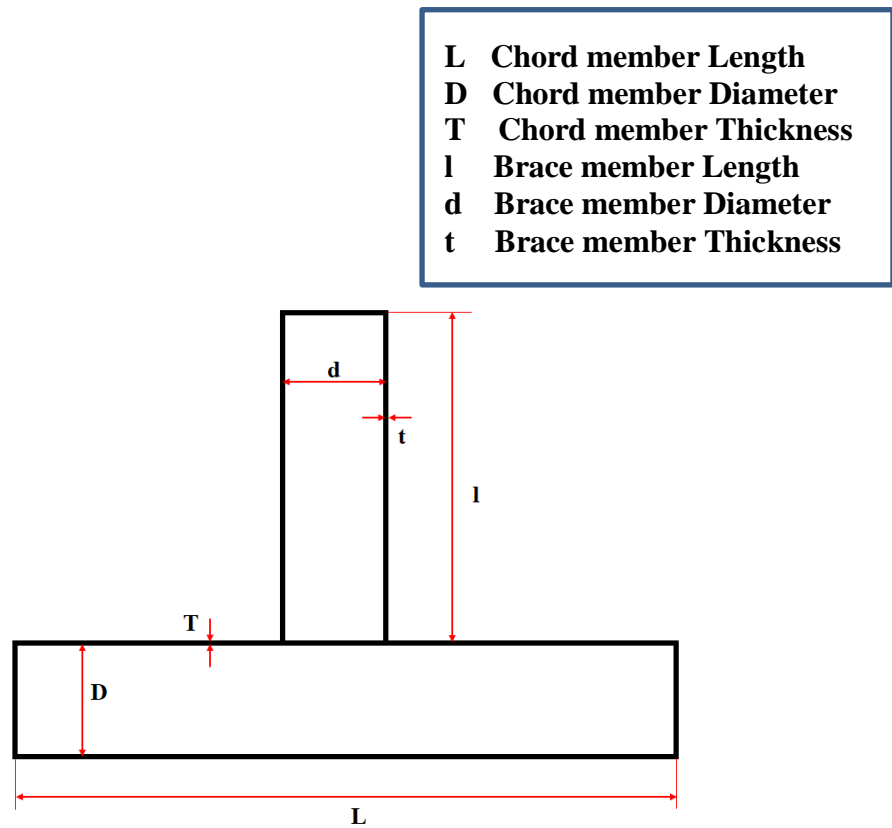


Figure 3.11: Schematic arrangement of T joint specimen

The experimental study involves twelve experiments and is summarized in Table 3.2. The experimental program consists of four sets, and axial compressive load is considered for all cases. Three cases of Model 1's unstiffened or unreinforced joints are shown in Table 3.2 and are used as a reference. Additionally, three specimens are

strengthened with can-rings—four strips, another three specimens are reinforced with Can-rings-6 strips, and the remaining three specimens are reinforced with Can-rings-8 strips. The brace and chord member of T-joints are made from SS 304 material which is essentially employed in offshore structures. AWS D1.1 is followed in the welding process, and 7018 welding consumables are used.

Table 3.2. Specimen Details (Measured Dimensions)

	Joint type	D	d	T	t	L	l	Brace Loading
Model 1	Unstiffened	100	50	2	2	400	200	Compression
Model 2	Can -Ring- 4 strips	104	50	2	4	400	200	Compression
Model 3	Can -Ring- 6 strips	104	50	2	4	400	200	Compression
Model 4	Can -Ring- 8 strips	104	50	2	4	400	200	Compression

Notes: All dimensions are measured in mm

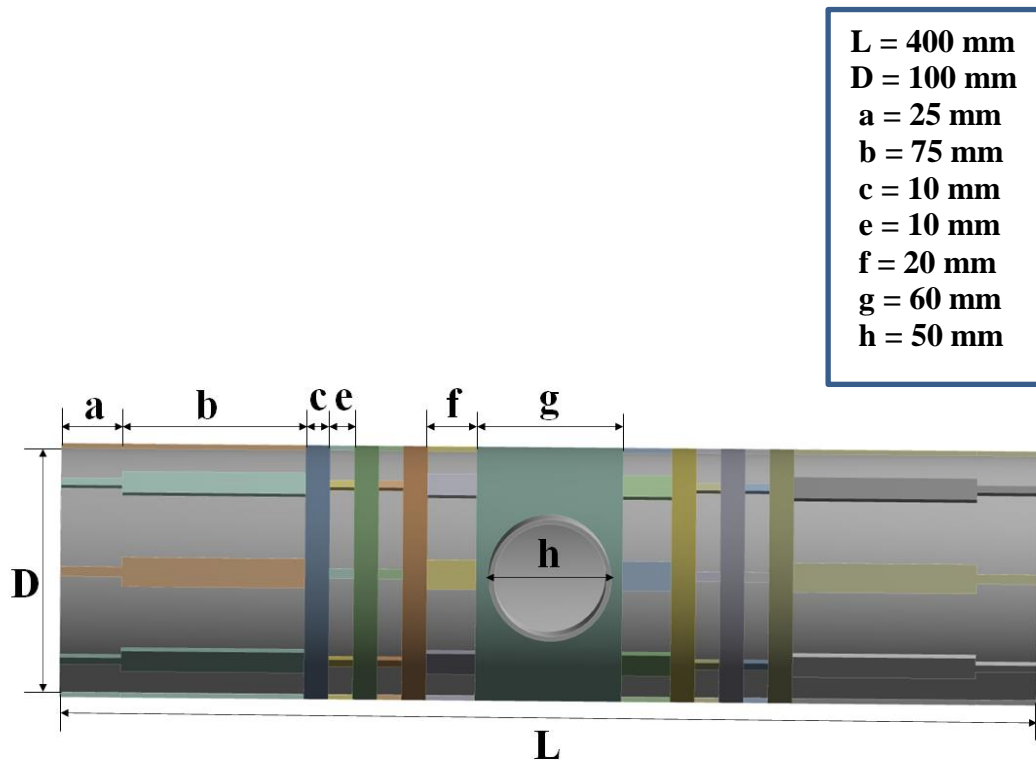


Figure 3.12: Tubular T-joint Specifications

The unstiffened and stiffened fabricated specimens are shown in Figures 3.13, 3.14, 3.15 respectively.



Figure 3.13: Unreinforced tubular T-joint

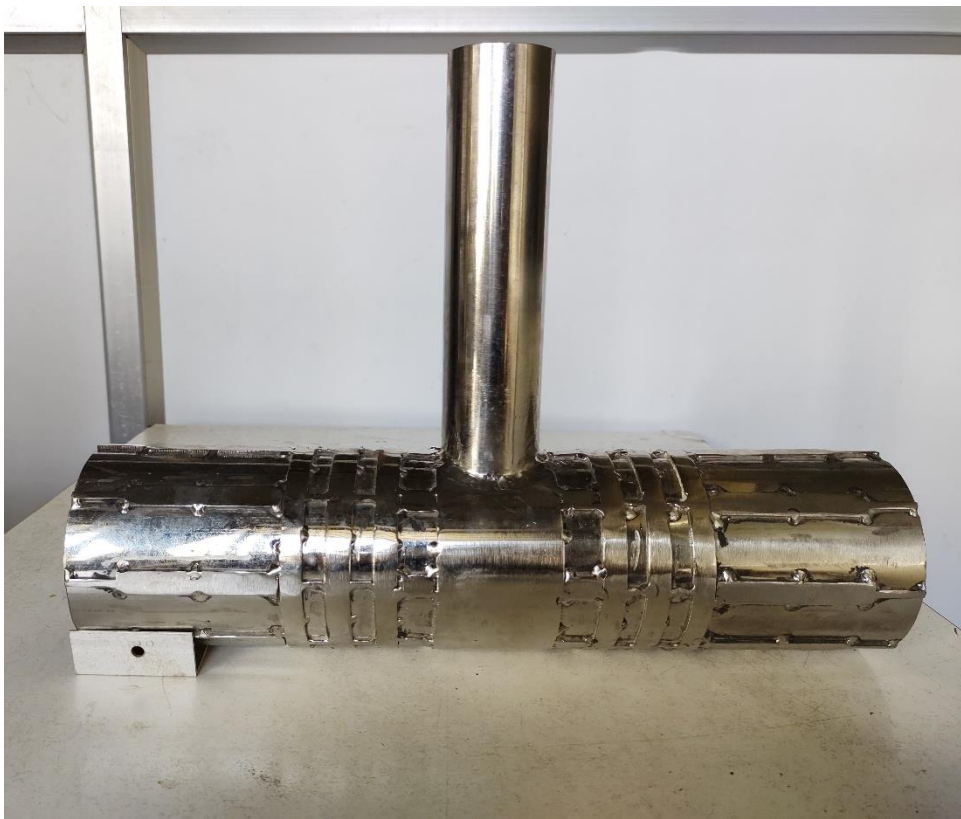


Figure 3.14: Reinforced tubular T-joint Can -Ring- 6 strips



Figure 3.15: Reinforced tubular T-joint Can -Ring- 8 strips

For the Can-Ring- 6 strips T-joint, the six strips are placed around the circumference of the chord member by means of welding and for the case of Can-Ring-8 strips T-joint eight strips are fixed around the circumference of the chord member.

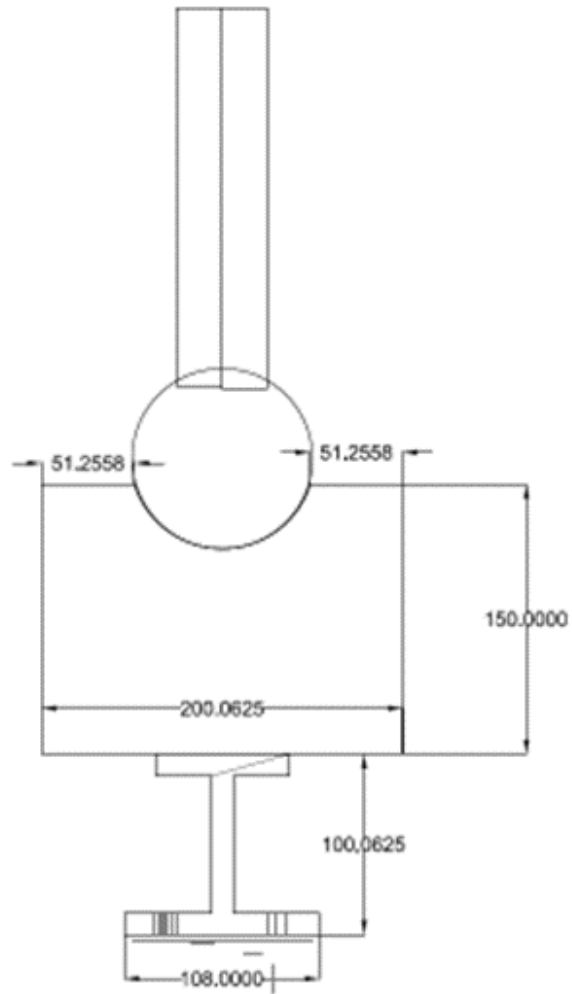


Figure 3.16a: Schematic diagram of specimen on saddle support

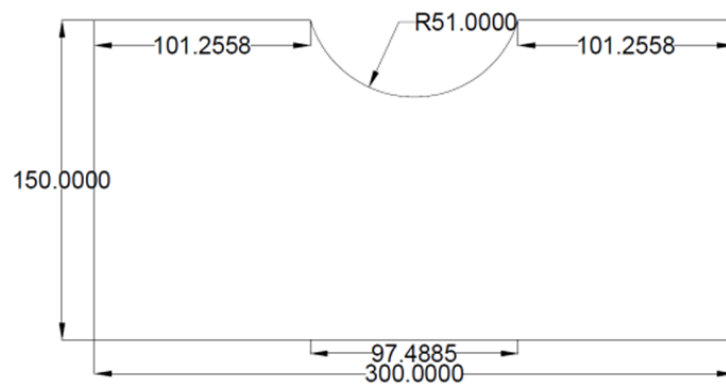


Figure 3.16b: Saddle Support 150 mm x 300 mm x 12 mm



Figure 3.16c: Fabricated saddle support

3.6. Instrumentation

The specimen is simply supported at the chord ends by means of saddle supports. The saddle support arrangement (Fig.3.16) was fixed by means of bolts to the base of movable crosshead of UTM machine to avoid any movement.

For each model, the instrumentation involves strain gauges (Figure 3.17) mounted around the brace member to measure the strain variation at the crucial portions and dial gauges (Figure 3.18 & Figure 3.19) to measure the displacements at the necessary locations.



Figure 3.17: Strain Gauge pasted over specimen

The strain gauges are pasted on the brace member along the circumference with an equidistant angle of 90 degree i.e. strain gauges are placed at 0 degree, 90 degree, 180 degree, 270 degree. They are placed nearer to the joint location with a distance of $0.65\sqrt{rt}$ mm (9.25 mm) from the weld according to OTH 354; Stress concentration factors for simple tubular joints.

The load-controlled actuator has a capacity of 40T. The brace load is applied to each test from 0 kg (0 N) and then increased gradually with a load interval of 25 kg (245.166 N) until the failure of the specimen.



Figure 3.18: Experimental setup with specimen (Unreinforced)

Figure 3.18 and 3.19 show the experimental set up with unreinforced and reinforced specimen is fixed for carry out the experiments. The dial gauges are placed to measure the ovalization of the tubular T-joint in both stiffened and unstiffened configurations.



Figure 3.19: Experimental setup with specimen (Reinforced)

COMPUTATIONAL STUDY

4.1. Introduction

In this chapter, stiffened and unstiffened tubular T-joints are numerically simulated under an axial compressive force. An initial linear static analysis is carried out for grooved stiffening mechanism. To validate the experimental results, a non-linear numerical study also carried out successfully. The numerical study involves pre-processing, solving and post processing stages.

4.2. Linear Static Analysis

The three-dimensional finite element study is performed using the general-purpose finite element program ANSYS. The thicker chord part has grooves formed around its perimeter. They are 5 grooves (one in the centre, four set 16.5 mm apart on either side), 3 grooves (one in the centre, two placed 16.5 mm apart on either side), and 3 grooves (one at middle, two are placed 33 mm apart from the middle on both sides). For the analysis, square grooves with dimensions of 1 mm by 1 mm and 2 mm by 2 mm are used. Steel is the material used in the analysis, and it has a 210 GPa Young's modulus and a 0.3 Poisson ratio.. In the present study, a linear static analysis was employed to investigate the behaviour of joints.

4.3. Geometric modelling

The geometrical model of a stiffened tubular T joint with five grooves is shown in Figure 4.1. The tubular T model taken into consideration for this study has brace length of 388 mm, brace diameter of 55 mm, and brace thickness of 4 mm. Its chord length is 1000 mm, chord diameter is 102 mm, and it has a chord thickness of 5 mm. ANSYS is used to create the tubular T-3-dimensional joint's model.

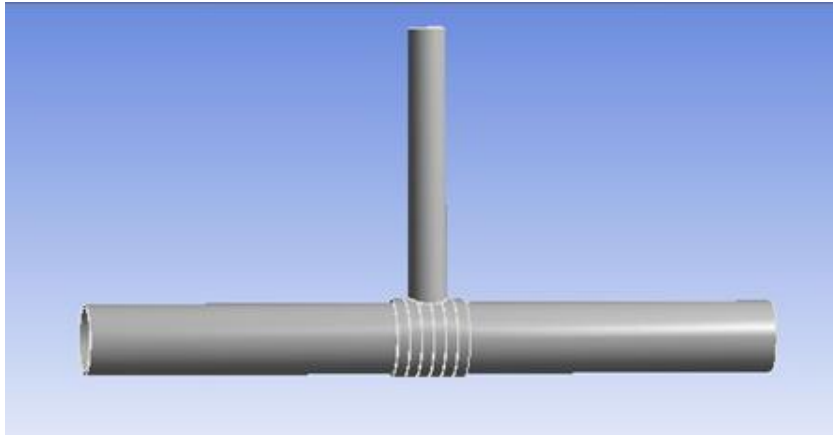


Figure 4.1: The geometry of Tubular T joint model with 5 grooves

4.4. Meshing and element details

The tubular T joint's meshing features are shown in Figure 4. 2. The model's meshing is done using hexa dominant mesh control. The number of nodes and elements considered for 5 grooves 2 mm model are 127730 and 24337. SOLID187 is the element that was used in the analysis. A 10-node, 3-dimensional higher-order element is called SOLID187. The element's displacement behaviour is quadratic, making it ideal for simulating uneven meshes.

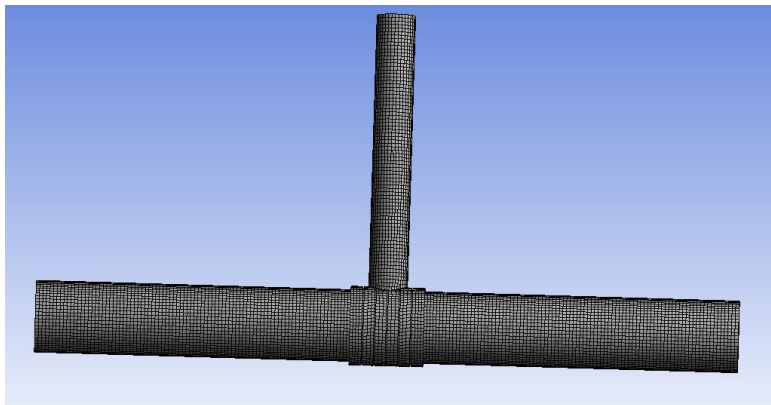


Figure 4.2: Meshed model 5 grooves 2mm model

4.5. Loading and boundary conditions

The boundary conditions are detailed in Figure 4. 3. An axial compression force of 20 kN is applied at one end of the brace member, and the chord member ends are fixed on both sides while being free to rotate. Through the use of static analysis, the behaviour

of joints was examined.. The boundary conditions are: $u (\pm l/2, y, z) = 0$; $v (\pm l/2, y, z) = 0$; $w (\pm l/2, y, z) = 0$, $F_y = -P$.

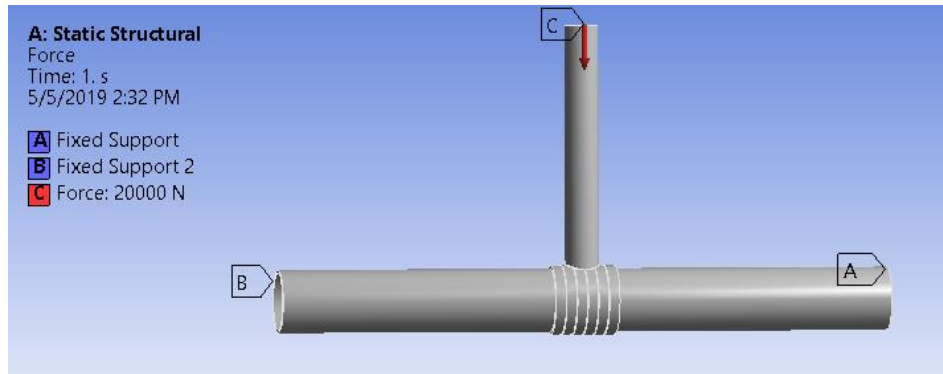


Figure 4.3: Boundary conditions for tubular T joint with 5 grooves

4.6. Non-Linear Analysis

The computer simulation was done by using the general-purpose finite element code ANSYS. The geometry and material nonlinearities are included in the simulation. The stress-strain graph can be assumed to be elastic-perfectly plastic includes work hardening, which can be defined in a piece-wise linear manner (Figure 6). The input simplified material model can be assumed to be a plateau with a small gradient right away after yield in order to prevent convergence issues.

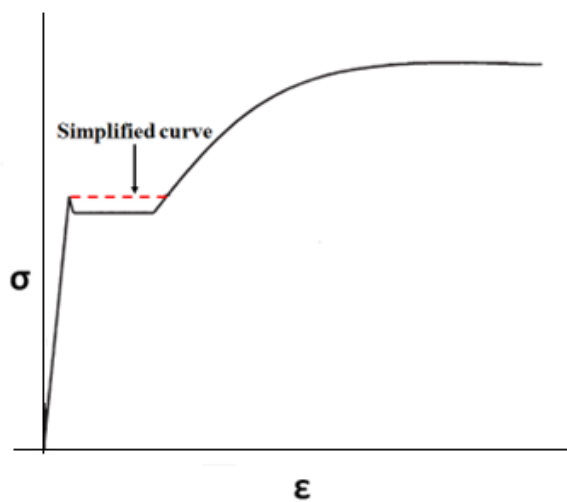


Figure 4.4: Material model for finite element input

From the experimental studies conducted at NITK strength of materials laboratory, the material properties are taken and the values are Young's modulus = 193 GPa, Yield strength = 210 MPa, Poisson's ratio = 0.31, Mass Density = 7750 kg/m³, Shear modulus = 73.66 GPa, Bulk modulus = 169 GPa. The displacement loading is considered to track the unstable, post-peak load shedding behavior of the model.

In this study, the joint behavior is examined by nonlinear static analysis. In the FE models, both material and geometric non-linearities significantly affect the ultimate capacity of tubular joints. The Newton-Raphson Method is an iterative procedure that ANSYS employs. Iterations of Newton-Raphson equilibrium deliver convergence within tolerance bounds at the conclusion of each load increase. Once the updation of stiffness matrix is done, a new solution is found, and the out-of-balance load vector is re-evaluated until convergence requirements are met. Until the convergence, this iteration continues.

4.7. Geometric model

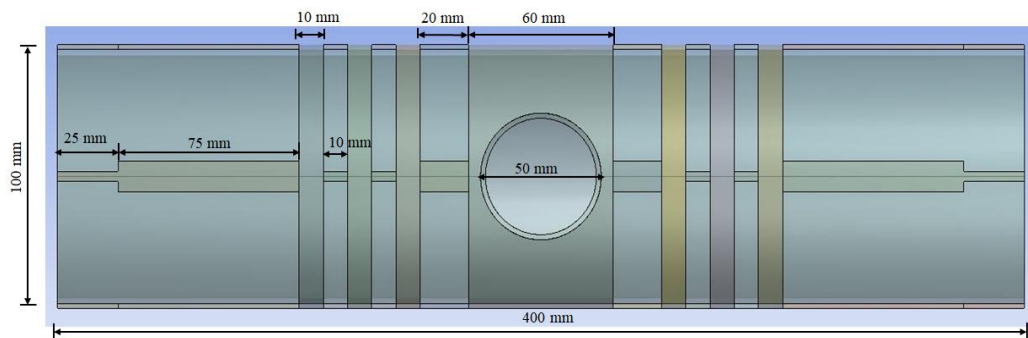


Figure 4.5: Tubular T-joint Specifications

The chord length, chord diameter, and chord thickness for the tubular T model used in this study are 400 mm, 100 mm, and 2 mm, respectively. The brace length, diameter, and thickness are 200 mm, 50 mm, and 4 mm, respectively. The geometric model of tubular T joint is drawn by using Design modeller tool of the commercial software package ANSYS workbench as shown in Figure 4.5. Figures 4.6 to 4.9 show the unstiffened and stiffened tubular T-joint models prepared for computational study.

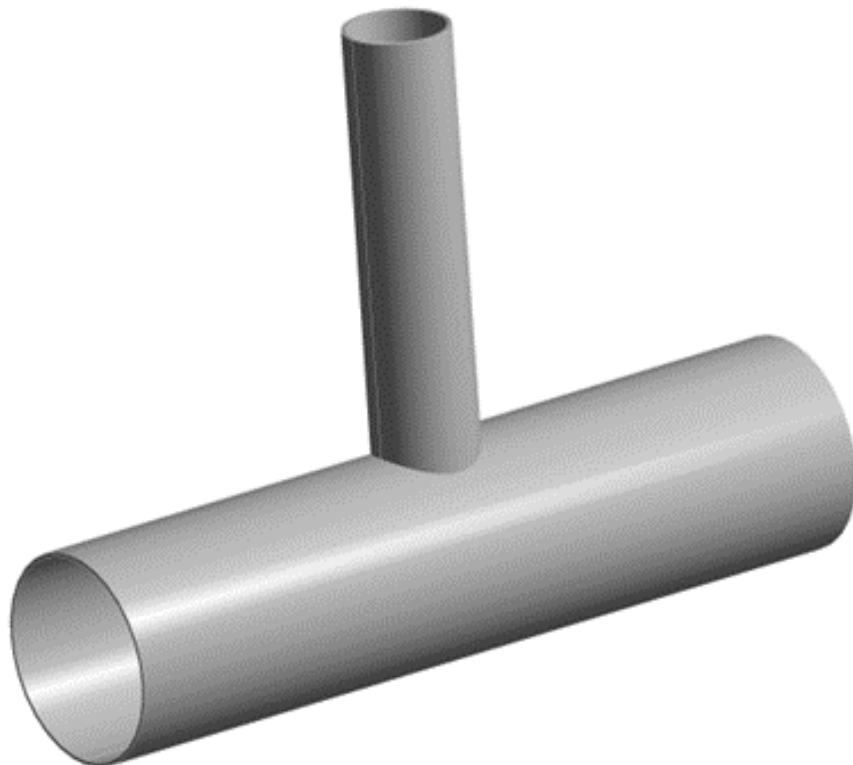
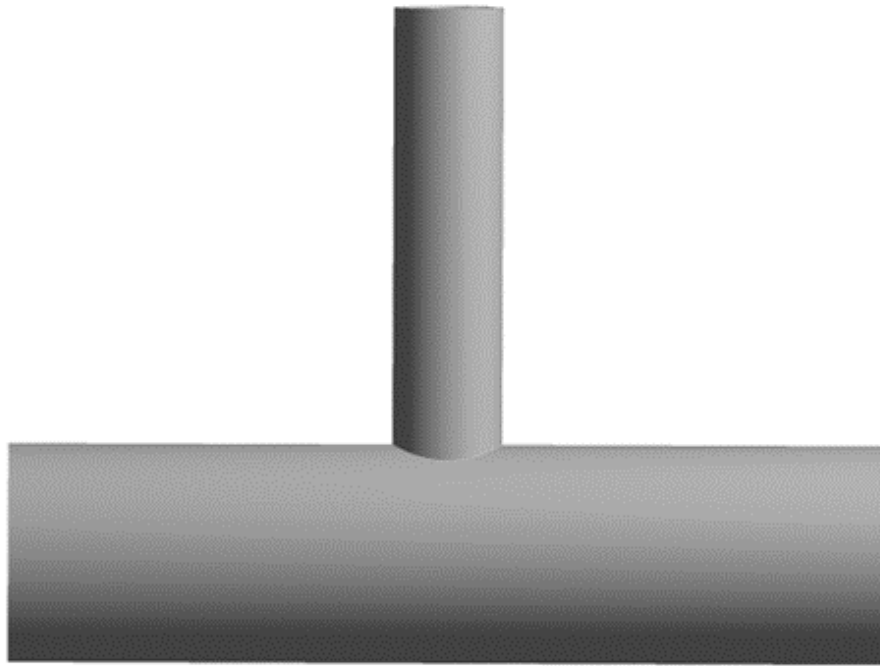


Figure 4.6: Unreinforced tubular T-joint model

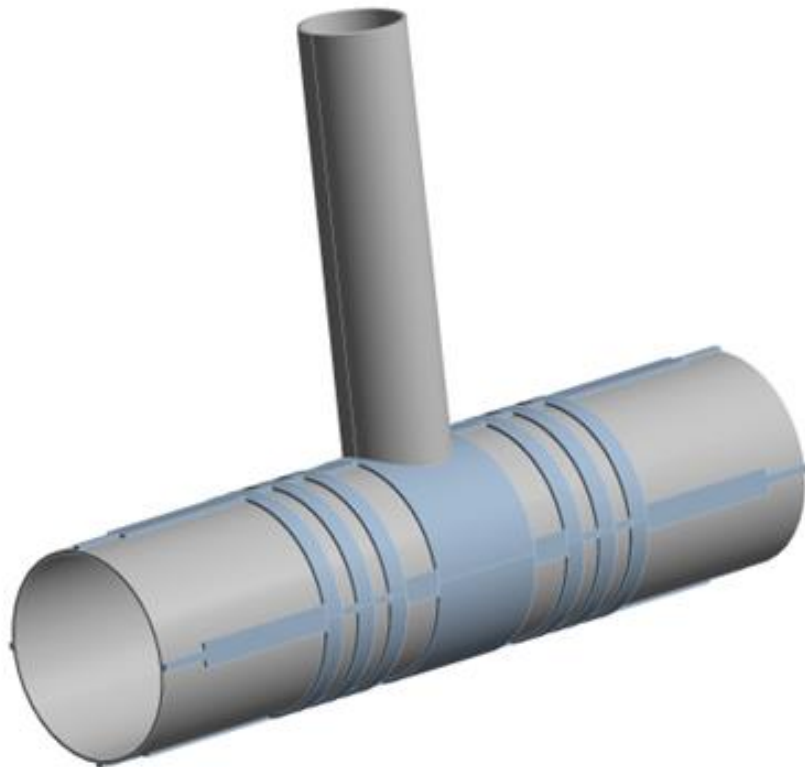
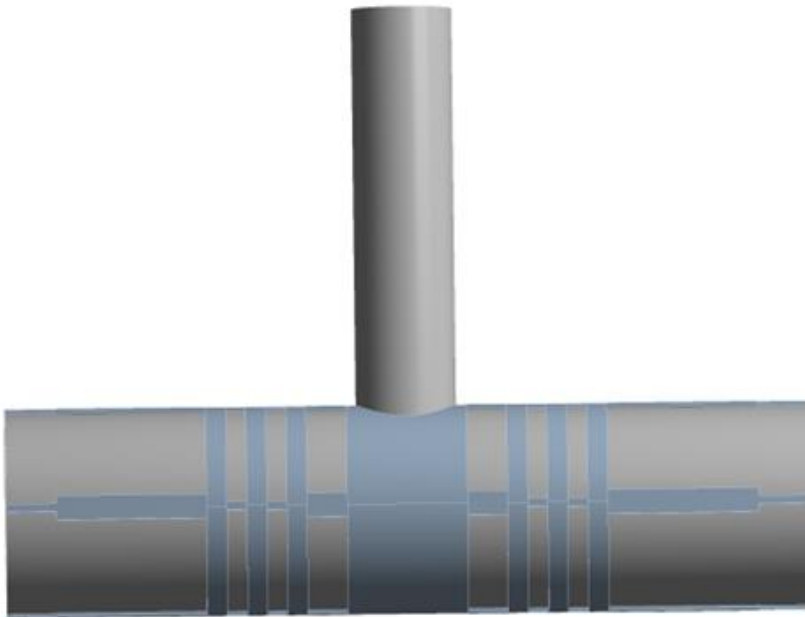


Figure 4.7: Reinforced tubular T-joint model (4 strips)

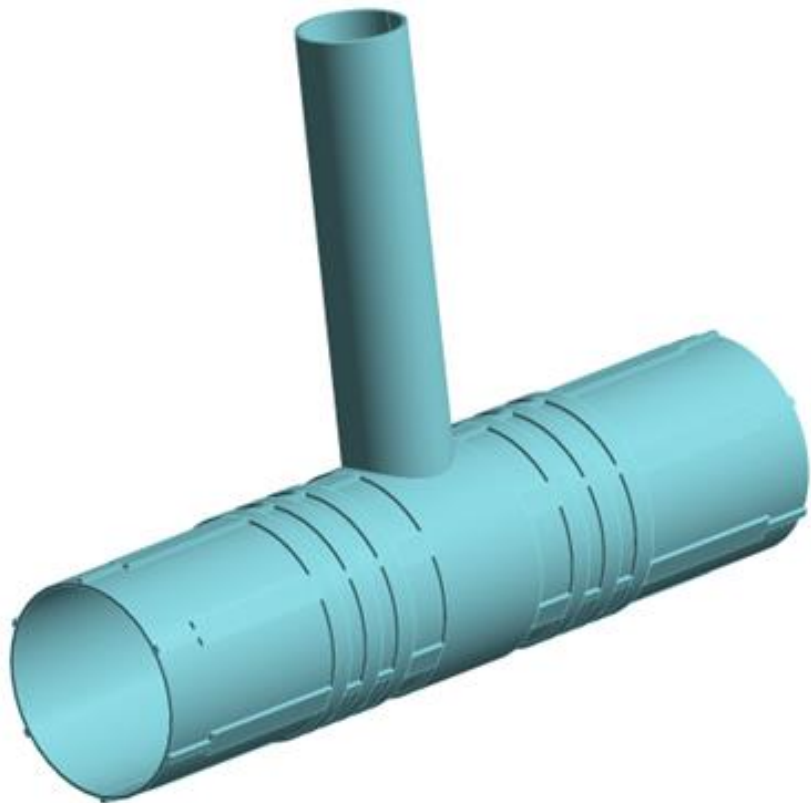
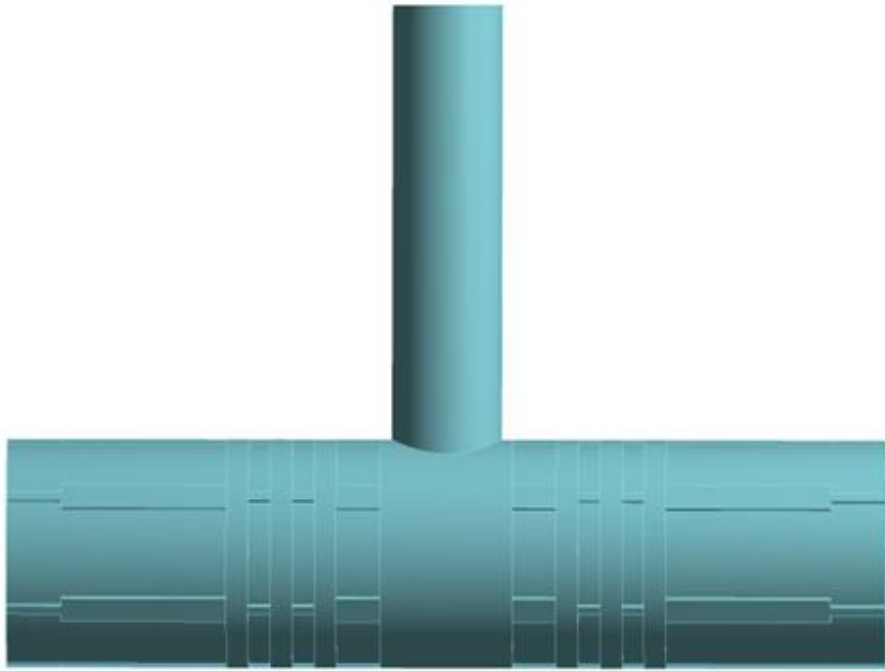


Figure 4.8: Reinforced tubular T-joint model (6 strips)

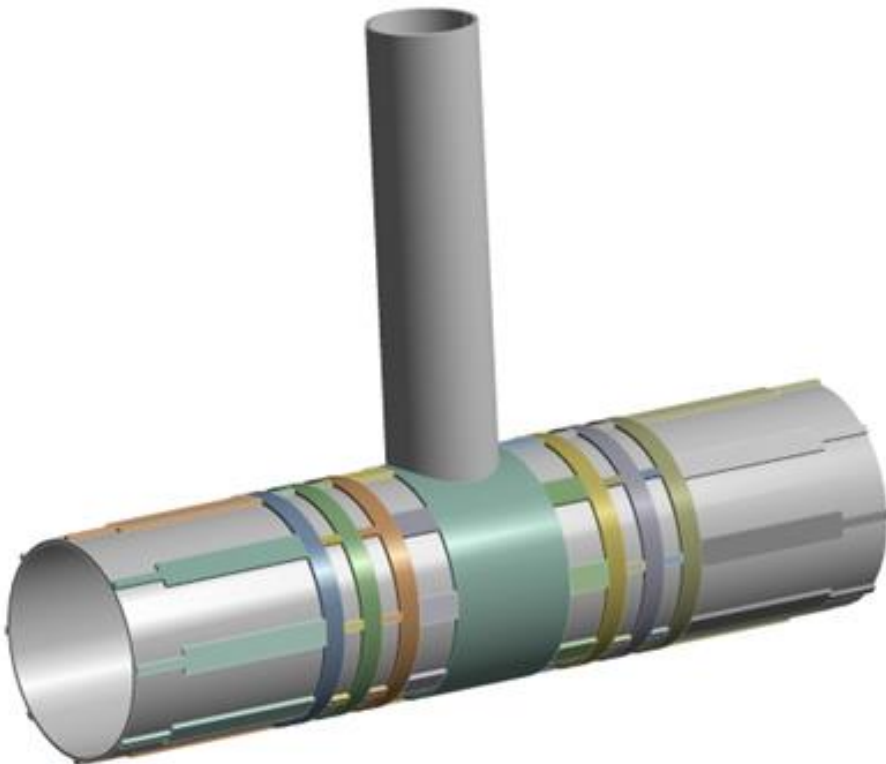
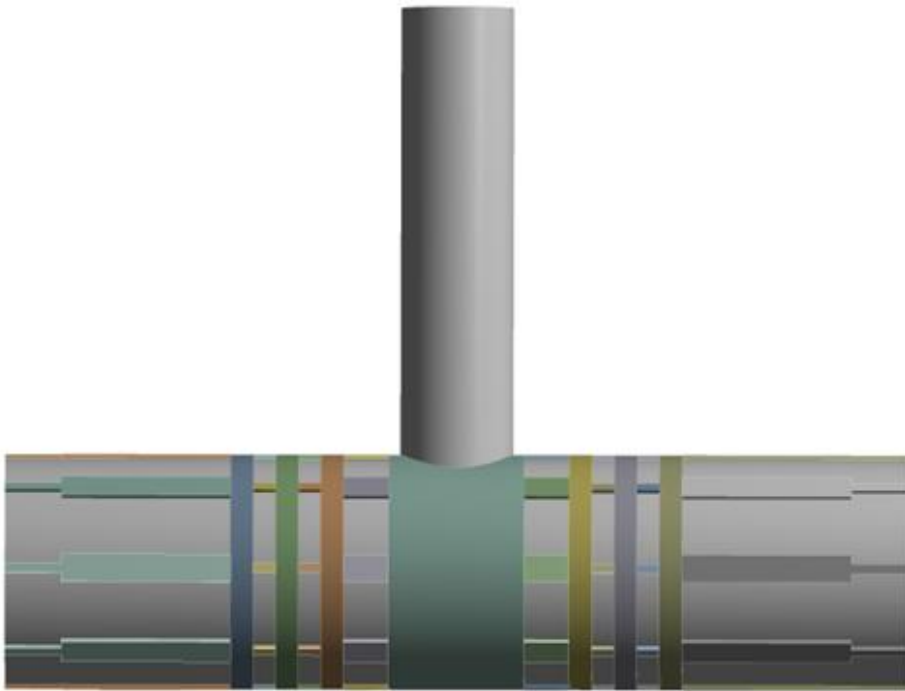


Figure 4.9: Reinforced tubular T-joint model (8 strips)

4.8. Meshing and element details

The tubular T joint's meshing features are shown in Figure 4. 10. The model meshing method of choice is hexa dominant mesh control. The SOLID 186, and SOLID 187 elements are employed to subdivide the domain into finite element forms. A 10-node, 3-dimensional higher-order element is called SOLID187. The element's displacement behaviour is quadratic, making it ideal for simulating uneven meshes. SOLID186 is a higher-order 3-D 20-node solid element that exhibits quadratic displacement behavior.

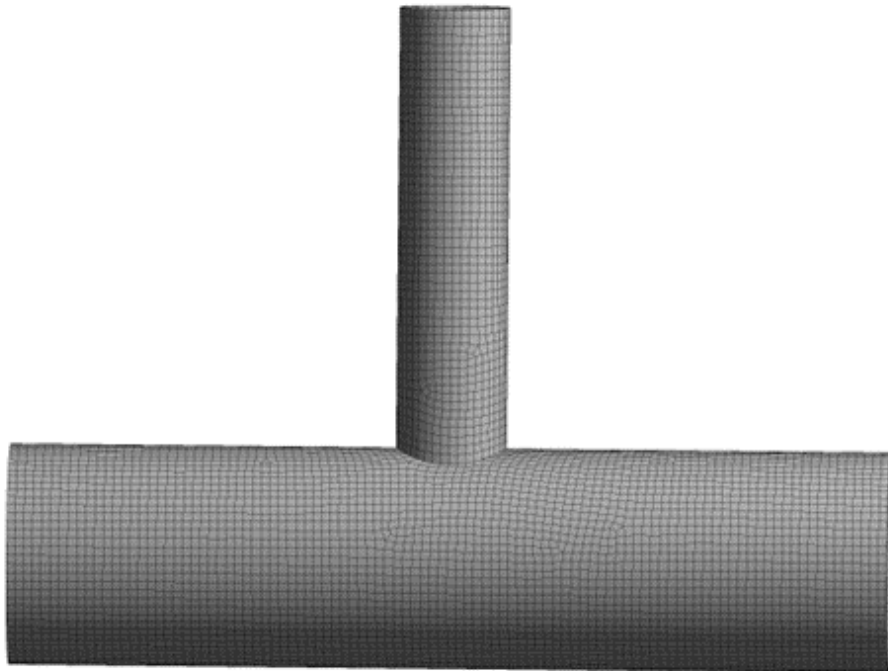


Figure 4.10: Finite element mesh

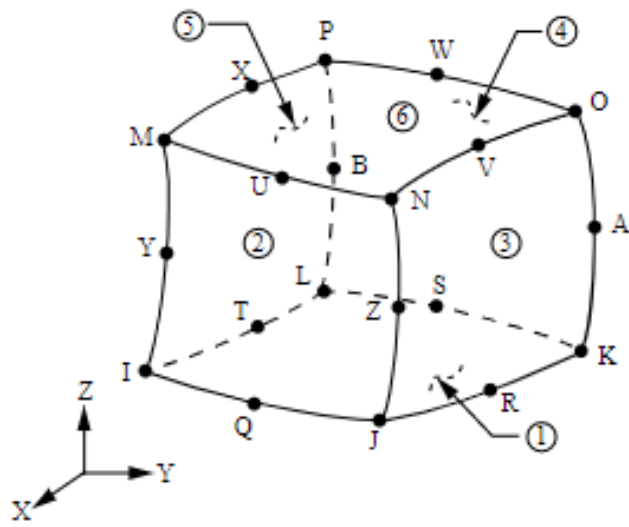


Figure 4.11: The geometry of SOLID186 element

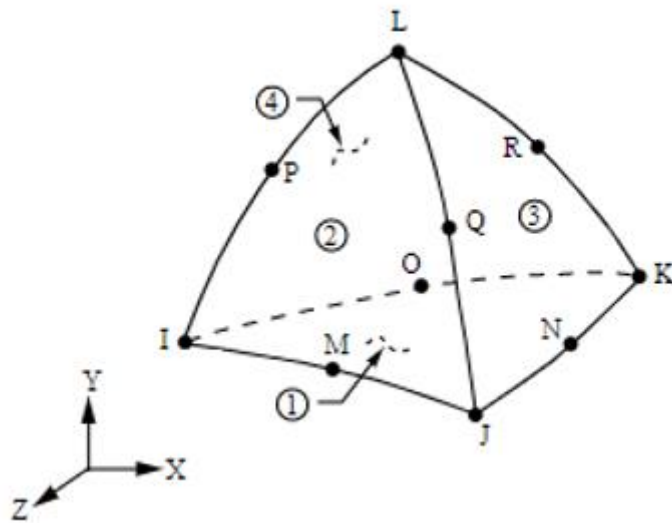
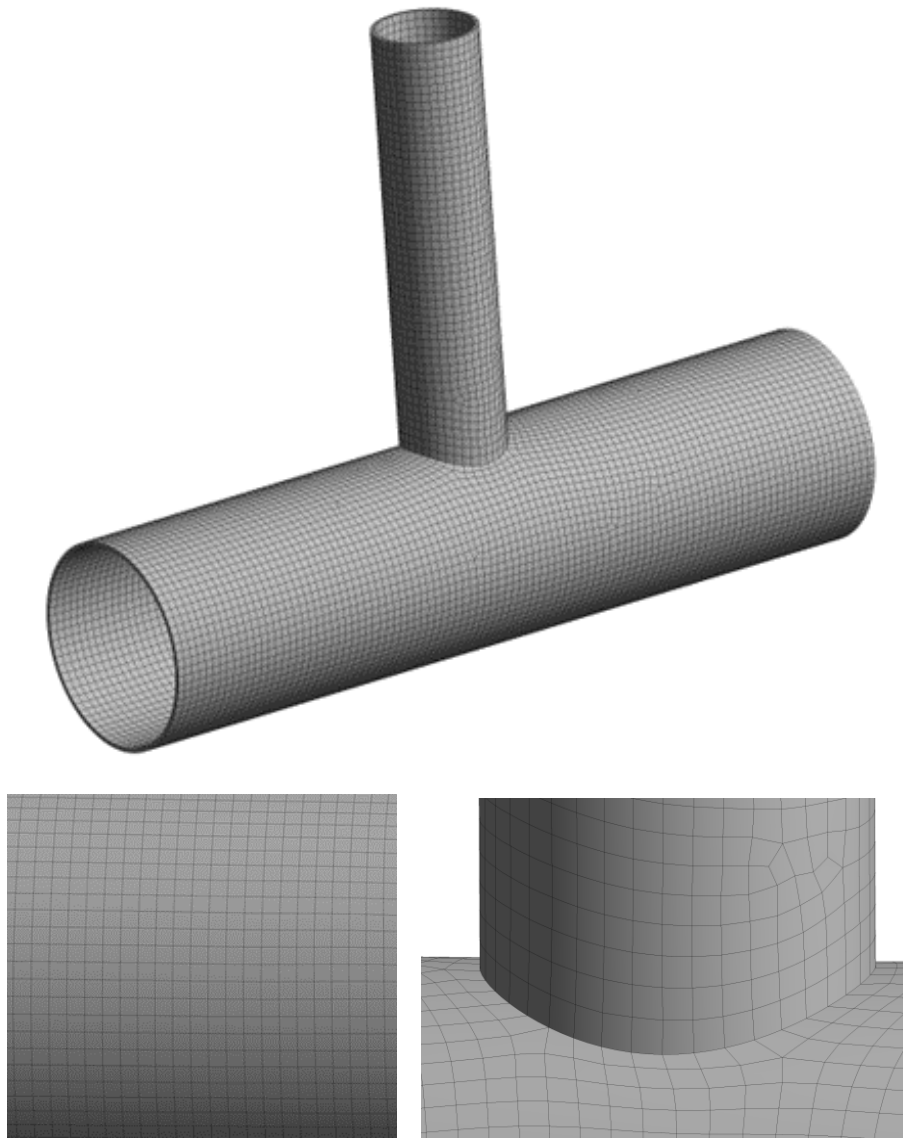


Figure 4.12: The geometry of SOLID187 element



(b) Meshing in chord member

(c) Meshing in chord-brace

Figure 4.13: Finite element mesh unreinforced model

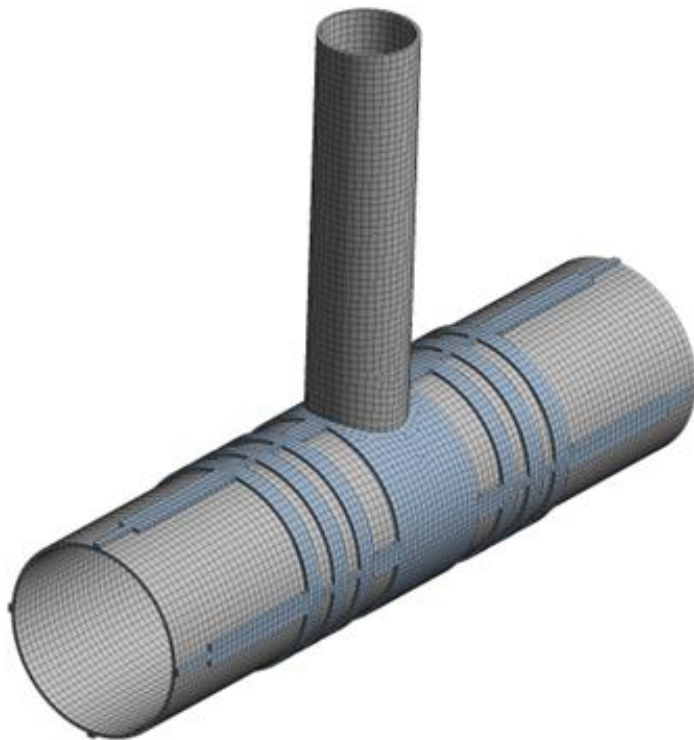
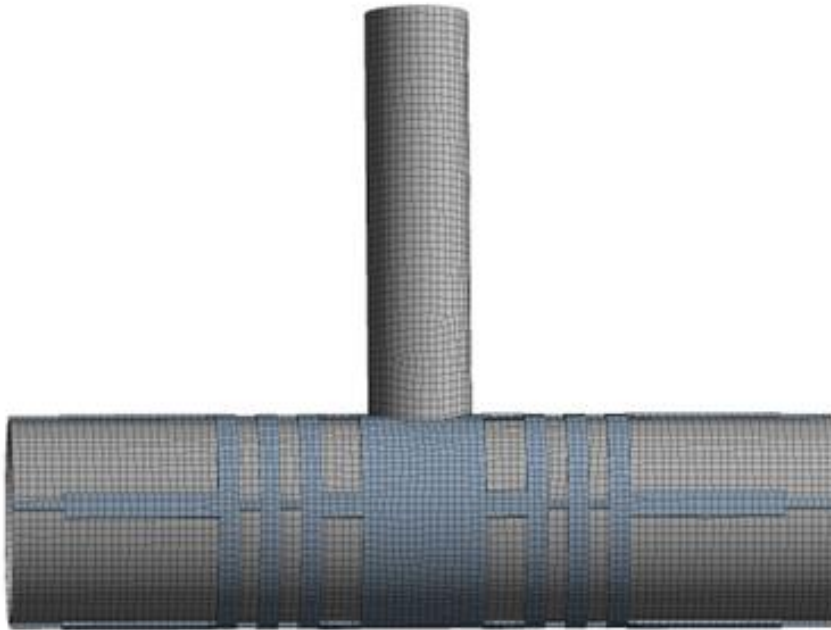


Figure 4.14: Finite element mesh 4 strips model

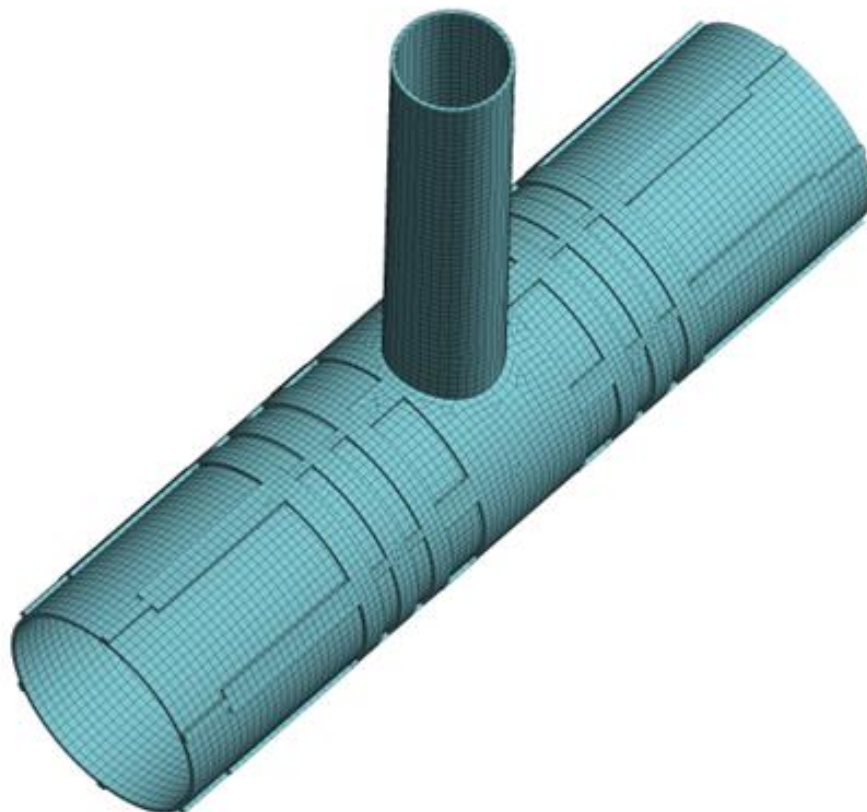
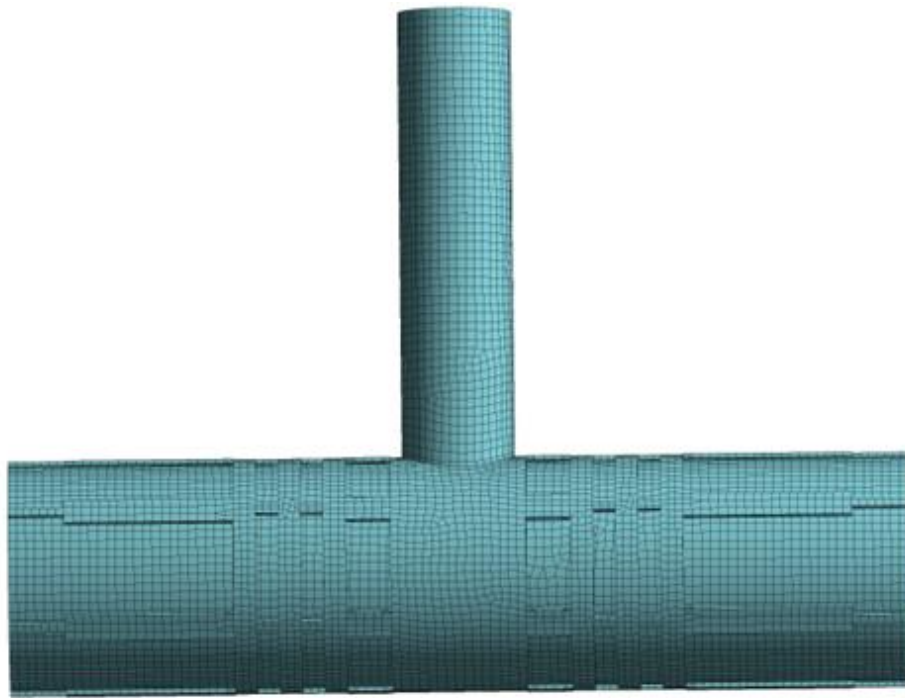
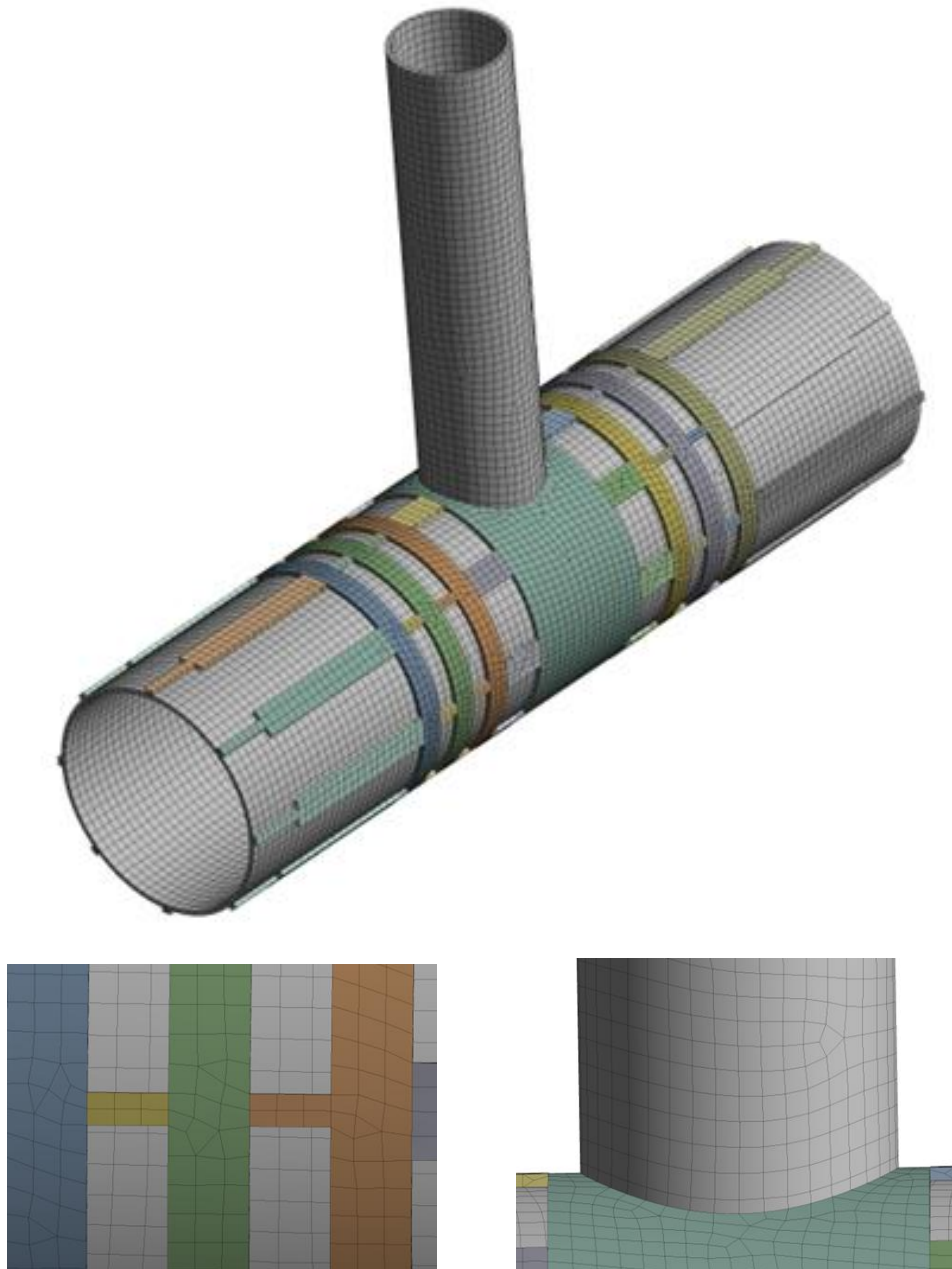


Figure 4.15: Finite element mesh 6 strips model



(b) Meshing in chord member (c) Meshing in chord-brace

Figure 4.16: Finite element mesh 8 strips model

4.9. Mesh convergence study

The results of the numerical finite element study are particularly sensitive to the type, size, and pattern of the mesh used because the solution is approximate. The suitable mesh size, wherein the solution is independent of mesh size, is to be found by trial-and-

error method by running simulations for different mesh sizes. Optimum mesh size is usually used to reduce computational duration and work. To get accurate results with reasonable calculation time, a convergence study is carried out as shown in Figure 4.17.

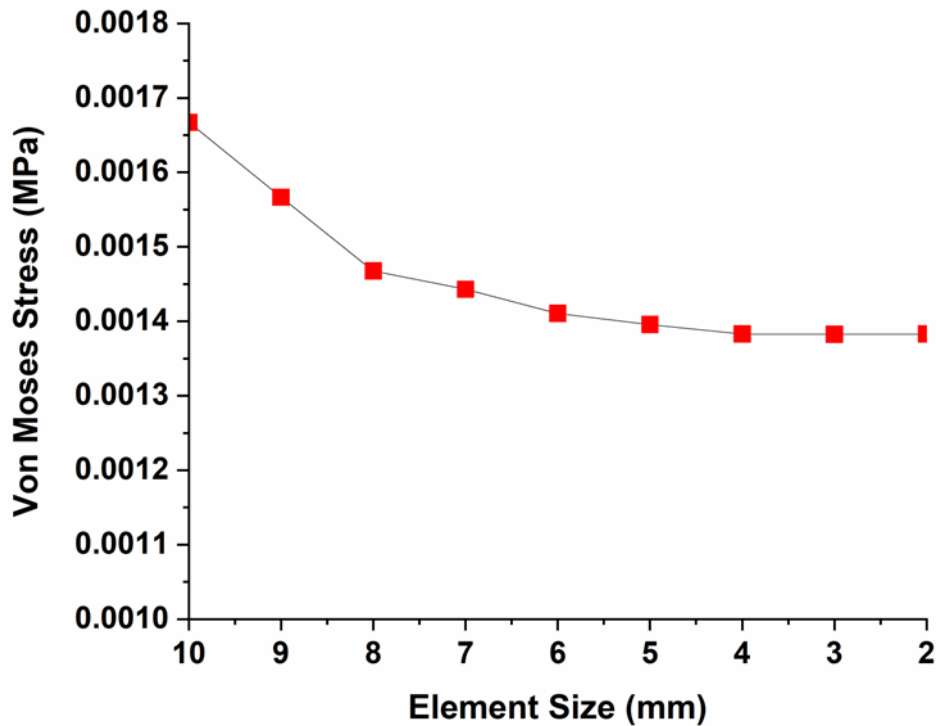


Figure 4.17: Convergence study

4.10. Loading and boundary conditions

Figures 4.18 to 4.20 illustrate the boundary conditions in more detail. Except for rotation on the z-axis, the degrees of freedom at the end faces of chord members are arrested. At the brace member's free end, a 20 kN axial compression force is applied. Through the use of static analysis, the behaviour of joints was examined.

The boundary conditions are:

$$u(\pm l/2, y, z) = 0; v(\pm l/2, y, z) = 0; w(\pm l/2, y, z) = 0; F_x(x, y, z) = -P.$$

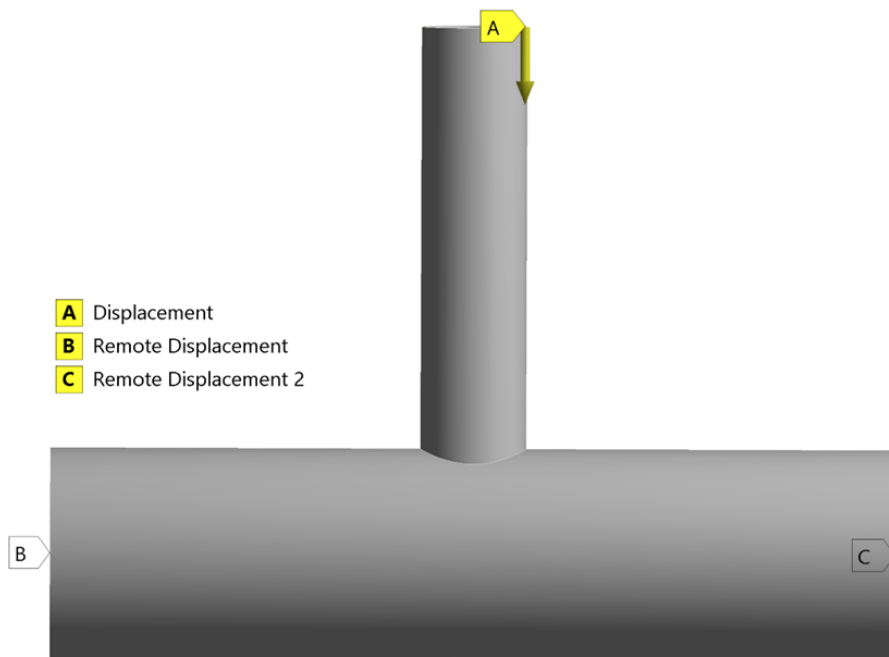


Figure 4.18: Boundary conditions for tubular T joint

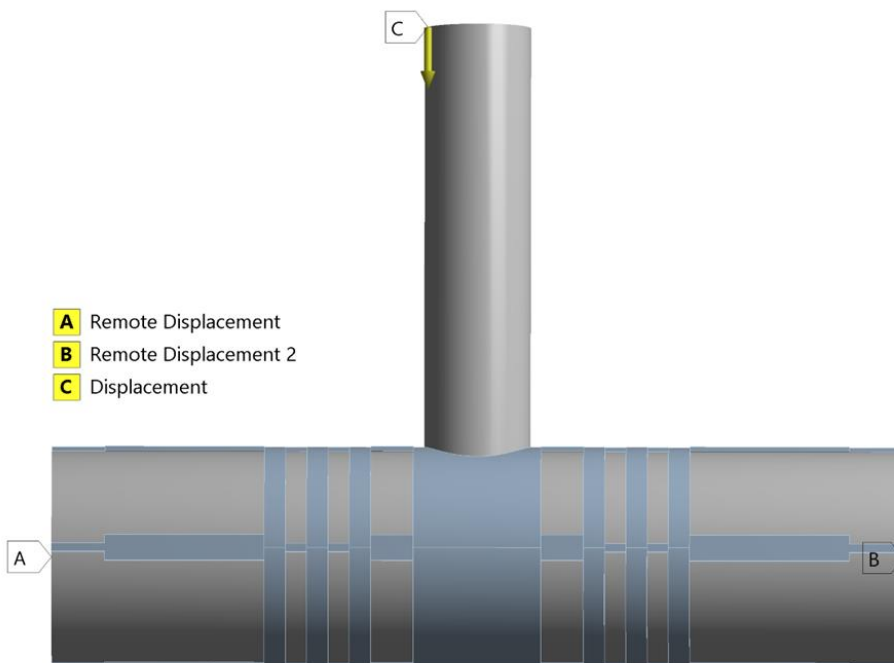


Figure 4.19: Boundary conditions for tubular T joint (4 strips)

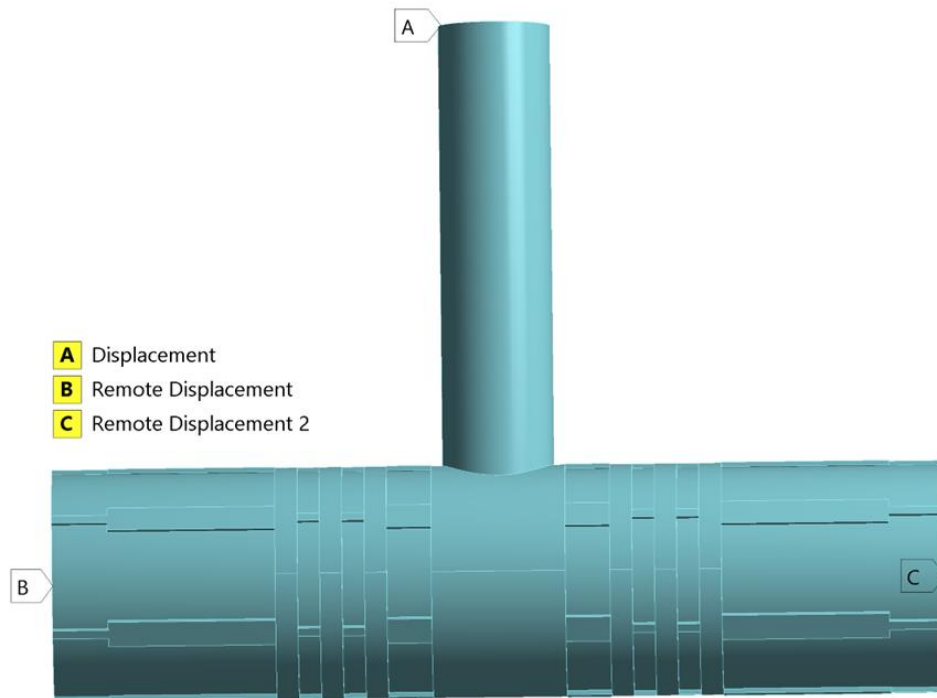


Figure 4.20: Boundary conditions for tubular T joint (6 strips)

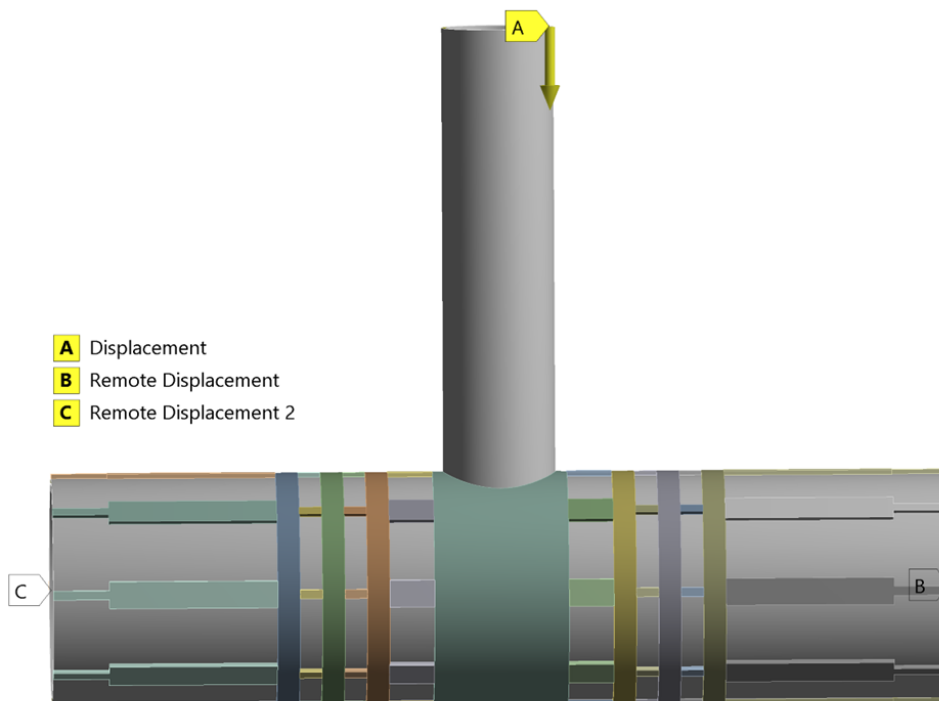


Figure 4.21: Boundary conditions for tubular T joint (8 strips)

RESULTS AND DISCUSSION

5.1. Introduction

The numerical study based on finite element code ANSYS, on linear and non-linear analysis, is done and experimental investigation is carried out to understand the effects of reinforcements on stiffness and static strength of the tubular T-joints.

5.2. Failure mechanism

Figure 5.1 depicts the cross section of the chord member before and after the load is applied. The chord member had a circle shape before the load was applied; when the load was applied, the shape changed to an oval. Ovalization is defined as the difference between the top displacement (Δ_t) and the bottom one (Δ_b) of the chord member. In terms of ovalization, the joint local stiffness against chord buckling failure can be compared.

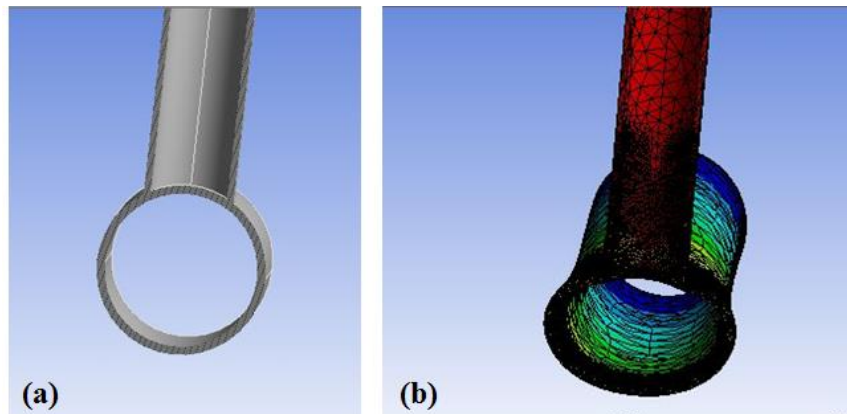


Figure 5.1: Shape of the cross-section of a chord member before (a) and after (b) applying a load

5.3. Von Mises Stress Variation

The von Mises stress value for unstiffened and grooved configurations for 20 kN are 204.87 MPa, 237.34 MPa (5 grooves 1 mm), 254.68 MPa (5 grooves 2 mm), 200.27

MPa (3 grooves 2-1-3 1mm), 240.92 MPa (3 grooves 2-1-3 2mm), 188.92 MPa (3 grooves 4-1-5 1mm), 207.79 MPa (3 grooves 4-1-5 2mm). It suggests that the grooved designs are stronger than the unstiffened model.

5.4. Load – Ovalization Relationship

The load-ovalization graphs in Figure 5.2 show how the joint local stiffness against chord outward buckling failure is shown. It is evident that the configurations with grooves are stiffer than those without. For the comparison analysis, the deformation of the six grooved configurations is displayed on a single graph. Due to the grooves' minimal effects, all six grooved configurations exhibit the same deformation pattern. The slope of the load- ovalization curve's straight section represents the stiffness of a joint locally.

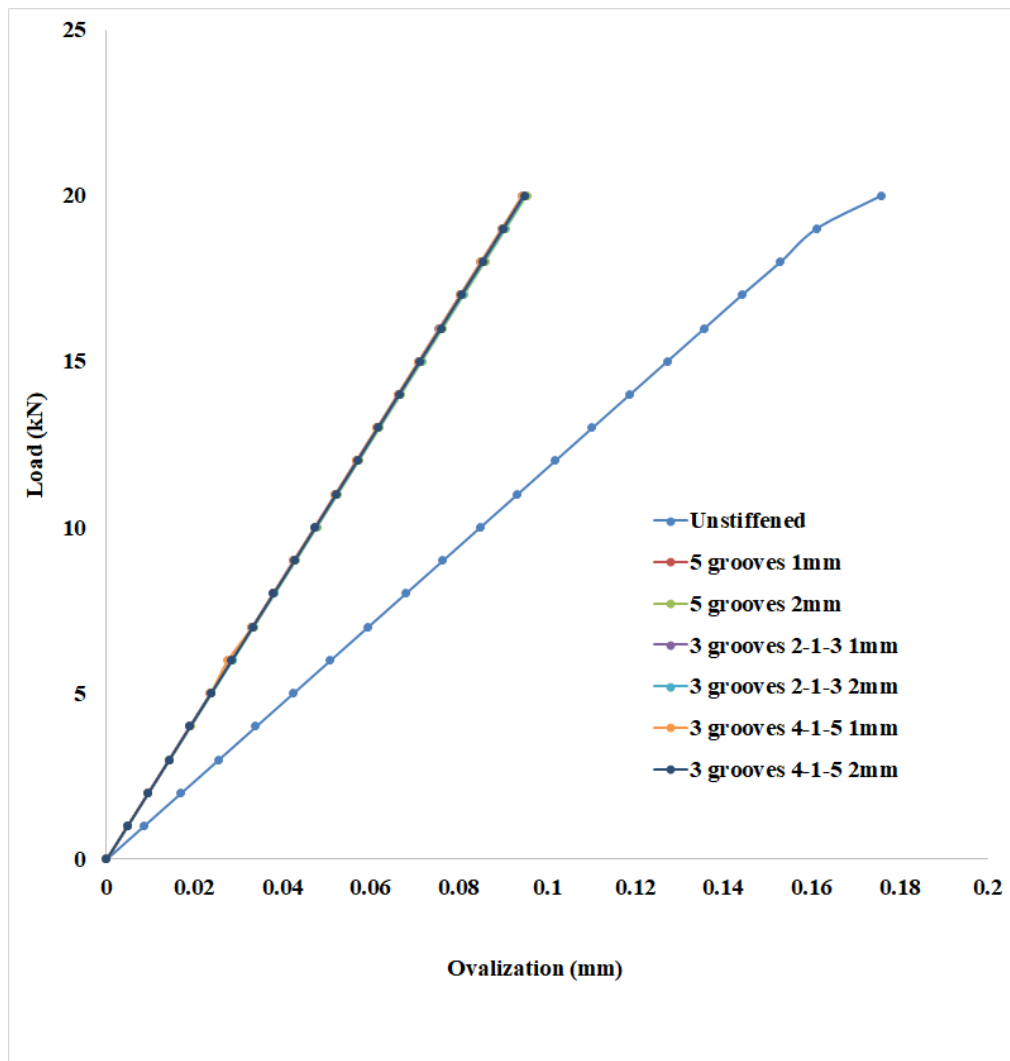


Figure 5.2: Load vs chord ovalization

The joint local stiffness values for various configurations are shown in Table 5.1. From the tabular values, it is observed that the stiffened configuration takes more load for the given deformation than that of the unstiffened one.

Table 5.1. T joint model Joint local stiffness

S.no	Model	Stiffness (N/mm)	% increment
1	Unstiffened	116.68	-----
2	5 grooves 1×1 mm	211.58	81.3
3	5 grooves 2×2 mm	209.51	79.55
4	3 grooves (2-1-3) 1×1 mm	211.79	81.51
5	3 grooves (2-1-3) 2×2 mm	210.47	80.38
6	3 grooves (4-1-5) 1×1 mm	211.53	81.29
7	3 grooves (4-1-5) 2×2 mm	210.83	80.69

5.5. Load - Ovalization Definition

The load-deformation values from the experiments are shown and discussed. Deformation in this context refers to chord ovalization at the middle of the T-joint, which is calculated by subtracting the value from the dial gauge reading at the load application point (brace top end) δ_1 to the value of the dial gauge reading at the chord bottom at the middle of the joint δ_2 , as shown in Figure 5.3. Here in the present study, the top deflection is measured by placing the dial gauge on the movable crosshead of the machine.

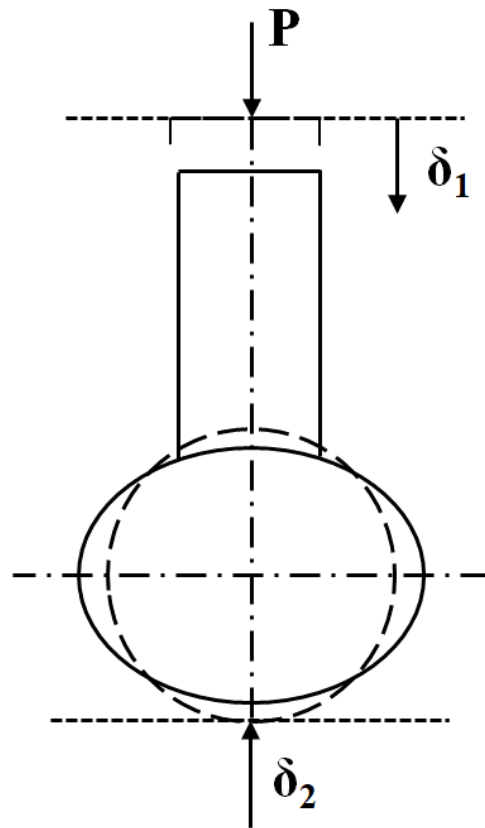
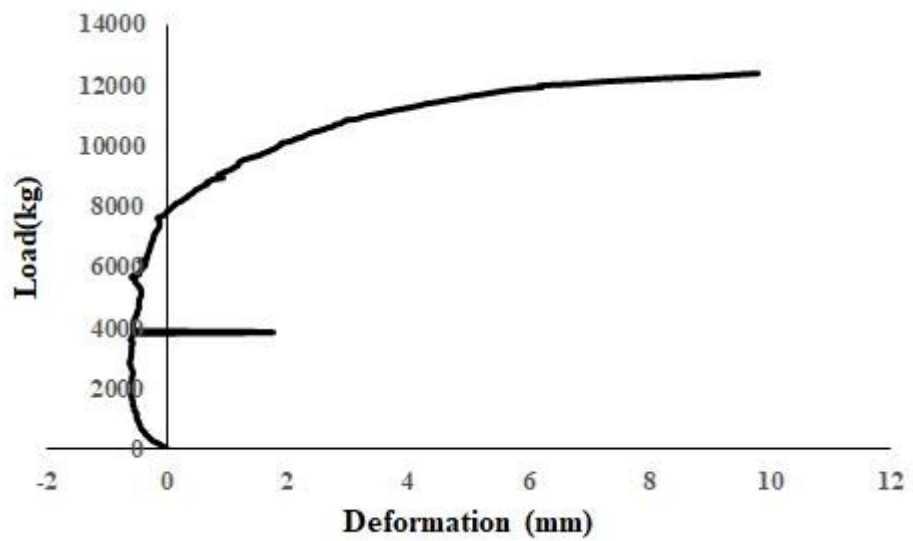


Figure 5.3: Definition of Ovalization

From the ovalization curve, it is observed that the ovalization starts at 8000 kg. The reason behind this was the failure started at the supports initially. The supports were failing till the failure starts at the joint. After that, the ovalization was taking place in the joints in the usual way. Figure 5.4 depicts the failure of the specimen at the supports and corresponding load-deformation information



(a) Failure at support



(b) Ovalization Curve (case 1)

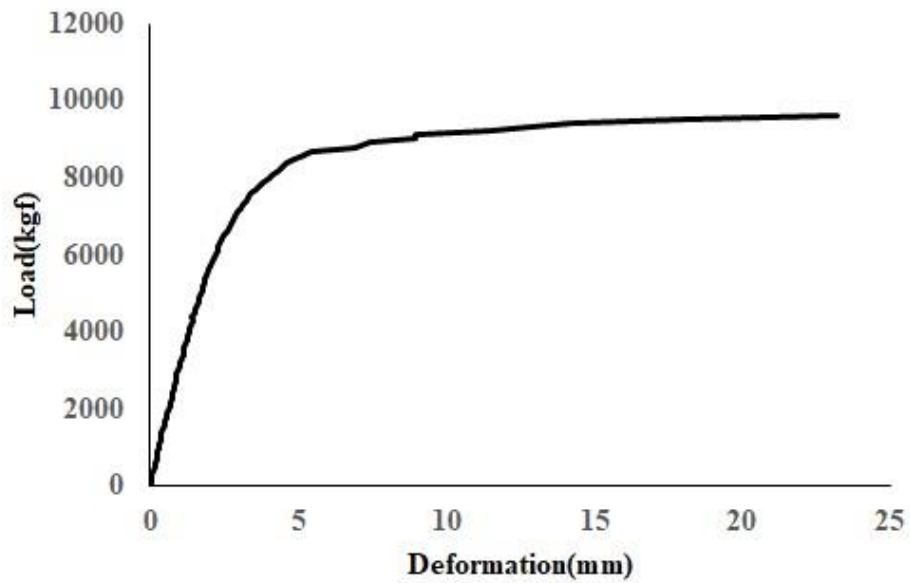
Figure 5.4: (a) Failure at support and (b) Ovalization Curve (case 1)

By observing the above ovalization curve we can judge that there is a negative ovalization up to 8000kg (78453.2 N) after that positive ovalization. During the experiment, we observed that the load was initially transferred to the support but the applied load should be transferred to the joint. So, this may be the reason for the negative ovalization up to 8000kg (78453.2 N).

Figure 5.5 shows the ovalized specimen after the experiment. Till the elastic limit, the load and deformation vary linearly as depicted. The welded joint was transferring the load from the brace member to chord member effectively. Once the load is crossing the elastic-plastic transition and entering into the plastic limit the chord wall starts to local buckling which results in ovalized shape of the specimen.



(a) Ovalized specimen

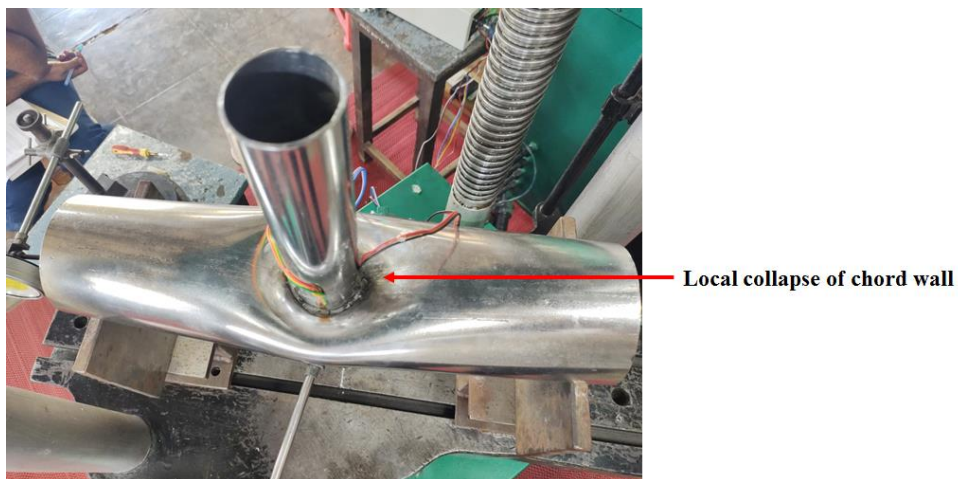


(b) Ovalization Curve (case 2)

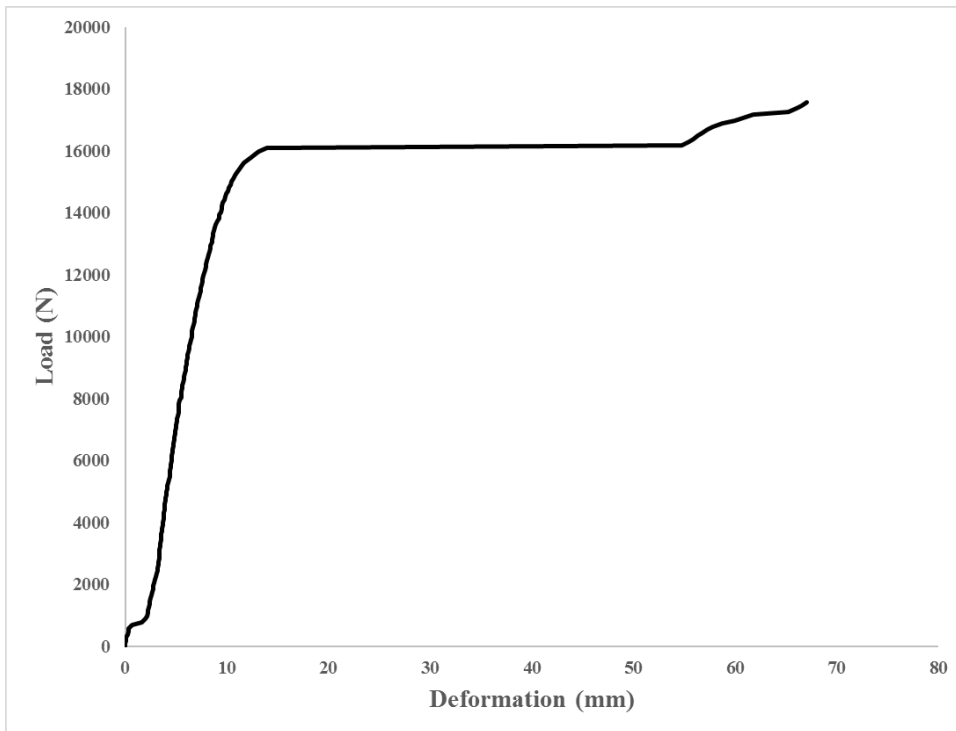
Figure 5.5: (a) Ovalized specimen (b) Ovalization Curve (case 2)

The Ultimate strength is defined as the brace load where the load ovalization curve shows a distinct peak.

Figure 5.6 displays the load ovalization curve of the unstiffened tubular T-joint specimen subjected to brace compression. As the load increases gradually, the joint deformation also increases in a linear fashion within the elastic limit. Once the elastic region is fully experienced then as the load increases, the plastification of the chord starts. As a result, the local chord wall starts buckling. The local collapse of the chord wall is shown in Figure 5.6.



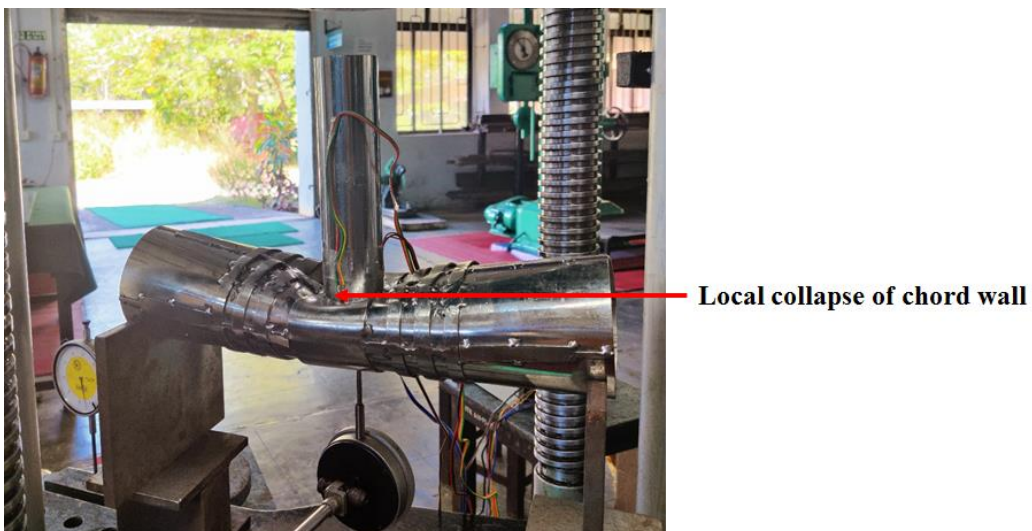
(a) Local collapse of chord wall



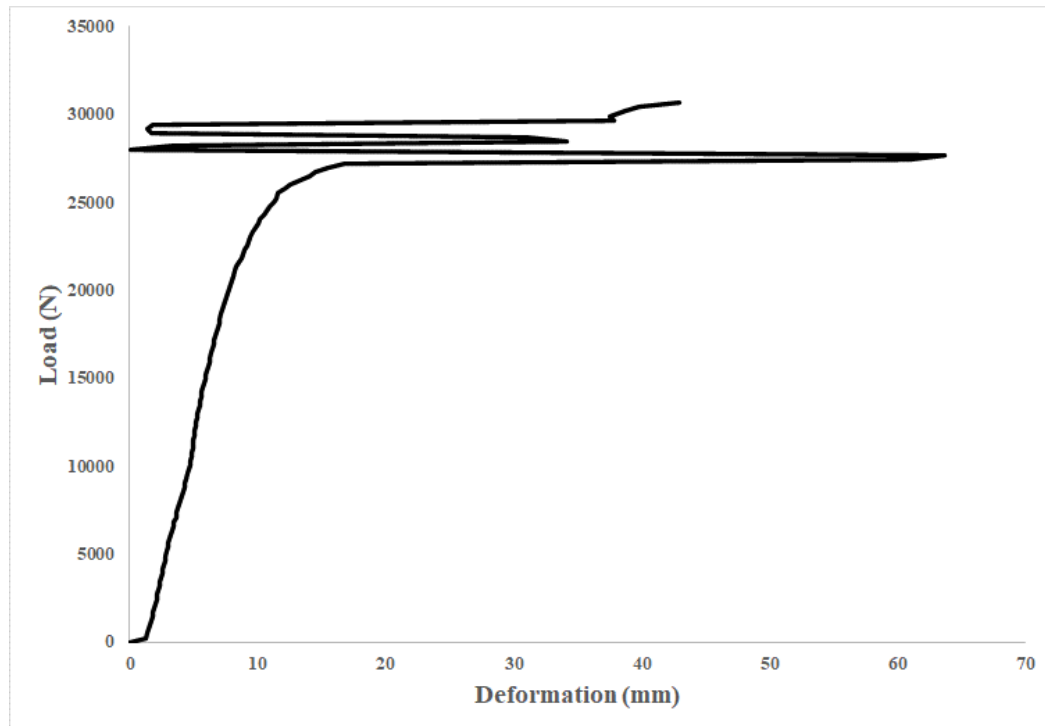
(b) Load ovalization curve (Unstiffened T- joint)

Figure 5.6: Unstiffened T- joint (a) Local collapse of chord wall

(b) Load ovalization curve (Unstiffened T- joint)



(a) Local collapse of chord wall



(b) Load ovalization curve (4 strips)

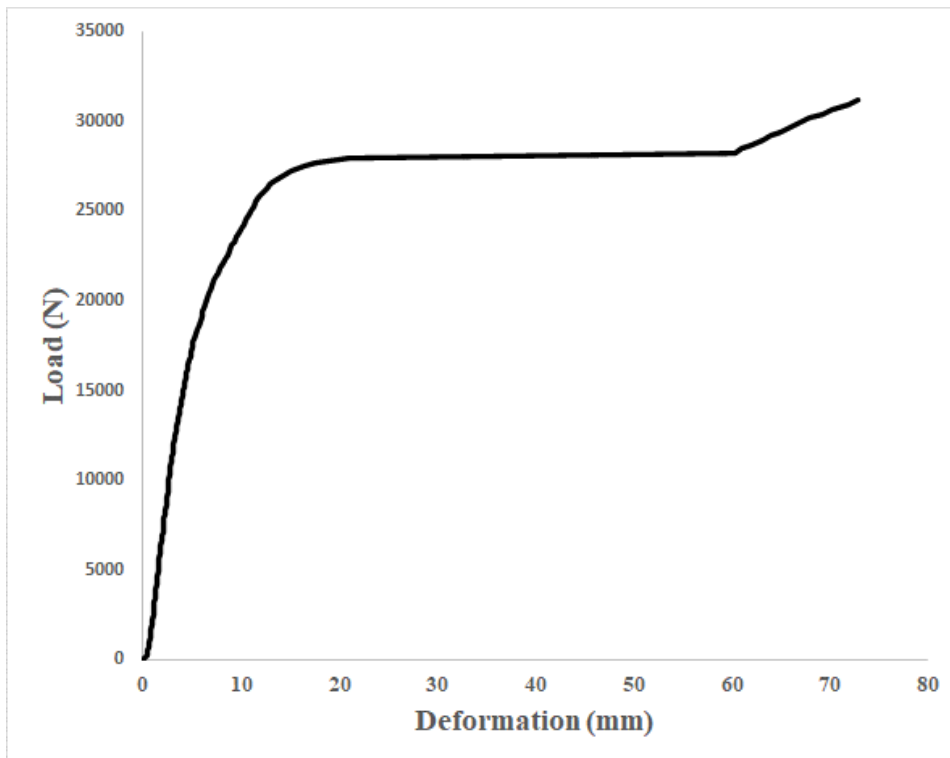
Figure 5.7: 4 strips (a) Local collapse of chord wall (b) Load ovalization curve

Figure 5.7 displays the load ovalization curve of the reinforced tubular T-joint specimen stiffened with 4 strips subjected to brace compression. As the load increases gradually, the joint deformation also increases in a linear fashion within the elastic limit. As reinforcements are introduced the load-carrying capacity of the joint increases in comparison with that of the unstiffened specimen. The plastification process takes more load than that of the unstiffened one. The local collapse of the chord wall is shown in Figure 5.7.

Figure 5.8 displays the load ovalization curve of the reinforced tubular T-joint specimen stiffened with 8 strips subjected to brace compression. As the load increases gradually, the joint deformation also increases in a linear fashion within the elastic limit. As reinforcements are introduced the load-carrying capacity of the joint increases in comparison with that of the unstiffened specimen. The plastification process takes more load than that of the unstiffened one. The local collapse of the chord wall is shown in Figure 5.8.



(a) Local collapse of chord wall



(b) Load ovalization curve (8 strips)

Figure 5.8: 8 strips (a) Local collapse of chord wall (b) Load ovalization curve

5.6. Unstiffened T-joint

According to Figure 5.9, the chord wall of an unstiffened T-joint begins to yield according to the load supplied up to the elastic limit. When the chord wall reaches its maximum capacity, it begins to buckle locally and ovalize globally as a result of

significant displacements at the joint. For displacement levels over the maximum allowable, buckling persists and results in the brace punching the chord wall, which causes further ovalization. The following describes the physical phenomena of failure.

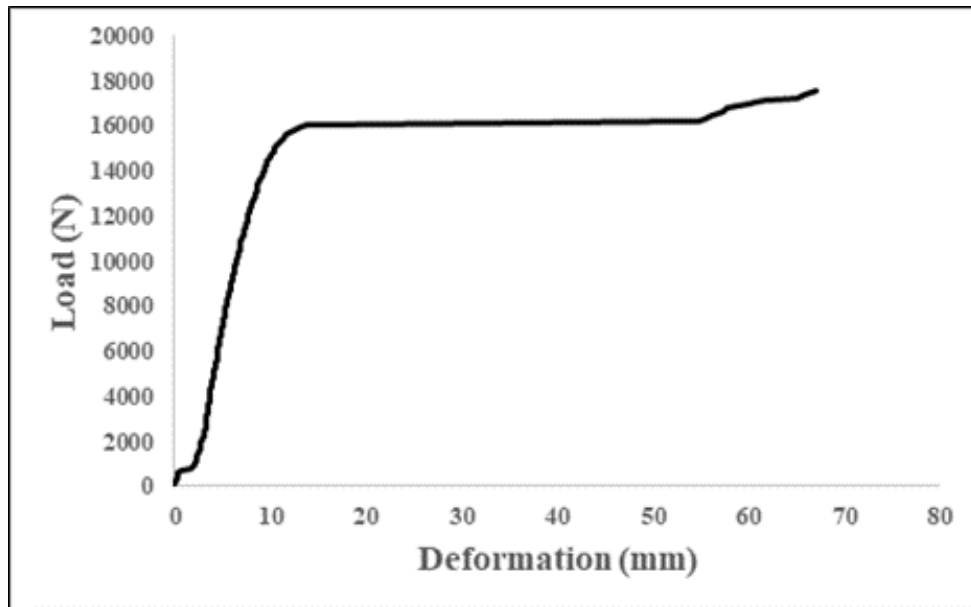


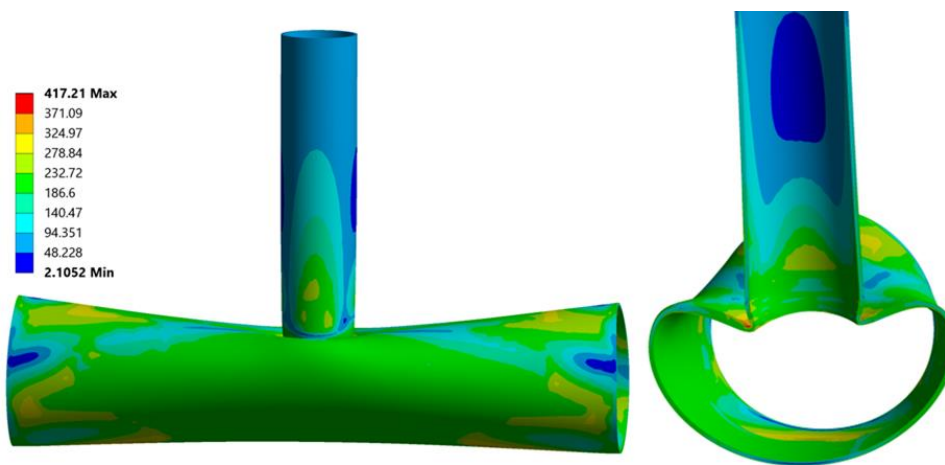
Figure 5.9: Load-deformation curve for unstiffened joint

With the exception of crown points, when a single point load will be present, the force applied to the brace is transferred to the chord at any point along the brace-chord intersection in the form of two symmetrical point loads. For large diameter ratios ($\beta = d/D$ close to 1.0), the load is transferred to the chord as a scattered load, whereas for small β (close to 0.1), the force is transferred as a concentrated load to the section of the chord. Assuming that for the diameter ratio of 0.50, the load transmission mechanism in the current study combines distributed and concentrated loads. By bending, the top piece of the chord bears the transferred weight, and a component of the chord adds to the stiffness of the bending motion.

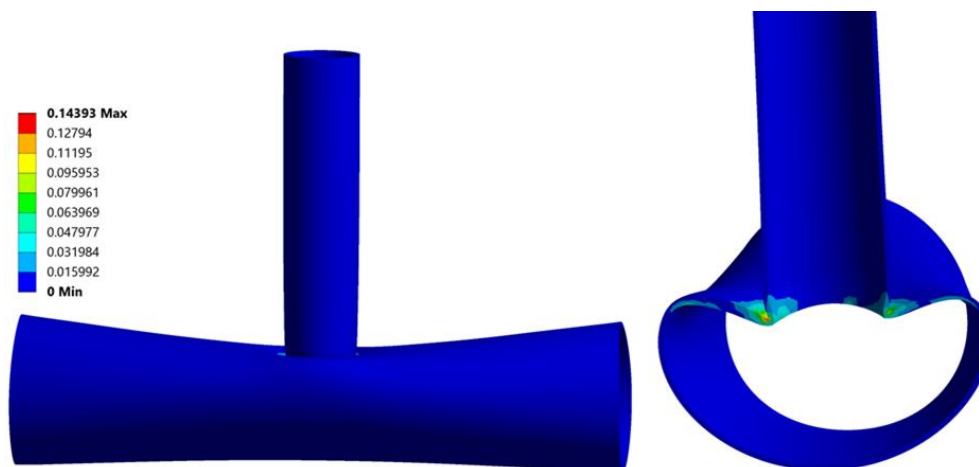
The bottom part of the chord is then subjected to the load as beam shear. The distorted shape near the intersection of the bracechords from the numerical simulation, as seen in Figure 5.10(b), is evidently similar to the failed specimen of the unstiffened joint shown in Figure 5.10. (a). Figure 5.10. (c), gives the variation of plastic strain in the T-joint.



(a) After-testing image of the specimen (experiment)



(b) The von Mises stress distribution (Numerical simulation)

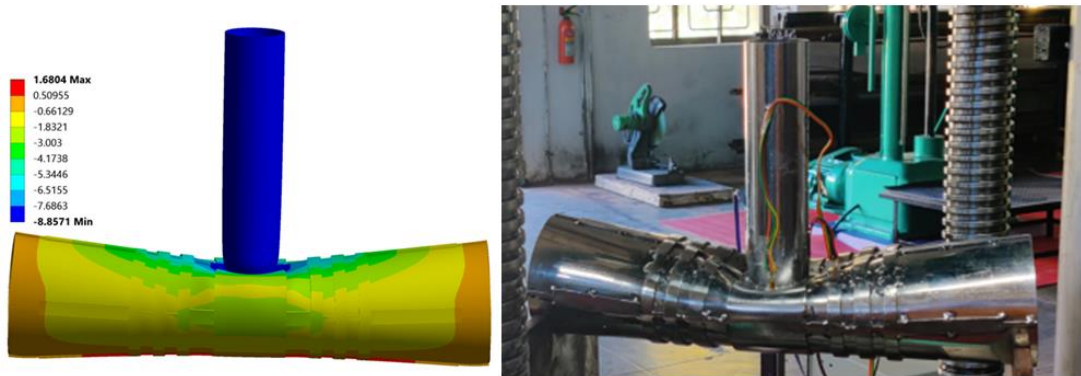


(c) Variation of Equivalent plastic strain (Numerical simulation)

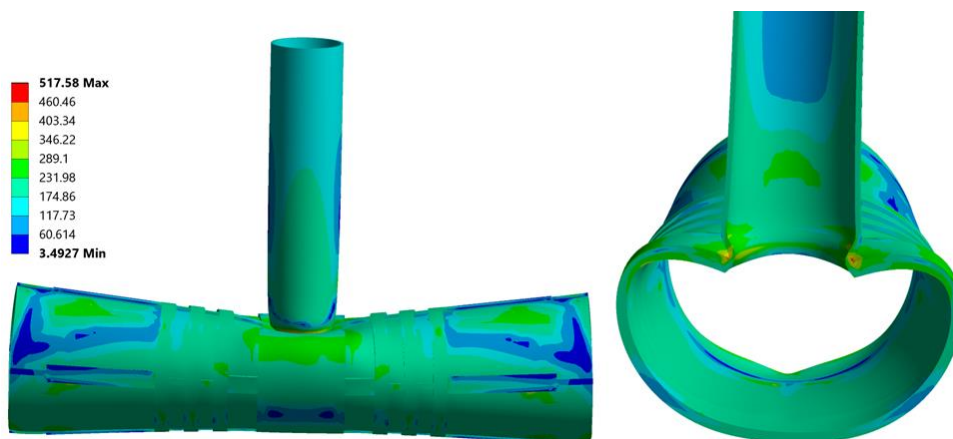
Figure 5.10: Unstiffened T joint (a) After-testing image of the specimen (experiment) (b) The von Mises stress distribution (Numerical simulation) (c) Variation of Equivalent plastic strain (Numerical simulation)

5.7. Behaviour of stiffened tubular T-joint

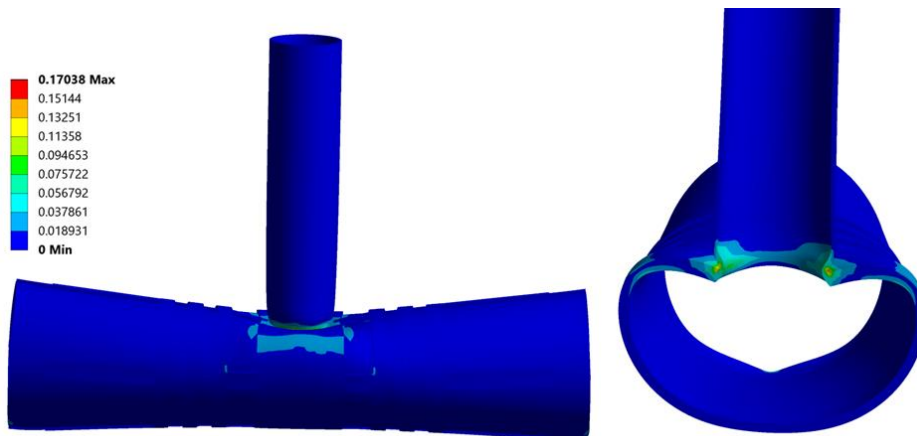
Below is an explanation of how stiffeners behave in relation to an unstiffened T-joint. As shown in Figure 5.11(b), the saddle region of an unstiffened T-joint bears greater stress than the crown region as a result of the axial load applied to the brace. In addition, there is an extensive region of high stress concentration around the brace-chord contact. According to Figure 5.11(c), the high stress distribution and high strain distribution both occur at the intersection of the brace and chord. The specimen after failure in both the experiment and the numerical study is shown in Figure 5.11 (a).



(a) After-testing image of the specimen (experiment)



(b) The von Mises stress distribution (Numerical simulation)



(c) Variation of Equivalent plastic strain (Numerical simulation)

Figure 5.11: 4 strips stiffened T joint (a) After-testing image of the specimen (experiment) (b) The von Mises stress distribution (Numerical simulation) (c) Variation of Equivalent plastic strain (Numerical simulation)

5.8. Ultimate capacity of the chord

Table 5. 2 shows the variation in ultimate capacity of the unreinforced and reinforced tubular T-joint models. From the data, it is evident that the stiffened configurations have more capacity in the bearing of the loads and the corresponding increase in strength is more than sixty percent than that of the unstiffened T-joint model

Table 5. 2. Ultimate capacity variation (kN)

Unstiffened	Four strips	Six strips	Eight strips
16.088	26.98	27.95	27.96
	69.25 %	73.73 %	73.79 %

Table 5. 3 shows the variation in joint local stiffness of the unstiffened and stiffened tubular T-joint models. From the data, it is evident that the stiffened configurations have achieved more stiffness.

Table 5. 3. Joint Local Stiffness variation (N/mm)

Unstiffened	Four strips	Six strips	Eight strips
1449.1	2420	3158.8	3489.4
	67.00 %	117.98 %	140.79 %

5.9. Verification of Numerical results with experimental data

Load versus deflection curves obtained from experiment and finite element analysis is depicted in figures 5.12, 5.13, 5.14, and 5.15 respectively. The case considered here is an unstiffened T joint and stiffened T joint with 4 strips, 6 strips, and 8 strips respectively and it is subjected to compression loading. A number of zones can be identified on the load-deflection curve, we have categorized the above load-deflection curve into three zones. Zone 1 as elastic region, Zone 2 as the elastic-plastic region and Zone 3 as yielding to fracture region. In zone 1, the load is transmitted to the strips and chord member through brace members. From figures 5.12 and 5.13, it is observed that for unstiffened T joint and stiffened T joint with 4 the load-deflection curve strips flatten up to a deflection of 1 mm (zone1) but in case of stiffened T joint with 6 strips (Figure 5.14) and stiffened T joint pipeline with 8 strips (Figure 5.15) flattening of the load-deflection curve is not observed at the initial loading. From Figures 5.12, 5.13, 5.14, and 5.15, it is observed that as the load increases the load-deflection curve varies linearly (elastic in nature) and it reaches the plasticity region up to a deflection of 3 mm (zone 2) which is a common observation in all the cases. As the loading increases, the materials start yielding and enter into the fracture region (zone 3). In the case of unstiffened, the material fails at a load of 16000 N but in the case of stiffened T joints the materials take more load when compared to unstiffened which can be observed in figures 5.13, 5.14, and 5.15 respectively contribution of stiffeners plays a very vital role in carrying more loads.

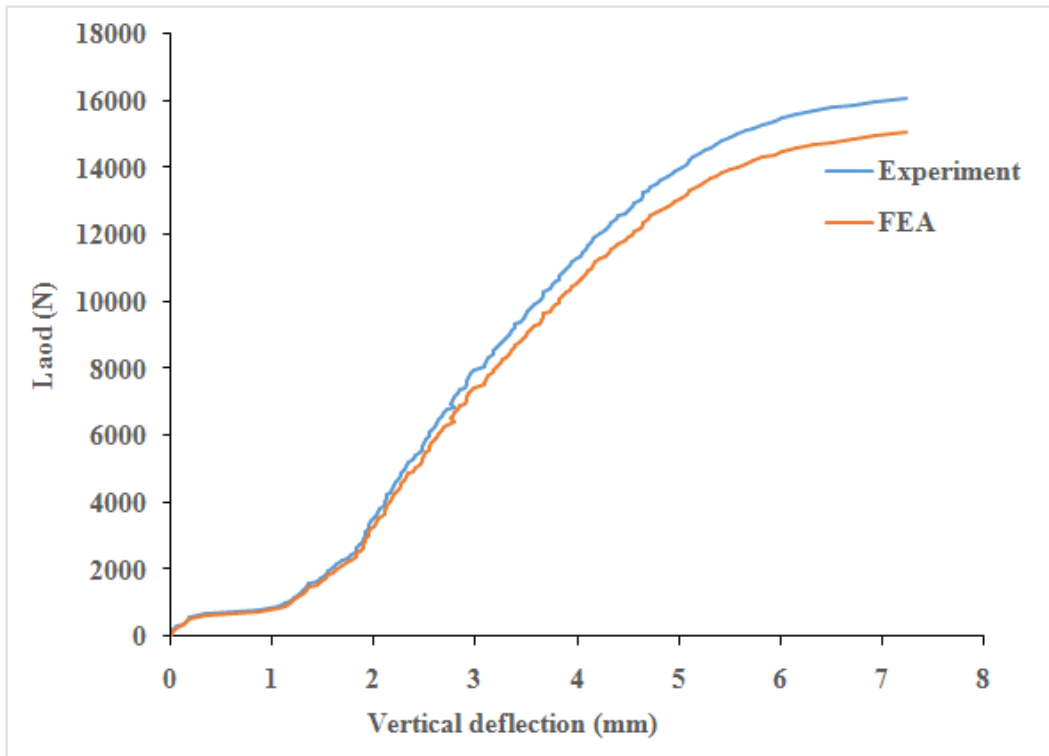


Figure 5.12: Comparison of Load v/s Vertical deflection between experimental and FE-simulated data for Unstiffened T-Joint

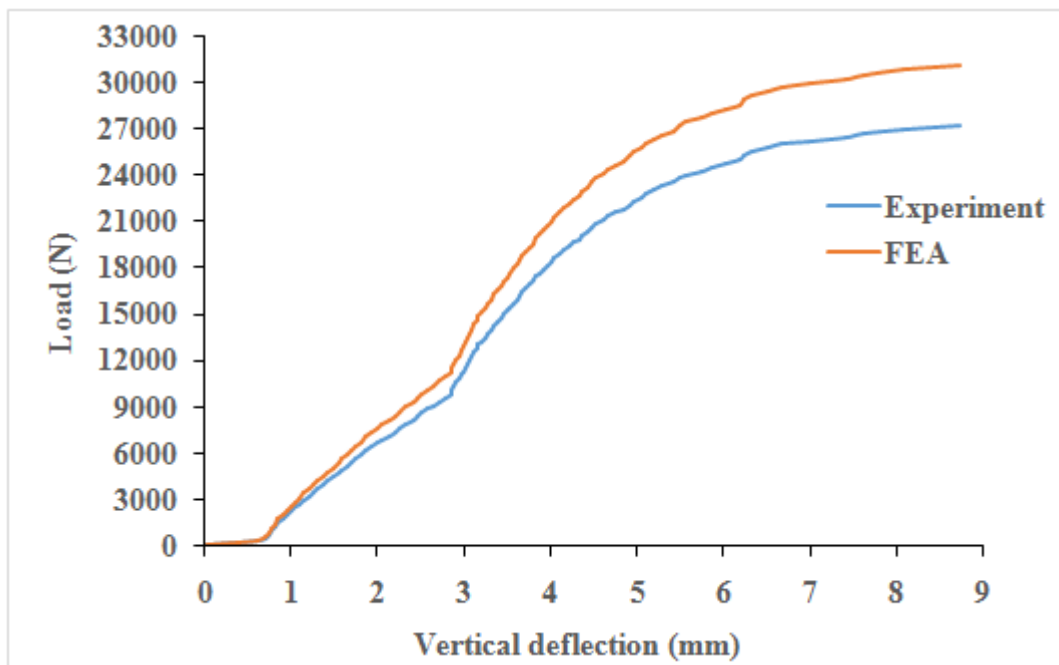


Figure 5.13: Comparison of Load v/s Vertical deflection between experimental and FE-simulated data for 4 strip stiffened T-Joint

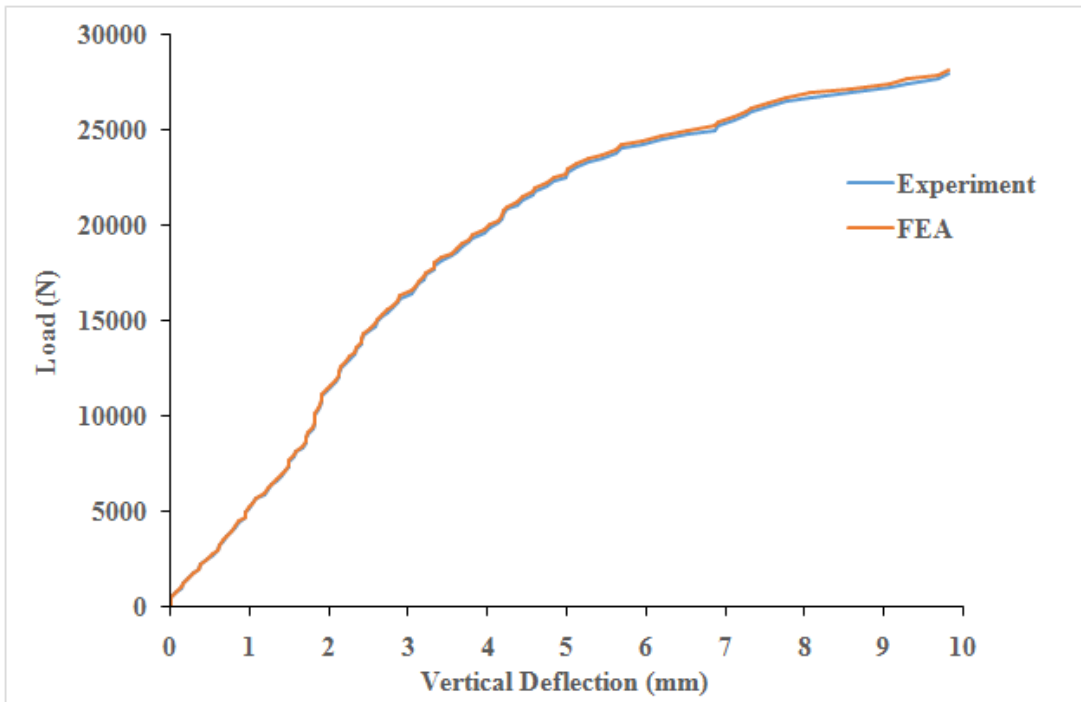


Figure 5.14: Comparison of Load v/s Vertical deflection between experimental and FE-simulated data for 6 strip stiffened T-Joint

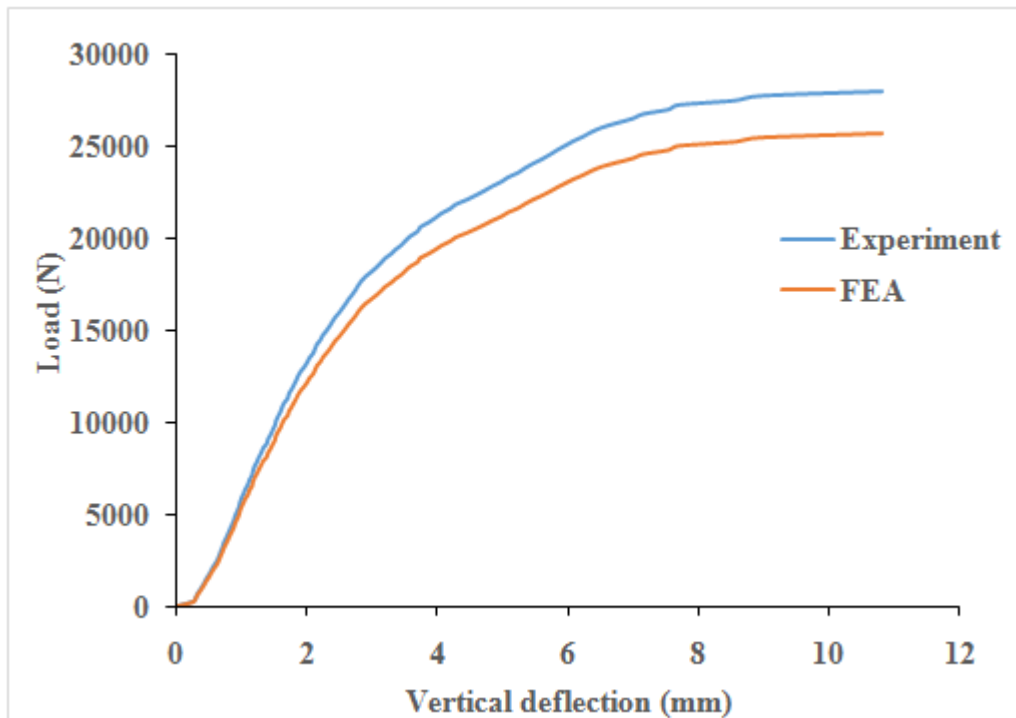


Figure 5.15: Comparison of Load v/s Vertical deflection between experimental and FE-simulated data for 8 strip stiffened T-Joint .

The experimental solutions illustrated in Table 4 are attained by taking into account of the residual stresses in the four tubular T-joint models: one unstiffened T-joint model and the other stiffened T-joint model. The finite element model does not take into account the residual stresses created during the pipe cutting, welding, and groove machining processes, hence the numerically projected compression loads differ from the actual values. From figures 5.12 -5.15, it is observed that the FEA results are in good correlation with the experimental results

Table 5. 4. Variation of load

Configurations	Displacement (mm)	Load (N)		% Error
		Experimental	Numerical	
Unstiffened	7.24	16088.4	15046	6.47
4 strips	8.75	27222.75	31102	14.25
6 strips	9.81	27958.5	28200	0.8
8 strips	10.8	27958.5	25681	8.14

CHAPTER 6

CONCLUSIONS

In summary, this study involves the design and analysis of unreinforced and reinforced tubular T-joints and it deals with the difficulties faced during fabrication process as well as experiments. From the study, the following conclusions were drawn:

6.1 CONCLUSIONS FROM EXPERIMENTAL STUDY

- T-joints under axial compressive force failed by plastification of the chord near the joint intersection, as can be seen from the distorted shapes of the specimens.
- According to the studies conducted for this study, T-joints that have been stiffened by stiffeners exhibit a considerable increase in strength when compared to joints that have not been stiffened.
- The stiffened joints have an improvement in the strength of more than 70 %.
- The local stiffness of the stiffened joints has increased by more than 60%.
- The various stiffening mechanism configurations should effectively distribute the axial load of the brace to a broader area of the chord, hence increasing the chord's strength.

6.2 CONCLUSIONS FROM NUMERICAL STUDY

- The finite element-based numerical study for both unreinforced and reinforced with grooves of tubular T-joint is carried out and observed that the groove mechanisms with different configurations effectively increase the joint local stiffness of tubular T joint.
- The different grooved configurations and their increment in percentage of stiffness are 5 grooves 1×1 mm 81.3 %, 5 grooves 2×2 mm 79.55 % 3 grooves (2-1-3) 1×1 mm 81.51% 3 grooves (2-1-3) 2×2 mm 80.38 %, 3 grooves (4-1-5) 1×1 mm 81.29 %, 3 grooves (4-1-5) 2×2 mm 80.69%.

6.3 LIMITATIONS OF THE STUDY

- The complete stress analysis to understand the behavior of the joint in the brace-chord intersection is not done due to instrumentation limitations
- The finite element model does not take into account the residual stresses created during the pipe cutting, welding, and machining processes.

6.4 SCOPE FOR FUTURE WORK

Further experimental studies are needed to identify the effects of parameters, which influences behaviour of tubular T-joint under axial compressive load. The parametric studies, which essentially give the information about the relationship between the various parameters of stiffeners and the resultant effect on the static strength and stiffness of the joint, are to be done. As a result, an analytical equation would be formulated involving the parameters that affect the behaviour of the joint.

REFERENCES

- A.A. Walvekar et al. (2014). “An experimental study and fatigue damage model for fretting fatigue.” *Tribology International*, 79, 183–196.
- A. Ramalho, Celis, J. (2003). “Fretting Laboratory Tests: Analysis of the Mechanical Response of Test Rigs.” *Tribology Letters*, 14, 187–196. <https://doi.org/10.1023/A:1022368414455>.
- API-RP American Petroleum Institute Recommended practice for planning, designing and constructing fixed offshore Platforms, 22nd edition, 2014.
- Chen, W. J., and Han, D. J. (1985), *Tubular members in Offshore Structures*, Pitman Advanced Publishing Program, Boston, MA.
- D. S. Ramachandra Murthy, A. G. Madhava Rao, P. Gandhi, and P. K. Pant (1992), “Structural efficiency of internally ring-stiffened steel tubular joints”, *Journal of Structural Engineering*, Vol. 118, No. 11, 3016-3035
- Designing, and Constructing Fixed Offshore Platforms—Working Stress Design. 21st Edition. 2000.
- Det Norske Veritas. Offshore Standard DnV-OS-C101 Design of Offshore Steel Structures, General. October 2000.
- Digre, K. A., Krieger, W., Wisch, D.J., and Petrauskas, C., 1994, “ API RP 2A Draft Section 17 Assessment of Existing Platforms”, Behavior of offshore structures, BOSS '94, Chryssostomidis, C., *et al.*, eds., Pergamon, Oxford, pp.467-478
- Dikshant Singh Saini, Debasis Karmakar, Samit Ray-Chaudhuri (2016), “A review of stress concentration factors in tubular and non-tubular joints for the design of offshore installations”, *Journal of Ocean Engineering and Science* 1, 186-202
- E. M. Dexter I and M. M. K. Lee (1999), “Static strength of axially loaded tubular K-joints. I: behavior”, *Journal of Structural Engineering*, Vol. 125, No. 2.
- Fenq Qi and TAN Jia-hua (2005), “The ultimate strength of doubler plate reinforced Y-joints under compression loading”, *Journal of Marine Science*

and Application, Vol. 4, No. 2.

- Fenq Qi, Tan Jia-Hua (2006), “Static Strength of Sleeve Reinforced X-joints Loaded By Compression Load”, 25th International Conference on Offshore Mechanics and Arctic Engineering.
- G. J. van der Vegte; Y. S. Choo; J. X. Liang; N. Zettlemoyer; and J. Y. R. Liew (2005), “Static Strength of T-Joints Reinforced with Doubler or Collar Plates. II: Numerical Simulations”, *Journal of Structural Engineering*, Vol. 131, No. 1.
- G. Raghava, A. G. M. Rao, D. S. R. Murthy (1989), “Behavior of Unstiffened and Stiffened Steel Tubular T-Joints”, *Journal of Offshore Mechanics and Arctic Engineering*.
- H. Qu, J. Huo, C. Xu, F. Fu (2014), “Numerical studies on dynamic behavior of tubular T-joint subjected to impact loading”, *International Journal of Impact Engineering*, 67, 12–26.
- Hamid Ahmadi, Mohammad Ali Lotfollahi-Yaghin, Shao Yong-Bo (2013), “Chord-side SCF distribution of central brace in internally ring-stiffened tubular KT-joints: A geometrically parametric study”, *Journal of Thin-Walled Structures* 70, 93–105.
- Hossein Nassiraei , Mohammad Ali Lotfollahi-Yaghin, Hamid Ahmadi (2016), “Structural behavior of tubular T/Y-joints with collar plate under static in-plane bending”, *Journal of Constructional Steel Research*, 123, 121–134.
- Hossein Nassiraei , Mohammad Ali Lotfollahi-Yaghin, Hamid Ahmadi (2016), “Static strength of doubler plate reinforced tubular T/Y-joints subjected to brace compressive loading: Study of geometrical effects and parametric formulation”, *Journal of Thin-Walled Structures*, 107, 231–247
- Hossein Nassiraei, Lei Zhu, Mohammad Ali Lotfollahi-Yaghin, Hamid Ahmadi (2017), “Static capacity of tubular X-joints reinforced with collar plate subjected to brace compression”, *Journal of Thin-Walled Structures*, 119, 256–265.
- Hossein Nassiraei, Mohammad Ali Lotfollahi-Yaghin, Hamid Ahmadi

- (2016), “Static strength of offshore tubular T/Y-joints reinforced with collar plate subjected to tensile brace loading”, *Journal of Thin-Walled Structures* 103, 141-156
- Hossein Nassiraei, Mohammad Ali Lotfollahi-Yaghin, Hamid Ahmadi (2016), “Static performance of doubler plate reinforced tubular T/Y-joints subjected to brace tension”, *Journal of Thin-Walled Structures* 108, 138–152
 - Hossein Nassiraei, Mohammad Ali Lotfollahi-Yaghin, Hamid Ahmadi (2016), “Static strength of collar plate reinforced tubular T/Y-joints under brace compressive loading”, *Journal of Constructional Steel Research*, 119, 39–49.
 - Hossein Nassiraei, Mohammad Ali Lotfollahi-Yaghin, Hamid Ahmadi, Lei Zhu (2017), “Static strength of doubler plate reinforced tubular T/Y-joints under in-plane bending load”, *Journal of Constructional Steel Research*, 136, 49–64.
 - ISO/CD 13819-2: Petroleum and Natural Gas Industries—Offshore Structures—Part 2: Fixed Offshore Structures, May 1999.
 - Jie Yang, Yongbo Shao, Cheng Chen (2012), “Static strength of chord reinforced tubular Y-joints under axial loading”, *Journal of Marine Structures* 29, 226–245.
 - Lei Zhu n, Yan Zhao, Shuwen Li, Yuxing Huang, Liren Ban (2014), “Numerical analysis of the axial strength of CHS T-joints reinforced with external stiffeners”, *Journal of Thin-Walled Structures*, 85, 481–488.
 - Lei Zhu, Shuo Han, Qiming Song, Limeng Ma, Yue Wei, Shuwen Li(2016), “Experimental study of the axial compressive strength of CHS T-joints reinforced with external stiffening rings”, *Journal of Thin-Walled Structures*, 98,245–25.
 - M. Lesani, M.R. Bahaari, M.M. Shokrieh (2015), “FRP wrapping for the rehabilitation of Circular Hollow Section (CHS) tubular steel connections”, *Journal of Thin-Walled Structures*, 90, 216–234.
 - M.H. Li, H.J. Xing, X.G. Hu, Y. Gao, Research on load-carrying capacity

- of smaller angle K-joints for power transmission steel tubular tower, *Build. Struct.* 43 (5) (2013) 48–53 (in Chinese).
- M.Lesani, M.R. Bahaari, M.M. Shokrieh, “Experimental investigation of FRP strengthened tubular T-joints under axial compressive loads”, *Journal of Construction and Building Materials* 53(2014) 243-252
 - M.Lesani, M.R. Bahaari, M.M. Shokrieh, “Numerical investigation of FRP strengthened tubular T-joints under axial compressive loads”, *Journal of Composite structures* 100(2013) 71-78
 - M.M.K. Lee, A. Llewelyn-Parry (1999), “Strength of ring-stiffened tubular T-joints in offshore structures-a numerical parametric study”, *Journal of Constructional Steel Research* 51, 239–264.
 - M.R.Shiyekar, M. Kalani, R.M. Belkune (1983), “Stresses in Stiffened Tubular T joint of an Offshore Structure”, *Journal of Energy Resources technology*, 1983
 - Nelson J. Cossa, Narayanan S. Potty, Mohd Shahir Liew, Arazi B. Idrus (2011) “Reliability Analysis of Tubular Joints of Offshore Platforms in Malaysia”, *International Journal of Civil, Environmental, Structural, Construction and Architectural Engineering* Vol:5, No:12.
 - Offshore Oil and Gas magazine (2017), Vol 77, Issue 4.
 - R. B. Pan, F. B. Plummer, J. G. Kuang (1977), “Ultimate Strength of Tubular Joints”, *Journal of Petroleum Technology*, Volume 29, Issue 04, 449-460.
 - T. C. Fung, T. K. Chan, and C. K. Soh (1999), “Ultimate capacity of Doubler plate–reinforced tubular joints”, *Journal of Structural Engineering*, Vol. 125, No. 8.
 - T. S. Thandavamoorthy (2000), “Investigations on Internally Ring-Stiffened Joints of Offshore Platforms”, *Journal of Offshore Mechanics and Artic Engineering (OMAE)*, Vol. 122, 233-242.
 - W. J. Craff. (1981), *Introduction to offshore structures: Design Fabrication Installation*”, Gulf publishing company, ISBN: 9780872016941.
 - W. Visser (1975), “On the Structural Design of Tubular Joints”, Sixth

Annual Offshore Technology Conference, OTC 2117, *Journal of engineering for Industry*, 391-399.

- Wimpey structures. In-service database for ring-stiffened tubular joints report WOL 035/91; 1991
- Y. Fu and L. Tong (2015), “Experimental Study on Behavior of CFRP-Strengthened Circular Hollow Section Gap K-Joints”, 6th International Conference on Advances in Experimental Structural Engineering.
- Y. Fu, L. Tong, L. He, X.L. Zhao (2016), Experimental and numerical investigation on behavior of CFRP-strengthened circular hollow section gap K-joints, *Journal of Thin-walled Structures*, 102, 80–97.
- Y. S. Choo , G. J. van der Vegte, N. Zettlemoyer, B. H. Li, and J. Y. R. Liew (2005), “Static Strength of T-Joints Reinforced with Doubler or Collar Plates. I: Experimental Investigations”, *Journal of Structural Engineering*, Vol. 131, No. 1.
- Y. Sawada, S. Idogaki, and K. Sekita (1979), “Static and fatigue tests on T-joints stiffened by an internal ring”, Offshore Technology Conference.
- Y. Zhao, S.W. Li, Y.X. Huang, L.R. Ban, L. Zhu, Experimental study on strength of CHS T-joints retrofitted by external stiffeners, *China Civ. Eng. J.* 47 (9) (2014) 70–75 (in Chinese).
- Y.K. Pan. Experimental investigation on static behavior of uniplanar gapped K-type CHS joints reinforced with longitudinal plates Harbin Institute of Technology. China (in Chinese) 2013.
- Y.S. Choo, J.X. Liang , G.J. van der Vegte, J.Y.R. Liew (2004), “Static strength of collar plate reinforced CHS X-joints loaded by in-plane bending”, *Journal of Constructional Steel Research*, 60, 1745–1760.
- Y.S. Choo, J.X. Liang, G.J. van der Vegte, J.Y.R. Liew (2004), “Static strength of doubler plate reinforced CHS X-joints loaded by in-plane bending”, *Journal of Constructional Steel Research*, 60, 1725–1744

PUBLICATIONS BASED ON PRESENT RESEARCH WORK

Publication in Journals (Indexed in SCI/Scopus/ Web of Science)

1. N. Murugan, Vadivuchezhian Kaliveeran, and M. K. Nagaraj (2020), “Effect of Grooves on the Static Strength of Tubular T-Joints of Offshore Jacket structures”, **Materials Today: Proceedings**, DOI: 10.1016/j.matpr.2019.10.132

Journal Articles (Submitted for Publication)

1. N. Murugan, Vadivuchezhian Kaliveeran, Subrahmanya Kundapura (2023), “Experimental investigation of the behaviour of tubular T-joint of Jacket structures”, **A Springer book series Springer Proceedings in Materials**.
2. N. Murugan, Vadivuchezhian Kaliveeran, Raveesh R M, Subrahmanya Kundapura (2023), “Experimental and numerical studies on the stiffening of tubular T joint of Offshore Jacket structures”, **Iranian Journal of Science and Technology, Transactions of Civil Engineering**.

International Conferences

1. N. Murugan, Neeraja J, and Vadivuchezhian Kaliveeran (2017), “Dynamics analysis of Jacket structure using finite element method”, 7th International Conference on Recent Advances In Material Chemistry - ICRAMC 2017, February 15-17 2017, SRM University, Chennai.
2. N. Murugan, Vadivuchezhian Kaliveeran and M. K. Nagaraj(2019), “Effect of Grooves on the Static Strength of Tubular T Joints of Offshore Jacket structures”, International Conference on Materials and Manufacturing Methods - 2019, July 5-7 2019, NIT Tiruchirappalli, Tiruchirappalli (**Awarded Best Paper**)
3. N. Murugan, Vadivuchezhian Kaliveeran, Subrahmanya Kundapura (2022), “Experimental investigation of the behaviour of tubular T-joint of Jacket structures”, 13th International Symposium on Plasticity and Impact Mechanics-IMPLAST 2022, August 21-26 2022, IIT Madras, Chennai

CURRICULUM VITAE



Name : N. MURUGAN

Permanent Address:

. 4/58, Sivanandanoor Road, Thiravianagar, Mathalamparai post, Tenkasi District,
Tamil Nadu, PIN: 627814.

Contact No. : +91-9566424949.

Email ID : nmurugan.ezhilarasi@gmail.com

Experience:

Assistant Professor (2013-2016)

College : Veltech Dr RR & Dr SR Technical University, Chennai

Assistant Professor (2011-2013)

College : Gopal Ramalingam Memorial Engineering College, Sri Krishna
Group of Institutions, Chennai.

Education:

Master of Engineering (2009-2011)

Discipline : Aerospace Technology

College : Madras Institute of Technology, Anna University, Chennai

Bachelor of Engineering (2005-2009)

Discipline : Aeronautical Engineering

College : Noorul Islam college of engineering, Kanyakumari